UCLouvain

AGRO LOUVAIN BIOINGÉNIEURS

Faculté des bioingénieurs

Optimisation of the microfluidic system of Dolomite for nanoparticle production

Author: Arthur CARBON

Supervisors: Prof. Anne DES RIEUX
Prof. Christine DUPONT

Readers: Prof. Ana BELOQUI GARCIA
Prof. Arnaud DELCORTE

Academic year 2023–2024

Master thesis presented in a view of obtaining the Bioengineer diploma: environmental sciences and technologies

Acknowledgements

I would like to express my gratitude to :

Everyone who supported me in any way during the writing of this master thesis;

My two supervisors, Mrs des Rieux and Mrs Dupont, for their explanations, their advice and their availability to help me understand;

The ADDB research team at UCLouvain's Woluwé-Saint-Lambert laboratories, especially Floriane for her help and invaluable advice;

Mr Delcorte and Mrs Beloqui Garcia, for agreeing to be on my jury;

Mrs Rasse, who helped me with the whole part on using the JMP software;

My parents, my family and friends, for their constant support.

During the writing of this thesis, I acknowledge the use of ChatGPT 3.5 (OpenAI, https://www.openai.com/chatgpt) for rephrasing sentences and understand concepts, the use of DeepL Translator (https://www.deepl.com/en/translator) to translate text from French to English.

Table of contents

´

List of Figures

List of Tables

List of abbreviations

τ	Residence time of the fluid
τ_{agg}	Time for a particle to nucleate, grow and aggregate
τ_{mix}	Mixing timescale
F_a	Flow rate of the organic phase
F_w	Flow rate of the aqueous phase
M_n	Number average molecular weight
M_w	Weight average molecular weight
ACN	Acétonitrile
ADDB	Advanced Drug Delivery and Biomaterials
D	Diffusivity of the solvent
Doxil	Doxorubicin Liposomal
EMA	European Medicines Agency
EUA	Emergency use authorization
FDA	Food and drug administrations
FEP	Fluorinated ethylene propylene
FRR	Flow rate ratio
HFF	Hydrodynamic flow focusing
HPLC-UV	High-Performance Liquid Chromatography-UV
IDW	Inverse Distance Weight
IDW	Inverse distance weight

LDRI Louvain Drug Research Institute

milliQ water Ultra pure water

mRNA Messenger RNA

mTORC1 Mammalian target of rapamycin complex 1

mTORC2 Mammalian target of rapamycin complex 2

N Replicates

Np(s) Nanoparticule(s)

NS Not significant

NTA Nanoparticle Tracking Analysis

O/W emulsion Oil-in-water emulsion

P1 Pump 1

P2 Pump 2

P3 Pump 3

PDI Polydispersity index

PEG Polyethylene glycol

PEO Polyethylene oxide

PGA Polyglycolic acid

PLA Polylactic acid

PLGA Poly(lactide-co-glycolide)

PPG Polypropylene glycol

PPO Polypropylene oxide

PS100 Polystyrene 100nm

S significant

SMCS Support en Méthodologie et Calcul Statistique

TCI Tokyo Chemical Industry

TFR Total flow rate

V1 Valve 1

V2 Valve 2

V3 Vavle 3

W/O emulsion Water-in-oil emulsion

Chapter 1

Introduction

1.1 Overview

The research question of this master's thesis concerns the production of nanomedicines using a microfluidic system supplied by the company Dolomite. This system was new and had never been used before in the research lab where this study was conducted (Advanced Drug Delivery and Biomaterials (ADDB) / Louvain Drug Research Institute (LDRI) / UCLouvain).

Before directly discussing the experiments carried out during 2024, Chapter 1 will be devoted to the context and the justification of this research question. Firstly, the history of nanomedicines will be briefly discussed, with a focus on nanomedicines in recent years and the importance of nanoparticles (NPs) in medicine. Secondly, a point will be dedicated to the different polymers and drugs used during this work. Thirdly, this chapter will discuss the different criteria used to assess the quality of NPs, which will therefore be evaluated during the experiments in this work. A point will be made about NP production methods with a focus ont the conventional method and its limitations. Finally, before discussing the microfluidic system used for this work, the use of microfluidics for the production of nanomedicine will be discussed.

1.2 Context

Nanomedicine is a discipline that aims to improve application from medical diagnostics, treatments and therapies to prevention by applying nanotechnologies in medicine in order to exploit material properties at the nanoscopic scale. This branch of medicine appeared thanks to Richard Feynman in 1959 with the production of nanometer-sized materials [1]. Nanomedicine has made possible the increase of precision, efficacy, and safety of treatments compared to more conventional ones [2][3]. It leads to a wide range of benefits, such as early diagnosis and improved monitoring of disease progression, improved medical imaging, drug delivery, etc [2].

Nanomedicine has rapidly gained in importance. Numerous treatments based on it are currently available on the market. For example, Doxorubicin Liposomal (Doxil®) was approved in 1995 by the Food and Drug Administration (FDA) in the United States. Doxil® consists of encapsulating doxorubicin in liposomes. It was designed to improve the efficacy of doxorubicin while reducing its side effects. Traditionally, doxorubicin has been highly effective in treating cancer but exposes patients to significant side effects (e.g. cardiac toxicity). Liposome encapsulation of doxorubicin allows better control in order to target cancerous tissues and better spare healthy tissues while increasing the accumulation of doxorubicin in these cancerous tissues. Doxils® have been extended to many cancers [4][5][6][7].

Another example of a recent nanomedicine application is Moderna's COVID-19 vaccine, known as mRNA-1273. The design of this vaccine is based on the use of lipid NPs to deliver messenger RNA (mRNA) to human cells. This vaccine induces an immune response that protects against infection and reduces the severity of the disease. It plays a crucial role in preventing infection by the SARS-CoV-2 virus, which causes COVID-19. It is one of the first COVID-19 vaccines to receive emergency use authorization (EUA) from the FDA in December 2020. Lipid NPs protect the mRNA during intramuscular injection and facilitate its entry into cells. The mRNA is then translated into a protein by the cell's ribosomes, which is then recognised as foreign and triggers an immune response. It is the memory of the immune system which, when subsequently exposed to SARS-CoV-2, triggers a rapid and effective immune response [8][9][10].

As the previous examples illustrate, nanomedicine has been a constantly expanding science for many years, offering a wide range of new avenues of discovery. Nanomedicine covers a wide scope of applications. Concrete examples are dendrimers, which are branched polymers used to transport substances to specific cells; fullerenes and nanocages, forms of carbon with specific configurations used to transport drugs or for medical imaging; quantum dots, semiconductor nanocrystals used mainly for biomedical imaging because of their unique fluorescent properties and many more [11].

Among the most recent and promising advances, the use of NPs for drug encapsulation is an area of considerable interest. NP encapsulation increases the effectiveness, precision and safety of bioactive molecules through a number of key benefits including improved solubility and stability, decrease toxicity, controlled release, targeting. This enthusiasm for nanomedicine opens up new prospects for new and effective treatments. This is reflected by the large number of clinical trials for a wide variety of diseases [12][13]. These new treatments offer a new approach to cure diseases which, until now, have had no effective treatment, or, have had high infection or mortality rates. For example cancer, which is one of the leading causes of death worldwide, making it a major public concern, with high biological complexity. Cancer presents therapeutic challenges, as some

cancers remain difficult to treat and some treatments have violent side effects [14][15][16].

The FDA has already approved 64 formulations of NPs in 2023, most of them are lipid, polymeric and inorganic/metallic [17]. Applications for lipid NPs and their role have already been discussed. Metallic NPs are involved in a wide range of diseases. Their metallic composition gives them unique properties such as electrical conductivity, magnetism and specific optical properties [18][19]. This enables various applications, such as the use of gold NPs to fight cancer by converting light energy into heat [18]. Metallic NPs are also used for more specific diseases such as iron deficiency anaemia, an iron-related disease. Ferumoxytol, an iron oxide NP, is used to improve the distribution of iron in the body to counter iron deficiencies [20][21].

Finally, polymer NPs are also used in the treatment of various diseases such as cancer, cardiovascular disease, etc. Their use is popular thanks to their high biocompatibility and biodegradability, their controlled release property and subcellular size [22]. These NPs also have the ability to encapsulate a wide range of drugs, both hydrophobic and hydrophilic [22][23]. One example is the use of poly(lactide-co-glycolide) PLGA NPs to encapsulate irinotecan (a chemotherapeutic agent). PLGA is a polymer described in section 1.3.1.1. These NPs provide prolonged circulation in plasma and controlled release of irinotecan, making treatment more effective [24].

Although nanomedicines have many advantages, they face challenges and limitations. NPs can be toxic and non-biocompatible. They can induce undesirable immune responses due to their small size and specific properties, which is not the case with conventional methods [25]. Moreover, the production of homogeneous and reproducible NPs on a large scale remains a major challenge. The techniques must therefore become more reliable to obtain mass production economically while ensuring good efficiency and safety in the homogeneity of the size, the shape, the composition of the NPs [26].The approval of nanomedicine is subjected to strict and long-term regulation by the FDA and the European Medicines Agency (EMA) [27].

NPs can be coated with biocompatible materials such as silica (improves targeted delivery), hydroxyapatite (frequently used in bone regeneration), chitosan (for drug delivery and gene therapy) or more commonly PEG (increases residence time in the bloodstream and reduces recognition by the immune system) [28][29][30][31]. These materials make them less detectable by the immune system, allowing them to circulate for longer periods in the body and, for example, to accumulate selectively in tumours [32]. This shows that NPs are enabling the emergence of more effective and targeted drug therapy. They also pave the way for a promising future that will meet the challenges of disease treatment and nanomedicine [33][34].

1.3 Nanomedicines

Nanomedicine refers to the use of nanotechnology in medicine, i.e. the use of engineered materials generally on a scale of several nanometers for therapeutic treatments and diagnostics. Nanomedicines can also refer to NPs in which a bioactive molecule is encapsulated [35][36]. NPs are nanoscale structures, usually in the range of a few nanometers to a few hundred nanometers, which can be made from a variety of materials, such as polymers, lipids, metals, and inorganic materials. These materials offer a versatile platform for the design and manufacture of NPs with specific physicochemical properties such as the size, the electric charge on the surface, etc (described in section 1.4) [36][17][37]. There are a large number of production methods for these NPs, each with its advantages. The conventional method, some more modern methods, their advantages and limitations will be discussed in section 1.5. This master thesis focuses only on polymeric NPs more precisely PLGA NPs. NPs made from other materials will not be addressed.

1.3.1 Polymers used to form nanomedicines

Polymers represent the largest class of biomaterials. They are used in many areas of medicine, including orthopedics, dentistry, cardiovascular implants, ...[38] They can be of natural origin or obtained using synthetic organic processes. The polymer results from the association of several monomers repeated in a particular sequence, creating a long monomer chain. The properties of polymers therefore tend to be more complex than those of their monomers. It is important to understand the unusual properties of polymers. The choice of one polymer for one application rather than another depends on this understanding [38]. They range from the least water-soluble polymers to the most hydrophobic polymers through polymers with an intermediate polarity (such as PLGA). Polymers are associated with a specific molecular weight [38]. Molecular weight refers to a whole series of information on physical and mechanical properties (resistance, elasticity), thermal properties (melting temperature), rheological properties (viscosity, solubility). The number average molecular weight (M_n) is defined by formula 1.1 and the weight average molecular weight (M_w) is defined by formula 1.2.

$$M_n = \frac{\sum N_i M_i}{\sum N_i} \tag{1.1}$$

$$M_w = \frac{\sum N_i M_i^2}{\sum N_i N_i} \tag{1.2}$$

Where N_i is the number of moles of species i, and M_i is the molecular weight of species i.

Polymers finding their applications in the medical field have generally a M_n ranging from 25,000 to 100,00 and a M_w from 50,000 to 300,000 [38].

1.3.1.1 PLGA

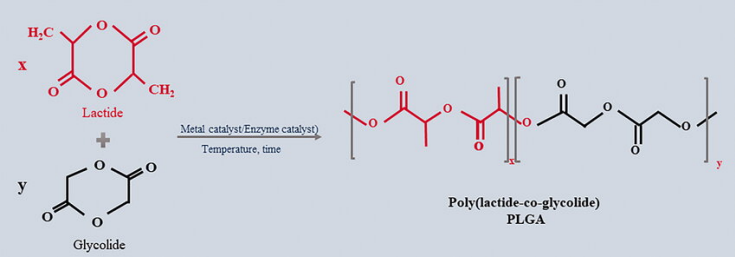

Figure 1.1: Structural Formula of the formation of PLGA

Among this diversity of polymers, PLGA is one of the most widely used in clinical medicine. Its structure is shown in Figure 1.1. It is a biocompatible and biodegradable polymer obtained from two monomers: polylactic acid (PLA) and polyglycolic acid (PGA). An ester bond binds them together to obtain the polymer (more precisely via ring-opening reaction between them). The degradation of this ester link by hydrolysis allows to reobtain the monomer of PLA and PGA, endogenous and non-toxic component that enters in the krebs cycle. Manipulating the monomer molar ratio (PLA:PGA ratio) allows to alter the hydrophobicity of the polymer and consequently the rate of degradation and release. PLGA is therefore an ideal biomaterial to encapsulate both hydrophilic and lipophilic therapeutic agents and to release them afterwards. When selecting PLGA for NPs production, it is essential to consider the molar ratio of the monomers, the mean molecular weight, the degree of crystallinity, as well as the size and shape of the monomers [38][39][40].

Table 1.1: Features of Resomer RG752S and Resomer RG502H [41][42][43][44][39]

Resomer RG 752S	Resomer RG 502H
Lactide :Glycolid (75 :25)	Lactide :Glycolid (50 :50)
HO[C2H4O2]n[C2H2O2]mCH3	[C3H4O2]x[C2H2O2]y
Ester terminated	Acid terminated
Mw = 13000	Mw = 14200

Table 1.1 shows the characteristics of the polymers used in this master's thesis. The experiments were carried out with resomer RG 752S and resomer RG 502H. They are well-known and have been widely used as nanomedicine polymers in several studies [39][44][45][43][46][47]. The variation in the lactide:glycolid ratio will have a direct effect on the degradation time of the NPs [38]. This is why it is interesting to study both Resomer RG 752S and RG 502H, even if some experiments

will be limited to the study of only one of the two polymers. The articles found in the literature testify to the ability of these two polymers to form NPs using both conventional methods and microfluidic systems. The studies also show to the ability of these polymers to form solid, stable and fairly reproducible NPs [39][44][45][43][46][47]. All polymers are purchased from Evonik.

1.3.2 Model Drug

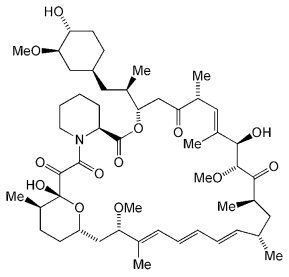

Figure 1.2: Rapamycin structural formula

The drug that will be used as a model drug in this work to test the efficacy of encapsulating a drug in polymeric NPs is rapamycin. Rapamycin, also called Sirolimus, is a macrocyclic compound discovered in the bacteria *Streptomyces hygroscopicus* (Figure 1.2). This substance was quickly identified as having immunosuppressive and anti-proliferative properties. This is why rapamycin quickly found medical use [48][49].

Rapamycin acts as an allosteric inhibitor of mammalian target of rapamycin complex 1 (mTORC1). This complex plays a regulatory role and can be implicated in development of diseases such as cancer. Indeed, the mTORC1 complex regulates the proliferation and growth processes cells. This complex regulates biogenesis of cellular components (such as proteins, lipids, ...) but also other processes such as energy metabolism and autophagy in response to growth-promoting signals such as nutrient intake, growth factors, oxygen, etc. Because of its action on this complex, making it immunosuppressive and anti-proliferative, medical research has developed an interest in rapamycin. Certain diseases, such as cancer or certain genetic diseases, presents a poor regulation of this complex. Rapamycin can also intervene in the treatment of neurological diseases, transplantation, age-related diseases, longevity and metabolism. Rapamycin has likewise a long-term inhibitory effect on complex 2 (mTORC2) in certain cell types. Little is known about the role of this complex 2. The literature describes in broad terms an impact of this complex on cell survival and on the organization of the actin cytoskeleton. The interest in rapamycin does not therefore stem from its weak influence on mTORC2. Rapamycin is generally used in the prophylaxis of organ rejection during renal transplantation. Cyclosporine, an immunosuppressive drug, and corticosteroids, drugs that imitates the effects of hormones produced by the adrenal glands, are generally used in combination with rapamycin for varying lengths of time depending on the patient's immunological

risk[48][49].

The molecular weight of rapamycin is 914.2 g/mol. This drug has a logP of 4.3 and is thus hydrophobic [49]. Rapamycin is a drug with a small therapeutic window, i.e. the concentration range for which rapamycin is effective without being toxic in the blood is small [50]. It fully justifies the encapsulation of this drug, which would make it possible to work over a wider concentration range while maintaining a prolonged and controlled release. It would therefore be possible to maintain more stable plasma levels over a longer period with less frequent administration. Targeting NPs would enable lower doses of rapamycin to be used, thanks to better accumulation of rapamycin in the target tissues, which would also reduce side effects. Rapamycin has already demonstrated good stability when encapsulated in NPs. This drug has thus often been used in the literature as a model drug [2][12][13][49][51][52]. Abnormalities resulting from the take of rapamycin (in general, regardless of the mode of administration) are generally mild, asymptomatic and self-limiting. Consequently it is rarely necessary to change the dose or to stop the treatment [49].

1.4 Physicochemical properties

Several parameters are essential to reflect NPs quality for medical applications and can easily be controlled.

One of the most critical properties is the size [nm] of the NPs. It influences the biodistribution of the molecule, the ability of NPs to cross physiological barriers, to penetrate cells and ultimately their rate of drug release. In this kind of application case, the goal is to minimize the size of NPs in order to optimize their accumulation in the target area [37][53][54].

Related to size, another property is the polydispersity index (PDI) [-]. PDI is defined as the narrow size distribution of NPs. Therefore a low PDI ensures reproducibility and homogeneity of NPs size and properties [37][53][54].

The third parameter to measure is the zeta potential [mV] which measures the apparent electric charge on NPs surface. The aim is to maintain the zeta potential with a sufficient charge ($>\pm 20$ mV) to ensure good colloidal stability (surface load can also affect interactions with proteins and cells in the body). It is thus necessary to target a zeta potential with a high magnitude without achieving an electrostatic overload. The surface charge is responsible whether the NPs repel each other sufficiently or agglomerate. An electrostatic overcharge, for example, could be the cause of colloidal instability leading to agglomeration or precipitation of the NPs [37][53].

The concentration of NPs [particles/mL] in a certain volume is also interesting for two reasons.

First, for industrial purposes, the goal is to produce NPs at large scales and high concentrations will maximize the amount produced. In addition, it can influence the delivery efficiency by controlling the amount of drug administered. For many drugs, the aim is to maintain a certain concentration of these drugs for example in the blood. An optimal concentration allows the frequency of administration to be reduced [49][55][56].

The proportion of encapsulated drug compared to the total amount of drug introduced is described by encapsulation efficiency [%] [57].This will vary from one drug to another, from one polymer to another as well as by changing the production conditions. The goal is to find the conditions that optimize it and thus maximize it. High encapsulation efficiency is important to maximize the use of the drug and reduce side effects [58].

Finally, the degradation/release is the last physicochemical properties to evaluate. The rate of degradation and the mechanisms leading to it will influence the lifetime of NPs in the body. A controlled release rate as well as a prolonged release is essential and involves a controlled degradation [59].

Other complex elements such as biological biocompatibility with target cells of the organism, surface functionalization, and mechanical properties of NPs can be examined but are more specific to certain applications [33][34][60][61].

1.5 Methods used to produce nanomedicines

One of the great challenges of using NPs in medicine is the transition from the research stage to the clinical stage and even further to scale up the production for industry.The conventional methods confront this limit. Conventional methods also have a high batch-to-batch variability and the NPs obtained have sub-optimal physicochemical properties [62][63]. On the one hand, this section will be devoted to the presentation of the conventional method most commonly used for the production of NPs. On the other hand, it will discuss more recent methods related to the research question of this master's thesis.

1.5.1 Conventional methods

The most common bulk method of production is traditionally the emulsion-solvent evaporation. Other methods exist like bulk mixing using nanoprecipitation, ultrasound or rapid mixing methods. Large scale industrialization and even clinical trials are difficult with these methods as these produce large and heterogeneous NPs. That can lead to toxicity, short circulation time and low tissue penetration. A high PDI leads to the obligation to use extra processes to ensure the quality of

the NPs, which is economically not favourable on a large scale. The large batch-to-bacth variability of these conventional methods are not ideal for continuous production [62].

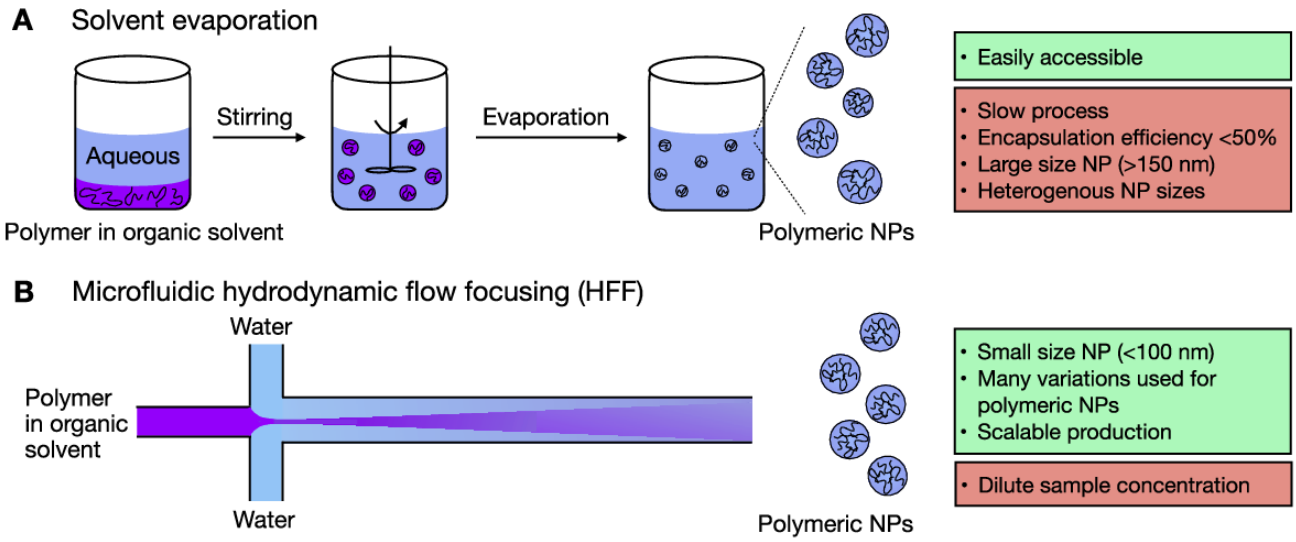

Figure 1.3: **Formulation methods for polymeric NPs** (A) Emulsion-solvant evaporation method (B) Hydrodynamic flow focusing method[62]

The solvent evaporation method is characterized by the formation of two solutions separately, namely an organic solution and an aqueous solution (Figure 1.3 (A)). Depending on the component to be encapsulated, this method will vary slightly. When encapsulating hydrophobic component, the polymer and the drug are solubilized in the organic phase which is added to the water solution in order to form an oil-in-water emulsion (O/W emulsion). Vigorous stirring is required to exerts shear forces that will decompose the organic phase into small droplets in the aqueous phase. For hydrophilic substances the idea remains the same but the emulsion will be different. Given the solubility of the compound in water, NPs will be produced via a water-in-oil emulsion (W/O emulsion). A further step is necessary in which the W/O emulsion is added to an aqueous phase to form a double emulsion (water-in-oil-in-water). In both cases, surfactants can be added to the phases to promote emulsion and evaporation of the organic phase [62][64].

By manipulating the polymer concentration, surfactant concentration, stirring method and choosing a solvent with specific properties, it is possible to have an impact on physicochemical properties (Section 1.4) such as the size [62][65]. The disadvantages of this method are repeated in Figure 1.3 (A).

1.5.2 Production of nanomedicines using microfluidics

Microfluidics technologies appear in NP formulations as an innovative approach to better meet the limits of conventional methods. It allows a better control on the NP productions and their

physicochemical properties. It also allows to produce continuously, rapidly and on a large scale while saving reagents and handling small quantities of volumes, which is economically advantageous. Microfluidics allows to reach smaller NP sizes, better percentage of EE and slower release (Section 1.4) [62].

A microfluidic system allows to manipulate and study fluid on a small scale (at the picoliter to nanoliter scale). This type of system is made up of a set of microscopic components used to control flows. Components can be made of different materials such as polymers, glass, silicon, paper or metal. Each material has its advantages. Microfluidic allows liquid to be transported to a zone whose architecture allows a desired function : mixing, pumping, sorting, bio-chemical environmental control, droplet generation, or nanoprecipitation device. They offer a wide range of avenues for new discoveries, in the field of nanomedicine and others like tissue engineering or biosensing [62][66][67].

One of the most common microfluidic approaches for the formulation of polymeric NPs is hydrodynamic flow focusing (HFF). As shown in Figure 1.3 (B), a central laminary stream of organic solvent containing the polymer is projected between two streams of aqueous solvents. This flow configuration allows to synthetise NPs by nanoprecipitation. In other words, the HFF method allows NPs to be synthesised by self-assembly in sub-microseconds [62].

1.5.3 Hydrodynamic flow focusing variation

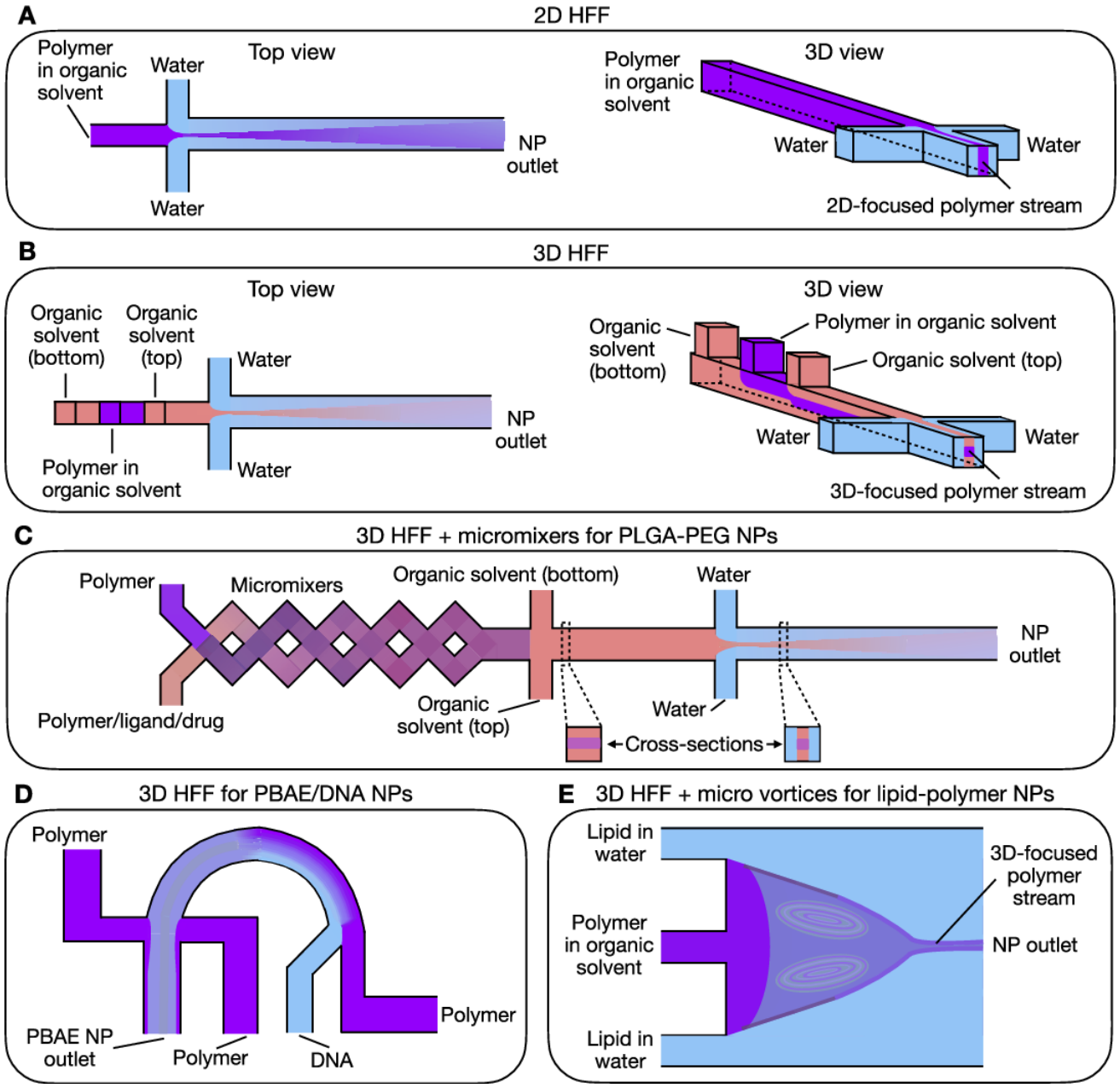

Figure 1.4: **Variations of HFF for polymeric NP production** (A) 2D HFF (B) 3D HFF (C) Micromixers HFF (D) architecture of HFF with 3 inputs (E) microvortices architectures in HFF [62]

Many changes can be made to the architecture of the devices, allowing slight modifications to be made while retaining the original HFF concept. The purpose of these changes is to better adapt the NP formulations to the desired applications. This is the case of the emergence of the 3rd dimension in HFF (Figure 1.4 (B)), to counter polymer aggregation at the interface between the different streams. Indeed, unwanted precipitation is problematic for microfluidic systems because

it can eventually result in a clog of the channel, and even further, in a device failure [62]. Taking the third dimension into account means that the organic stream containing the polymer can be focused between two other organic streams. Other examples include the use of micromixer-type designs (Figure 1.4 (C)), the incorporation of microvortices (Figure 1.4 (E)) or the use of three-entry polymer designs (Figure 1.4 (D)) [62].

All this is reflected in a wide range of chip designs, adapted to different needs. This is also a cause and consequence of the acceleration of research on microfluidics and, more broadly, on nanomedicine. This development has also led to the invention of other structures, such as herringbones (a structure that improves fluid mixing by inducing chaotic and turbulent movements), which can be applied to architectures that enable HFF as well as others [62]. The interest in microfluidics and the importance of chip design can therefore be seen in the wide variety of experiments carried out on the subject. Software (such as AutoCAD® 2015, Autodesk Inc, San Rafael, CA, USA) is being used to optimise chip design [68].

1.5.4 Microfluidic systems using a chip

This point will focus on the presentation of chip-based microfluidic system. Generally, microfluidic systems involving HFF techniques use a chip. However, it is possible to find other microfluidic systems using HFF technology without using a chip [69].

A microfluidic chip corresponds to a network of micro-channels engraved in a material such as glass, silicon or PDMS. The chip and microchannels are connected to tubes, syringe adapters or to nothing (the device rests only on holes in the chip) via inputs and outputs drilled through the chip. After the entry of the desired reagents, the chip performs the mixing or other function, via external active means, such as pumps and/or passive mechanisms as hydrostatic pressure, convection (which allows the focusing of flows), diffusion (molecular scale movement of molecules). Mixing is also controlled by design parameters and specific flow conditions. The precursors combine to form polymeric NPs. By adjusting microchannel operating parameters and flow conditions, it is possible to vary the properties described in section 1.4 [66][70][67][71][72].

1.5.5 Microfluidics system used in this work

The device used in this project is the Dolomite microfluidics system. In this section, the different components and specific properties of the device will be briefly detailed.

1.5.5.1 Configuration

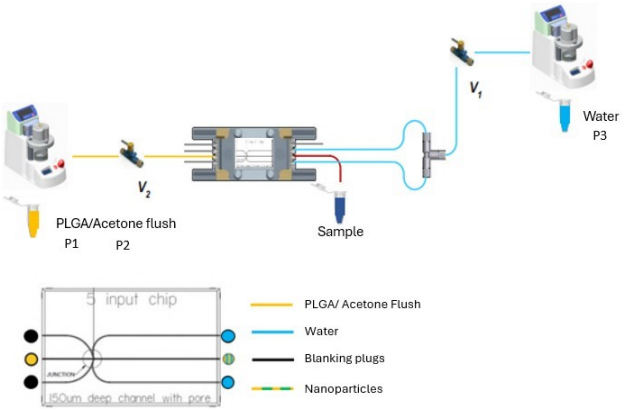

Figure 1.5: Microfluidic device of Dolomite[73]

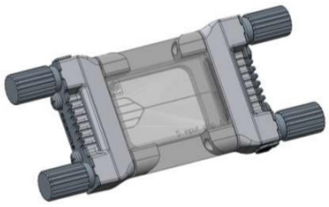

Figure 1.6: H Interface 7-way and two Linear Connectors 7-way[74]

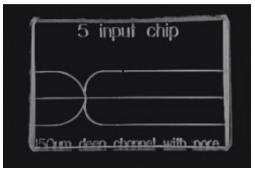

Figure 1.7: 5D Input Chip[73]

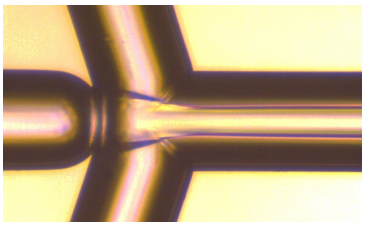

Figure 1.8: Y-junction of the 5D Input Chip

This microfluidic system consists of three pressure pumps (one for PLGA, one for acetone flush, and the last for water) defined by pump 1 (P1), pump 2 (P2), and pump 3 (P3) to move the fluids to the chip (Figure 1.5).

P1 delivers the PLGA in acetone solution (with rapamycin for some experiments) (organic phase) and is completed by a flow rate sensor setting an adjustable value range for the flow between 1-50µL/min. P2 is responsible for the movement of the acetone flushing fluid and work in combination with a 1-50µL/min flow rate sensor. The last pump, P3, and a 30-1000µL/min flow rate sensor, deliver the filtered ultra-pure water (milliQ water) (aqueous phase). The fluids are transported via a network of fluorinated ethylene propylene (FEP) tubing with an inside diameter of

0,25mm and outside diameter of 1,6mm. The assembly also has a T connector. This separates the flow of water into two fluxes of equivalent flows. The length of the two tubes after the connector is identical to ensure this equivalence. Higher in the device, the tubing is interrupted by three 2-way-in-lin-valves, one for each fluid. They allow to quickly open or close the flow streams. The tubing is connected to the chip, (Figure 1.7 and 1.8), via an assembly consisting of an H Interface 7-way and two Linear Connectors 7-way, (Figure 1.6) [73][74].

Dolomite is a pioneer in the field of microfluidic systems guaranteeing EE percentages of up to 99%, a coefficient of variation (standard deviation from the mean particle size) of up to 1%, a particle size distribution described as narrow, a high reproducibility, a high degree of control over NP formulations and a waste percentage of around 0% [75]. The various microfluidic systems from other companies agree with Dolomite on some of the advantages offered by such systems like the high reproducibility of formulations, the large-scale production and the ability to work with small volumes. However, only Dolomite presents its microfluidic system with attractive numbers. Some systems will highlight other qualities, such as the low risk of clogging [76][77][78].

1.5.5.2 5D input chip

The 5 Input chip, (Figure 1.7 and 1.8), is a hydrophilic flow focusing chip in glass designed to form a central laminar flow surrounded by two external laminar streams. In this kind of application, the central stream is connected to one side of the chip and contains the PLGA solution. The two lateral flows come from the other side of the chip and correspond to the aqueous phase [73].

1.5.5.3 Nanoprecipitation by solvent diffusion

The microfluidic system of Dolomite makes possible the formation of NPs via solvent diffusion. This concept is based on a rapid exchange between the PLGA acetone solution and the water thanks to the flow-focusing strategy described in the previous section (section 1.5.5.2). Indeed, the two lateral streams, which are faster than the central stream, will compress the latter and thus cause this rapid exchange and the precipitation of NPs at the interface. This rapid interaction between the two phases, resulting in the formation of an azetopic mixture, creates favorable conditions for the development of NPs. Different nucleation sites will appear along this mixture initiating the precipitation of PLGA. The growth of NPs is obtained by the accumulation of PLGA on neoformed particles and their hardening through the diffusion of the solvent outside the polymer matrix during and after the growth stage [74].

Theoretically, it is possible to influence the final average size of NPs as well as the size distribution by manipulating the mixing timescale (time for the mixture to occur, τ_{mix}). This control on τ_{mix} comes from the fact that by influencing the ratio of the flows between the organic phase (F_a) and

the aqueous phase (F_w) (also called flow rate ratio FRR with $FRR = \frac{F_A}{F_W}$), it is possible to play on the width W of the focused central stream. Indeed, τ_{mix} can be described by $\tau_{mix} \approx \frac{W^2}{4D}$ with D = the diffusivity of the solvent ($D \approx 10^-9[m^2/s]$) and W = the width of the central stream [74].

This is true only in the case where $\tau_{mix} > \tau_{agg}$, τ_{agg} denoting the time it takes for a particle to nucleate, grow and aggregate $\approx 10^1 - 10^2$ ms. In this case, the NPs begin to nucleate before the mixture is even finished. The medium is therefore heterogeneous and this results in the formation of large NPs. By reducing τ_{mix}, it is possible to reduce the size of NPs. In the other case, when $\tau_{mix} < \tau_{agg}$, polymer precipitation, initiated in a homogeneous medium, provides better stabilization to NPs through the hydrophilic portion of the polymer. Size is suspected not longer to be influenced by τ_{mix} and the polymer concentration [74].

Ultimately, all of this hinges on one final condition: $\tau > (\tau_{mix}, \tau_{agg})$, with τ the residence time of the fluid, which will be discussed in the following section. It seems logical that a NP, to be created must reside longer in the channel than the time it takes to create and mature, but also to experiment long enough mixing [74].

This variation of the TFR can be found in studies, which confirms the importance of the TFR [39][40].

1.5.5.4 Influence of total flow rate (TFR)

The calculation of average residence time (τ) is based in particular on knowledge of the total flow rate (TFR) where $TFR = F_a + F_w$, F_a= the flow rate of the organic phase and F_w the flow rate of the aqueous phase. Indeed, τ is obtained from the following calculation: $\tau = A \times L/(F_w + F_a)$ where L= the length of the straight outlet channel and $A = \pi d^2/4$ with d the cross-sectional area of the outlet channel of average diameter. Another variable that can be controlled by the microfluidics provided by Dolomite is the TFR, which influences the physicochemical properties of the NPs [74].

During a call with the Dolomite experts, the company also confirmed that increasing TFR could be a solution to counter excess polymer precipitation in the channels, which can lead to the formation of a clog, which is bad for the devices.

Experiments involving variations of the TFR are available in the literature on the formulation of NPs using microfluidics [39][40].

1.5.5.5 Variables that influence NPs physicochemicals properties

As presented in sections 1.5.5.1 and 1.5.5.1, the microfluidic system allows to adjust the flow rates of the different phases. In other words, this allows two key parameters to be configured, namely the FRR and TFR. The influences of these two variables on NPs have already been discussed in the previous sections 1.5.5.3 and 1.5.5.4. Concerning the Dolomite microfluidic system and the literature about the formulations of NPs via microfluidic, no other experimentally adjustable variable influences the characteristics of the NPs. In this work, the impact of varying these two parameters on NP production will be studied. Dolomite tested and recommended five different ratios with five associated total flows (Table 1.2) [74].

Table 1.2: Flows rate, TFR, FRR[74]

F_w [µL/min]	F_a [µL/min]	$TFR = F_a + F_w$ [µL/min]	$FRR = F_a/F_w$
30	10	40	0,333
40	10	50	0,250
50	10	60	0,200
60	10	70	0,167
70	10	80	0,143

Chapter 2

Objectives

2.1 Overview

Chapter two will discuss the different objectives of this master thesis. First, the broader context will be set out, with a discussion of the broader aim and long-term objective of this master thesis. Secondly, a discussion of the various sub-objectives that have guided this dissertation over the year will follow.

2.2 Objectives

The machine presented in section 1.5.5 arrived in ADDB laboratory of UCLouvain in Woluwe-Saint-Lambert this year. The only information available on this microfluidic system was provided by the Dolomite company. We had to start from scratch because no research of the subject had yet been carried out in the laboratory.

The objective of this master thesis and other work that will be carried out on it, will initially be to improve as much as possible our knowledge about the microfluidic device supplied by Dolomite, with the aim of producing optimised NPs. It is therefore necessary to experiment several variables like different polymers and drugs to be encapsulated, different concentrations of these, and the influence of the TFR and FRR on the physicochemical properties. Depending on the results obtained, adjustments will have to be made and new avenues of discovery investigated. As seen in section 1.5, this machine offers the potential to confront the challenges currently encountered by conventional methods. By understanding and optimising the microfluidic system, it would thus be possible to produce NPs adapted to different medical applications, for a large number of different polymers and drugs and with sufficient production flow. The ultimate goal, in the long term, is to generate a predictive model capable of informing the variables to be set (TFR and FRR) to produce

NPs adjusted according to the desired properties (and therefore suitable for medical applications). This could ideally be used for different polymers and drugs at different concentrations. This is bearing in mind that one of the aims of using a microfluidic system rather than a conventional method is to produce NPs in a more industrial way. Since the objective is to discover as much as possible about the microfluidic system in order to build this predictive model is broad, vague and not defined in terms of quantified results, several sub-objectives have been defined. This allows to assess the progress of this master thesis and one day achieve this goal step by step.

The first sub-objective was simply to get to grips with the machine and succeed in producing NPs without encapsulating drugs under the basic conditions recommended by Dolomite. In other words, to explore the unknown that this machine represented in order to succeed in producing NPs avoiding any problem with the installation (like chip blocking, leaks, ...). The protocols can then be refined on the basis of the conclusions drawn from the experimentation. This enabled the identification of certain limitations and avenues of exploration, which led to the development of the following sub-objectives. It was observed that the production of NPs was subject to precipitation in the chip channels. This is inherent in the production process and can increase the risk of chip clogging.

The second sub-objective was thus, based on the observations made during the initial experiments, to define and test FRR and TFR in order to reduce precipitation. The impact on size and PDI was also measured.

The final sub-objective was to define the TFR and FRR conditions favourable to the production of NPs optimised according to their physicochemical properties for a fixed polymer and this time by encapsulating a drug, rapamycin, in the NPs. Part of this sub-objective has been translated into the statistical study of observed trends and the generation of a model that can be used to return the values of the TFR and FRR that need to be set in order to obtain one or more desired physicochemical properties.

To summarise, the objective of this first master thesis on this new microfluidic system was to find out the unknown about its use.

Chapter 3

Reliable and Comparative Data Acquisition

3.1 Overview

Chapters 3, 4 and 5 will each be dedicated to an experiment. These experiments were selected because they were the most relevant. They were carried out in chronological order.

For this first experience, before designing it, several small anecdotal experiments were carried out in order to understand the operation and sensitivity of the microfluidic system. For example, this allowed to establish the protocols used in this experiment. These are the result of adjustments to previous protocols.

The aim of this first project was therefore to obtain, for the first time, a set of usable, complete and relevant data.

Firstly, the materials used will be discussed. Next, a section will review the methodology followed, presenting : the methodology for preparing the solutions and liquids used in the microfluidic system, the protocol followed for producing the NPs using this system, and the characterisation of the NPs. Finally, the results obtained for each physicochemical property and the observations will be discussed.

3.2 Materials

Resomer RG 752S was purchased from Evonik. Resomer RG 502H was also purchased from Evonik. The properties of these polymers can be found in Table 1.1.

3.3 Methods

3.3.1 PLGA solutions and liquids

A polymer solution was used for the organic phase of the microfluidic device. This solution was obtained for all the experiments in this work from a dilution of a 2% PLGA solution. This choice is justified by the fact that higher concentrations cannot be used in this microfluidic system [74]. The use of higher concentrations would increase the risk of clogging the channels by promoting particle-to-particle aggregation and heterogeneous nucleation on the channel walls. From this solution, various lower concentrations could be obtained by dilution.

The following protocol was recommended by members of the ADDB research laboratory at UCLouvain. The 2% PLGA solution was obtained by adding acetone to the polymer in a glass tube previously rinsed with acetone. Once homogenised by vortexing, the solution was filtered using a 0.22µm membrane filter and a glass syringe. The stock solution was then stored at -20°C, in a closed glass container covered with parafilm.

Resomer RG 752S and Resomer RG 502H 0.5% solutions were used in this experiment. One percent concentrations are often used to start [74][40]. However, the first tests on the microfluidic system, not mentioned in this master thesis, showed that it was very efficient at 0.5% and that at 1%, the chip quickly clogged.

Filtered milliQ water was used for the aqueous phase of the microfluidic system and filtered acetone was used to flush the system.

3.3.2 Production of NPs using Dolomite's microfluidic system

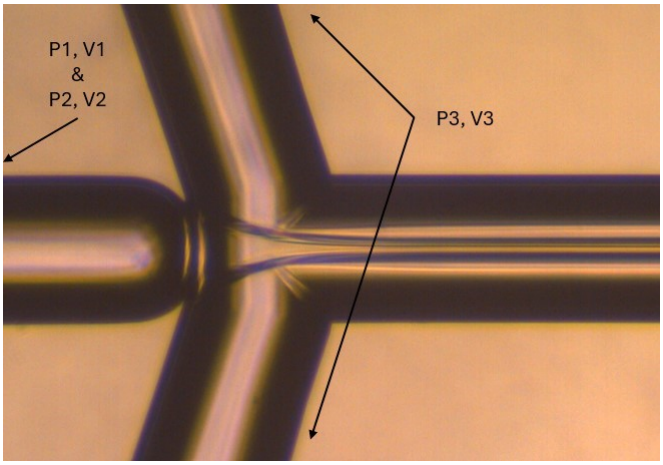

Figure 3.1: Pumps and valves location

Based on the protocol provided by Dolomite for the use of the microfluidic device and the initial tests carried out on it, the following protocol has been designed [74]. As a reminder, Section 1.5.5.1 describes the microfluidic system. At the chip's Y junction, the water supplied by P3 arrived both upstream (top channel) and downstream (bottom channel) of the chip (Figure 3.1). Acetone and PLGA supplied by P2 and P1 respectively were injected from the left of the chip (Figure 3.1).

First, P3 was activated to flow the aqueous phase at an arbitrary pressure sufficient to allow the fluid to flow. The corresponding valve (valve3, V3) was then opened. The pump was then switched to flow mode and the desired target value of flow rate was implemented. Once the first flow was stabilised, the same protocol was applied to the acetone-flush stream (P2) except that instead of switching to flow mode, the pressure was simply adjusted to obtain a flow rate close to the target flow rate for the PLGA.

Once the two flows have been stabilised and the pump pressures adjusted, the pressure at P1 was set close to P2 pressure. Based on the principle that since PLGA was solubilised in acetone, the same solvent used for flushing, the same pressure returns more or less the same flow for both streams. Since small variations in throughput can generate backflow, this avoids any problems by directly obtaining a throughput close to the target throughput. The corresponding valve for P1 (valve 1, V1) was quickly opened and the valve corresponding to P2 (valve 2, V2) was then closed. P1 was then switched to the flow mode to set the target value. The NPs were then collected in an eppendorf. Once collection was complete, the output channel of the microfluidic device was removed from the collection eppendorf.

After that, in this order, V2 was reopened followed by the closure of V1. Immediately after this,

P1 was switched off to prevent the pressure from rising to the limit of the pump (because the valve now prevents reaching the target flow). P3 was then switched back to pressure mode. Gradually, the pressure of P3 was decreased to a low pressure (100mbar) while the pressure of P2 was increased to a higher pressure (2000mbar). V3 was then closed and P3 was switched off. After two minutes, V2 and P2 was also closed and switched off. This enables a smooth transition from the production stage to the flushing stage, minimising persistent dross. This more gradual method optimises the PLGA flush and always keep a flow coming from the central channel preventing the PLGA to go back up into the channels.

The NPs were then evaporated in a hood for approximately three hours. The NPs were then stored in closed eppendorfs covered with parafilm at 4°C for three days before being characterized.

Table 3.1: Flow rates, TFR, FRR[74]

Number	F_w [µL/min]	F_a [µL/min]	$TFR = F_a + F_w$	$FRR = F_a/F_w$
1	30	10	40	0,333
2	40	10	50	0,250
3	50	10	60	0,200
4	60	10	70	0,167
5	70	10	80	0,143

For this experiment, five different FRRs and TFRs were used (Table 3.1). These have been defined thanks to Dolomite's application note [74]. Three replicates of each combination of TFR and FRR were performed for two different polymers. After waiting 30 seconds for the flows to become stable and for the NPs to begin to form, the NPs were harvested for 2 minutes.

3.3.3 Characterisation of NPs

The size, PDI and Zeta potential characterization of the different replicates were performed with Zetasizer Ultra from Malvern. NP concentration in the collected sample was measured using ZetaView® | Nanoparticle Tracking Analysis (NTA) Instrument. The parameters and the protocols used to operate the instruments are given in Appendix A.1.

3.4 Results and discussion

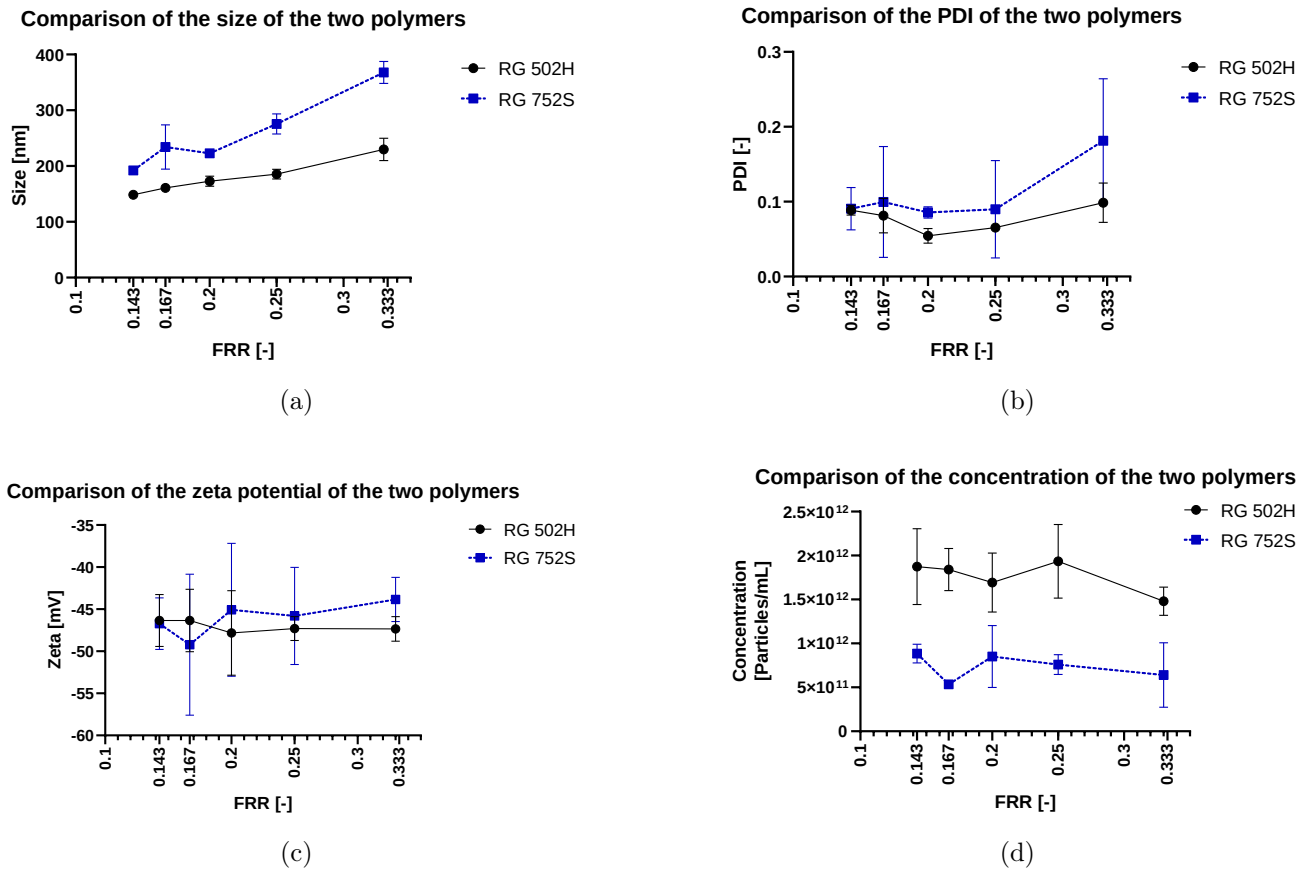

Figure 3.2: **Physicochemical properties of NPs of RG 502H and RG 752S for five FRRs** (a) Size of NPs (b) PDI of NPs (c) Zeta potential of NPs (d) Concentration of NPs

The values obtained are included in the appendix A.2. In this experiment, since the PLGA flow is fixed, the aqueous flow varies, the TFR increases while the FRR is decreasing. Although the two variables vary, the following graphs are expressed as a function of the FRR only, as carried out by Dolomite in their application note. It is therefore important to keep in mind that the TFR decreases along the X axis. For the concentration, only two replicates were measured for NPs made with Resomer RG 752S.

The results obtained are satisfactory. In the literature, for a different microfluidic system using the same or close polymers, the same size order overall is obtained (Figure 3.2(a)) [39]. A difference between the two polymers is observed, less marked in the literature [39]. RG 502H polymer produces smaller NPs.

The PDI values obtained are all acceptable (<0.2, Section 1.4) (Figure 3.2(b)). These seem to be higher for higher FRRs (and lower TFRs). It can also be observed that the standard deviation is high during PDI measurements for RG 752S, which is not the case for RG 502H.

Concerning the zeta potential, the average value between replicates is very stable from one condition to another for RG 502H and a little less stable for the RG 752S (Figure 3.2(c)). However, the standard deviation is very high, especially for the RG 752S. Zeta values are perfectly acceptable (> +/- 20mV, Section 1.4).

There is higher concentration of NPs when they are made of RG 502H rather than RG 752S (Figure 3.2(d)). This concentration is stable from one FRR to another. In the literature, the concentration values that can be found vary widely depending on the polymer, the production method, etc used. Values ranging from 10^8 to 10^{13} particles per mL have been reported [79][80]. The values obtained are therefore consistent. In comparison with the values obtained by a researcher from the research laboratory in ADDB at UCLouvain using the emulsion-evaporation-solvent method for the same polymer, the concentration values obtained were lower by a factor of 10^2.

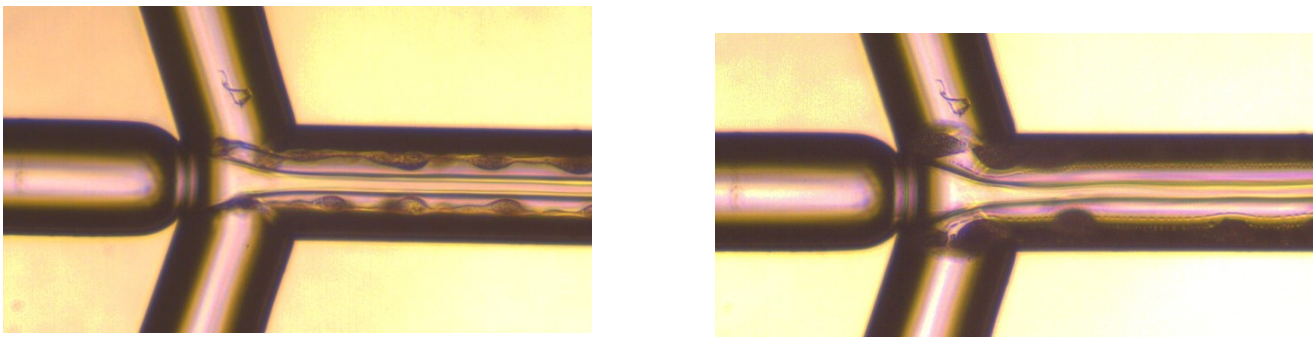

(a) (b)

Figure 3.3: **Precipitation during the production of NPs at a FRR of 0.143 after two minutes** (a) For RG 502H (b) For RG 752S

However, after a few minutes of production, precipitation is observable (Figure 3.3(a) and 3.3(b)). This precipitation has already been observed in the uses prior to this experiment and the longer the production is, the more the precipitation increases. The risk of this high precipitation is that the device could become clogged or even lead to device failure [62]. Precipitation can also modify the flows, disrupting the ideal environment created for NP production. The NP characterisation could consequently be affected.

Chapter 4

Impact of TFR and FRR on polymer precipitation in the chip channel during NPs production

4.1 Overview

As seen previously, the precipitation in the outlet channel of the chip is omnipresent. This precipitation has several risks (Section 3.4) and it is better to minimize it.

The aim of this second experiment was to explore the impact of two variables on precipitation, the TFR and FRR. This exploration will be done through different measurement points within a domain. This domain is defined in X axes by the FRR and in Y axes by the TFR. The NPs (without encapsulated drugs) produced were characterized and a precipitation score was assigned at the end of each production.

The final goal was therefore to create a map allowing to visually see the most favorable areas of the domain according to the different properties studied and the precipitation score. This would make it possible to know, for conditions that have not been experimentally tested, the values of the physicochemical properties and the precipitation score that could possibly be obtained.

Firstly, the materials used will be discussed. Then the methodology followed will be explained. The methodology will be divided into four sections. The protocol for the preparation of the solutions and liquids used in the microfluidic system will be described first. The second will cover the protocol followed for the production of NPs using this system. It will also deal with the development of the experimental plan. A section will then be dedicated to the characterisation of the NPs. The last one will cover the software used to create the map. Finally, the results obtained

will be discussed.

4.2 Materials

Resomer RG 502H was purchased from Evonik. The properties of this polymer can be found in Table 1.1.

4.3 Methods

4.3.1 PLGA solutions and liquids

The methodology for obtaining the solution of RG 502H for the organic phase, the aqueous phase and the acetone to flush the system was identical to the one presented in the section 3.3.1. The concentration of the polymer used in this experiment was also 0.5%.

4.3.2 Production of NPs using Dolomite's microfluidic system

The concentration, the choice of polymer were therefore considered as fixed parameters. Only RG 502H nanoparticles were produced at a concentration of 0.5%.

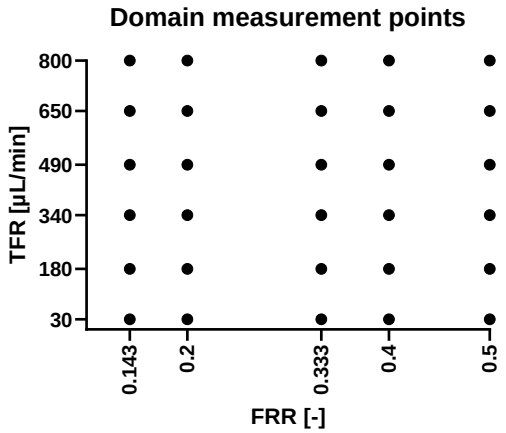

Figure 4.1: Experimental design

For the experimental design, it was estimated that it would be feasible to carry out 30 measurement points, i.e. 30 different NP formulations, while guaranteeing the best possible overview of the domain of study. The range of the area goes from a TFR of 30 to 800µL/min and an FRR of 0.143 to 0.5 (Figure 4.1). A single replicate was carried out for each point.

The experimental design was defined by selecting five FRRs. As the results of the previous experiment were satisfactory, reusing the same ratios was appropriate. As production went well with a ratio of 0.333, without too much precipitation, it was decided to test higher FRRs (0.4 and 0.5). The other three ratios were selected on the basis of the extremes and the central ratio from the previous experiment (0.143, 0.2 and 0.333).

Once the FRRs had been defined, the TFRs were defined accordingly on the basis of the limits of the microfluidic system (Section 1.5.5.1 for sensor limits). The calibration curve for RG 502H 0.5% in acetone, available in appendix B.1 was used to calculate F_a. For a ratio of 0.5, the maximum usable F_a was 278µL/min, i.e. 50µL/min. The corresponding F_w, to comply with the FRR, was 556µL/min. This gives a TFR of 834µL/min. For ease of use, the maximum FFR was approximated to 800µL/min and the minimum to 30µL/min. Six almost equidistant points were then defined between these two values (30, 180, 340, 490, 650, 800µL/min).

The protocol for using the microfluidic system and to store NPs after collection was identical to the one presented in section 3.3.2. Each production was carried out as follows. The NPs were collected 30 seconds after the target flow rates had been set for the two streams. This collection lasted two minutes. To estimate the precipitation level, a score between 1-5 was set with 1 being equivalent to no precipitation and 5 a chip blocking.

4.3.3 Characterisation of NPs

The size and PDI characterization of the different replicates was performed with Zetasizer Ultra from Malvern. The potential zeta was not measured because the experiment focused mainly on the study of precipitation. The parameters and the protocols used to operate the Zetasizer are the same as for the previous experiment and are described in Appendix A.1.

4.3.4 Modelling by R software

The construction of these prediction maps, at this stage of the master thesis, was carried out on the R software. Two interpolation methods were used to exploit the data. The use of two different methods allows a comparison of the results obtained and thus take a step back on the veracity of the results.

First, the inverse distance weight (IDW) is an interpolation method that estimates the value of unknown points relative to the inverse weighted distance of known points. In other words, this method will assign a weight, more or less important, to the points measured according to the inverse of the distance with the point to interpolate. Thus, the value of the furthest experimental points will have only a feeble or no influence [81].

$$\lambda_i = \frac{\frac{1}{h_{0i}^{\theta}}}{\sum \frac{1}{h_{0j}^{\theta}}} \tag{4.1}$$

With
λ_i = Weight of point I
h_{0i} = Distance to point I
h_{0j} = Distance to another point J
θ = Power given to distance with $\theta > 0$

The weight assigned to a point was calculated using the formula 4.1. The Theta parameter is the power given to the distance. This parameter was used in the calculation of the weight granted to a point. This has been optimized [81].

Kriging was the second prediction method used. Before explaining how this method works, here are a few explanations of different terms. The variance corresponds to the dispersion of a variable (properties and precipitation score) around the mean. Semi-variance measures the average dissimilarity between the values of the variable at two different points separated by a certain distance. It therefore varies as a function of distance. The variogram measures the variance of the differences between the values of a variable at two points separated by a certain distance. It tends towards the value of the variance. The semi-variogram measures the semi-variance of the differences between the values of a variable at two points separated by a certain distance. It tends towards the semi-variance, which at a long distance is half the variance [81].

Kriging relies on the construction of linear models that use variogram (or semi-variogram) models to describe the relationship between the semi-variance of a variable and the distance, to predict the other values of the map. To fit an empirical variogram to a theoretical model, variogram models are used, which are mathematical functions [81].

The kriging method is based on the assumption of second-order stationarity of a variogram. This means that the variance is constant and the covariance between the points depends only on the distance between them, not their position. If the second-order stationarity is not validated, the kriging may be biased and incorect, which compromises the quality of the predictions [81].

Since the differences in magnitude between the two axes of the field can generate failures in the prediction modelling, it was important to normalize the data according to the TFR and FRR. Indeed since the TFR has a magnitude much larger than the FRR, the distances along this axis

will have a disproportionate impact on the calculated weights. This ensures the proper functioning of both methods and explains why the axes extend over values from 0 to 1. As a reminder, the FRR therefore actually extends from 0.143 to 0.5 and TFR from 30 to 800µL/min.

4.4 Results and Discussion

The values obtained as well as the precipitation score for each formulation are included in the appendix B.2.

4.4.1 Prediction of physicochemical properties and precipitation score

The parameters chosen for both methods can be found in the appendices B.3. The linear model used for prediction via kriging are in the appendix B.4.

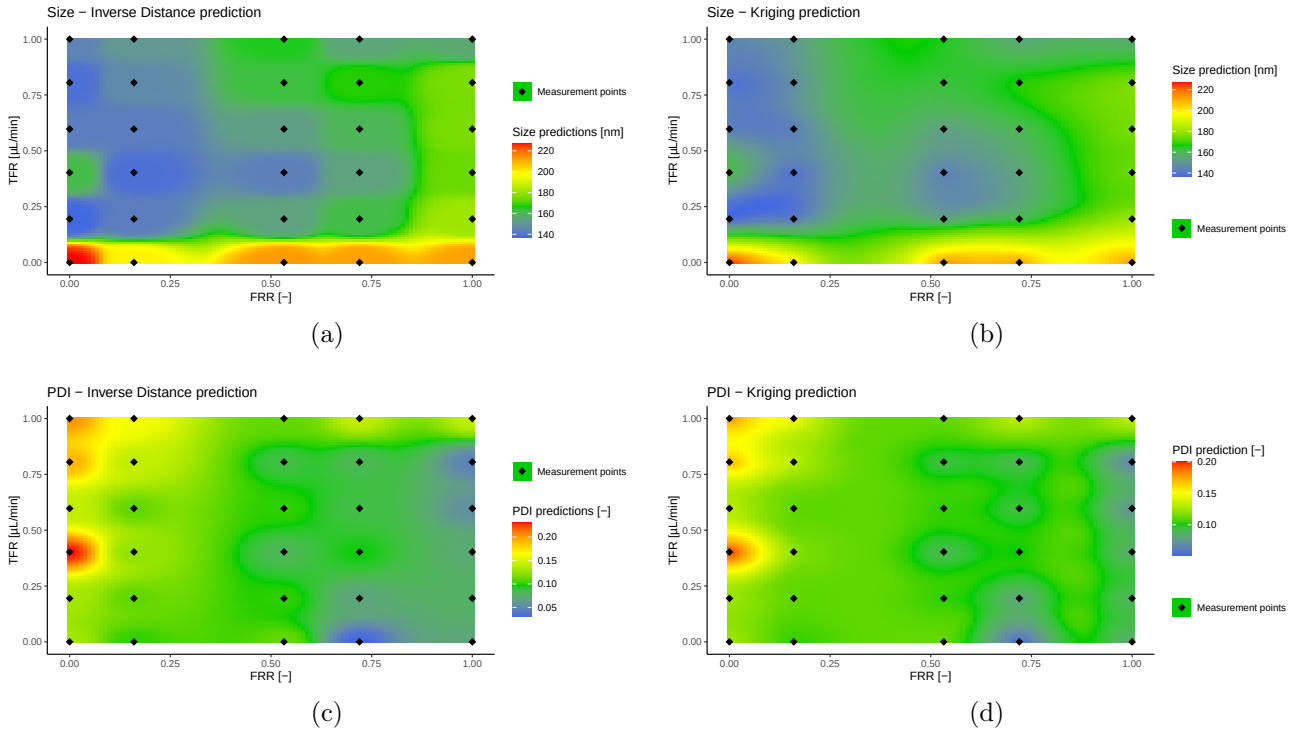

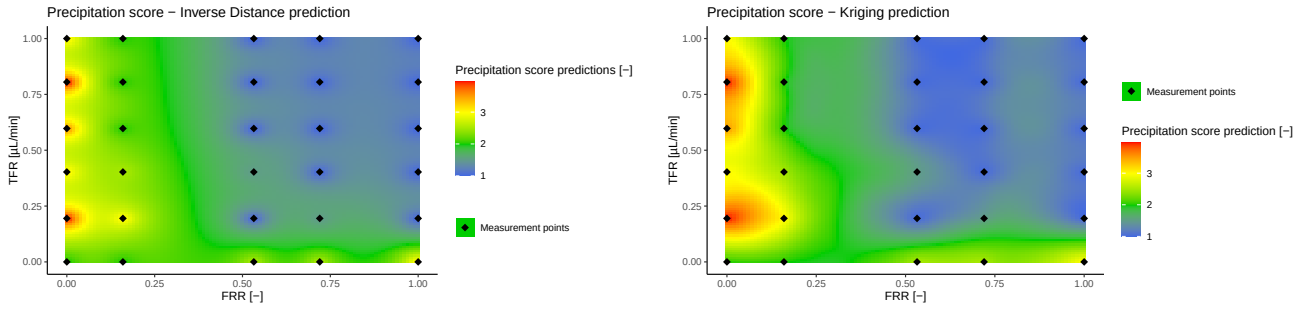

(e) (f)

Figure 4.2: **Predictions of physicochemical properties and precipitation score** (a) Size prediction using the IDW method (b) Size prediction using the Kriging method (c) PDI prediction using the IDW method (d) PDI prediction using the Kriging method (e) Precipitation score prediction using the IDW method (f) Precipitation score prediction using the Kriging method

The linear models used for prediction using the kriging method are not stationary of order 2. This may compromise the quality of prediction using this method.

Overall, the two methods gave us the same information. The differences between the two are a matter of detail. However, the overall information is sufficient to allows conclusions to be drawn. Considering the number of measurement points, the predictions may be of lower confidence for the predicted points furthest from the measurement points. This is particularly visible for Figure B.2(b), where the points furthest from the measurement points tend quickly towards the average. More different measurement points would make it possible to better cover the area and obtain more solid prediction models that enable more accurate predictions. These predictions are too imprecise to predict with certainty the values of the NPs properties obtained for a combination of TFR and FRR not tested experimentally.

A large demarcation is visible at the level of the NPs size between the NPs produced at a low TFR (TFR=30 µL/min, larger NPs) and those produced at other TFR (Figures B.2(b) and 4.2(a)). Similarly, a demarcation is visible between an FRR of 0.143 and the others in terms of precipitation score and PDI values (Figure 4.2(c), 4.2(d), 4.2(e) and 4.2(f)). In fact, the precipitation score and the PDI are higher (4 for precipitation score and > 0.2 for the PDI) for an FRR of 0.143.

4.4.2 Correlation between variables and properties

A possible correlation between the properties studied, the precipitation score and the two variables TFR and FRR were investigated.

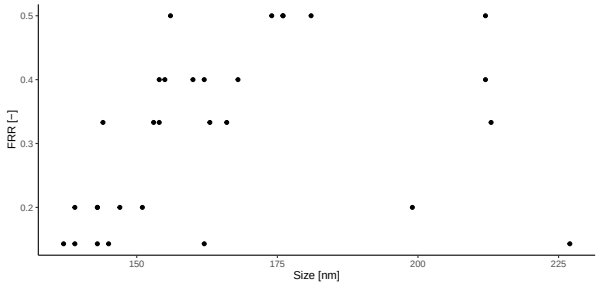
FRR [−]
0.5
0.4
0.3
0.2
150
175
200
225
Size [nm]

(a)

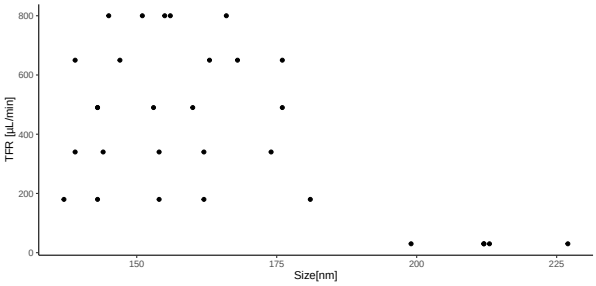
TFR [µL/min]
800
600
400
200
0
150
175
200
225
Size[nm]

(b)

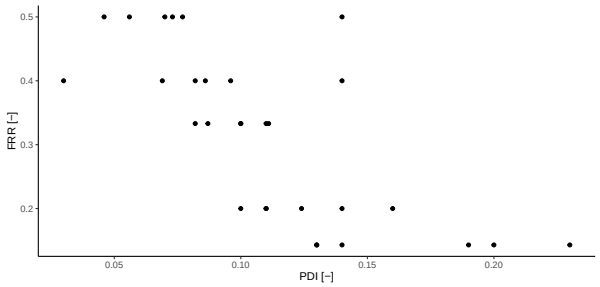
FRR [−]
0.5
0.4
0.3
0.2
0.05
0.10
0.15
0.20
PDI [−]

(c)

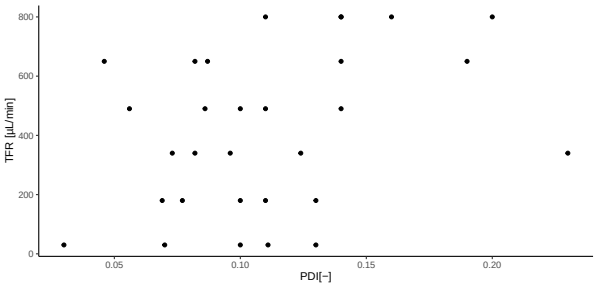
TFR [µL/min]
800
600
400
200
0
0.05
0.10
0.15
0.20
PDI[−]

(d)

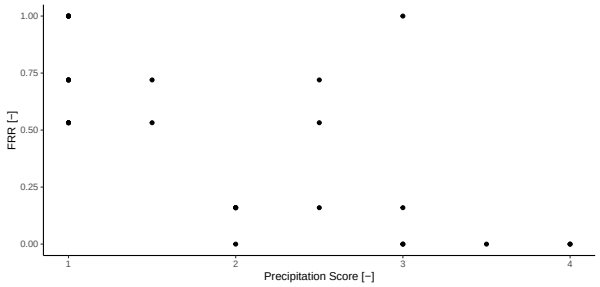
FRR [−]
1.00
0.75
0.50
0.25
0.00
1
2
3
4
Precipitation Score [−]

(e)

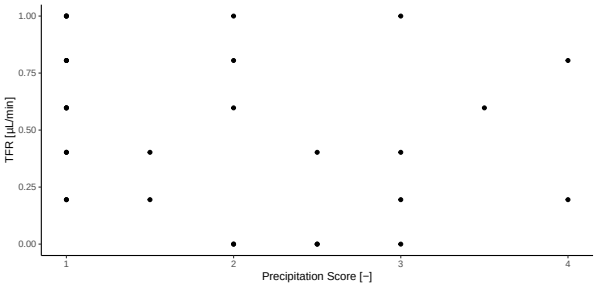
TFR [µL/min]
1.00
0.75
0.50
0.25
0.00
1
2
3
4
Precipitation Score [−]

(f)

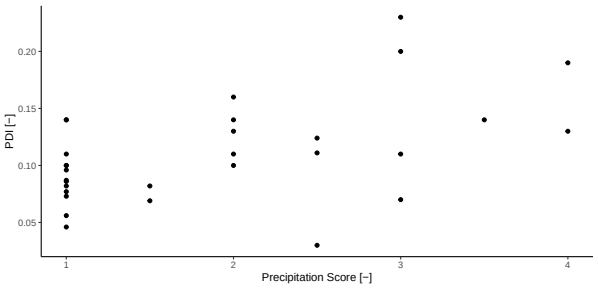
PDI [−]
0.20
0.15
0.10
0.05
1
2
3
4
Precipitation Score [−]

(g)

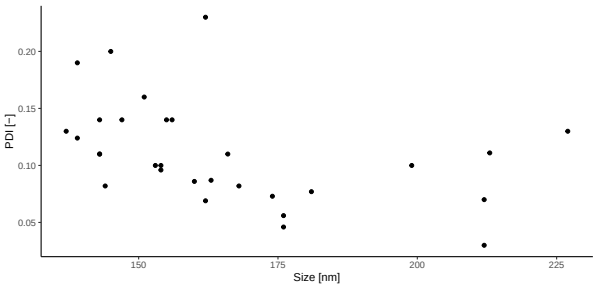
PDI [−]
0.20
0.15
0.10
0.05
150
175
200
225
Size [nm]

(h)

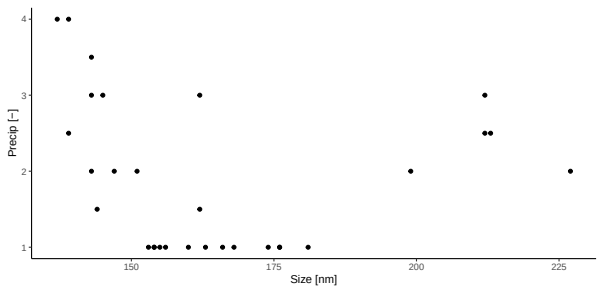

(i)

Figure 4.3: **Correlation between variables and physicochemicals properties/precipitation score** (a) Between size and FRR (b) Between size and TFR (c) Between PDI and FRR (d) Between PDI and TFR (e) Between precipitation score and FRR (f) Between precipitation score and TFR (g) Between precipitation score and PDI (h) Between precipitation score size and PDI (i) Between precipitation score and size

Looking at all the graphs in this section, very little correlation is visible between the variables and the properties. However, Figure 4.3(h) shows a certain correlation between PDI and size and Figure 4.3(c) between FRR and PDI.

Chapter 5

Drug Encapsulation, Statistical Analysis and Modelling

5.1 Overview

During this last experiment, the aim was to go further than the previous ones by encapsulating a drug in NPs. The drug used was rapamycin, presented in Section 1.3.2. Although rapamycin encapsulation had already been carried out in the literature, a few small tests were carried out beforehand to check that rapamycin encapsulation worked with this microfluidic system [52]. This enabled to refine the final protocol. The latter will be discussed in Section 5.3.

More precisely, the goal was to obtain final solid and complete data, until the encapsulation of rapamycin. Similar to the previous experiment, this experiment worked on a certain number of points within a domain of study. This will be detailed in section 5.3. One of the objectives pursued was to assess the influence of two variables, TFR and FFR, thanks to graphical analysis and modelling, on the various physicochemical properties studied. The EE (Section 1.4) was measured for the first time. With these data, another objective was to produce a predictive model capable of returning as a response the TFR and FRR to be set for a target physicochemical properties. Finally, the last objective of this experiment was to detect any influence of rapamycin and dialysis, the process used to separate unencapsulated rapamycin from encapsulated rapamycin, on the physicochemical properties.

Firstly, the materials and methods will be described. As in Chapter 4, the protocol for the preparation of the solutions and liquids used in the microfluidic system will be described first. This is followed by the methodology used for choosing the experimental design and for producing the NPs. The next section will deal with the methodology for the post-treatment of NPs, followed by a section on their characterisation and another on the software used. The results will then be

discussed, first the graphical results, then those of the models. Finally, the information will be summed up in a conclusion.

5.2 Materials

Resomer RG 502H was purchased from Evonik. The properties of this polymer can be found in Table 1.1. Rapamycin and Pluronic F-127 (Section 1.3.2) were purchased respectively from Tokyo Chemical Industry (TCI) and from Sigma-Aldrich. A description of pluronic acid and pluronic F-127 can be found in the Appendix C.1.

5.3 Methods

5.3.1 Solution of PLGA and rapamycin and liquids

In order to correctly isolate the effects of the TFR and FRR, the polymer, the drug and their concentrations used were fixed. Only the TFR and FRR were varied. A solution of PLGA (RG 502H) 0.5%, Rapamycin 0.1% was used for the organic phase. The choice of polymer concentration is justified by previous experiments in which a concentration of 0.5% gave good results. That of rapamycin is based on experiments carried out by one of the laboratory's researchers from the research laboratory in ADDB at UCLouvain.

This solution was obtained by dilution from more concentrated stock solutions of PLGA and rapamycin. The methodology used and the concentration for the PLGA stock solution is presented in section 3.3.1. The rapamycin stock solution had a concentration of 1%. The following protocol was recommended by a member of the ADDB research laboratory. This was obtained by mixing rapamycin with filtered ethanol in an eppendorf. The solution was then vortexed until homogenisation. The stock solution was stored at -20°C covered with parafilm.

5.3.2 Production of NPs using Dolomite's microfluidic system

Table 5.1: Measurement points

Number	TFR	FRR
1	180	0.2
2	180	0.5
3	387	0.3
4	387	0.4
5	593	0.3
6	593	0.4
7	800	0.2
8	800	0.5

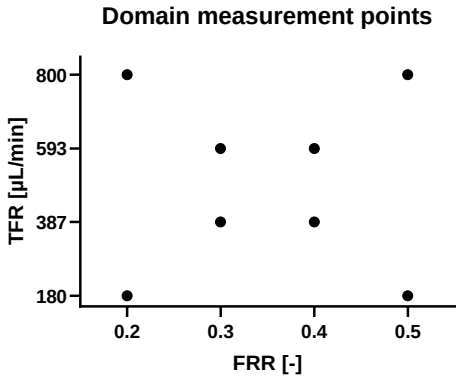

Figure 5.1: Experimental design

The field of study was defined on the basis of the results of previous experience (4.4.1). Since FRR=0.143 and TFR=30 µL/min gave poorer results, the range was redefined from 180 to 800µL/min for TFR values and from 0.2 to 0.5 for FRR. In order to obtain robust results, three replicates per point were carried out. Given the number of replicates, the experimental plan was designed with only eight measurement points (Table 5.1 and Figure 5.1). The idea behind this choice of plan was to progressively increase the TFR by testing two FRRs each time, representing as much of the surface area studied as possible. In Table 5.1, the darker the color, the higher the value.

The experimental design chosen does not allow the effect of TFR or FRR on the various physico-chemical properties to be isolated effectively. For a fixed TFR, the FRR sometimes varies differently from one TFR to another. It is therefore difficult to assess only the effect of the TFR on size for example, since for two different TFRs, the FRRs used are also sometimes different. The value of each property obtained could be influenced as much by one variable as by the other. For example, points 2 and 3 in Table 5.1 differ according to the TFR and the FRR. Other points, such as points 2 and 8, vary only at the TFR level.

In some sub-sections of the results, a number has been associated with each combination of variables so that all measurement points can be graphically represented based on the number, not the FRR. Plotting a property according to the FRR would hide a possible effect of the TFR. The associated numbers are shown in the Table 5.1.

Measuring EE requires a purification step for the NPs once they have been produced. The non-encapsulated rapamycin must be separated from the rapamycin encapsulated inside the NPs in order to be able to measure the encapsulated quantity. Centrifugation or dialysis are two com

monly used methods [82]. These were tested beforehand. It was observed that centrifugation formed a non deformable pellet which distorted the results of NP characterisation. Consequently the method chosen for this experiment was dialysis. A minimum of 1mL of each formulation was required for dialysis. NPs were produced to obtain 1.2 mL. 1mL was dialysed while the remaining 200µL was characterised without being dialysed. The dialysed NPs were then characterised. The aim is to check whether dialysis has an influence on the properties of the NPs. The production volume was calculated on the basis of the TFR [µL/min] where the time of each production was adapted.

The microfluidic device was used in the same way as described in Section 3.3.2. The directly characterised NPs followed the same protocol as presented in Section 3.3.2 except that they were characterised the day after they were produced. The other NPs were dialysed directly according to the protocol described in Section 5.3.3 and were characterised after dialysis.

5.3.3 Dialysis

The protocol used for dialysis was based on the user guide of the dialysis cassette and experiments conducted by one of the laboratory's researchers from the research laboratory in ADDB at UCLouvain [83]. Once the cassette membrane had been hydrated for two minutes, the dialysed sample was added to the cassette. The excess air was removed before plunging the cassette into the dialysis buffer in a hood on a rotating plate. The dialysis buffer was a solution of milliQ water containing 5% pluronic acid. The dialysis buffer was changed after four hours with milliQ water. The rest of the dialysis took place overnight (17h). The sample was then collected using a 1mL syringe with a needle. The cassettes used were Slide-A-Lyzer™ G2 Dialysis Cassette from Thermo Fisher Scientific.

5.3.4 Characterisation of NPs

Size, PDI and Zeta potential were measured for each result before and after dialysis in order to obtain robust data. EE could only be measured after dialysis. Size, PDI and zeta potential were measured with the same instrument as in Section 3.3.3. The parameters used to operate the Zetasizer are the same as for the previous experiments and are described in Appendix A.1.

Rapamycin was quantified by High-Performance Liquid Chromatography-UV (HPLC-UV). The HPLC-UV used is the HPLC SPD-20A from Shimadzu. The methodology for calculating EE, the protocol followed for the HPLC-UV and the parameters that have been set are listed in Appendix C.2.

5.3.5 Modelling by JMP software

JMP PRO 17 is the software that was used to model the data and produce graphs. The use of this software, the theory behind it, presented in section 5.3.5.1, 5.3.5.2 and 5.3.5.3, and the results and discussions obtained were carried out with the help of the plateforme technologique de Support en Méthodologie et Calcul Statistique (SMCS) from UCLouvain [84]. This software is easier to use and better suited to statistical analysis and prediction in chemistry than R. JMP is able to graphically represent all the data. It allows to draw conclusions on the trends of the effects of the two investigated variables (TFR, FRR) [84].

The graphical representation of the data is essential because, when modelling, it has a comparative role with respect to the conclusions made on the basis of valid models. It is also the only source of information when a model is invalid. The various graphs presented in this section allow to discuss the impact of the variables, but also the variability of the data, the quality of the data over the entire study field, the presence of outliers and/or an effect of the replicates [84].

The modelling and graphical analysis was carried out only on NP properties after dialysis. This choice is justified by the fact that it would make this work more cumbersome and confusing by increasing the number of models to be discussed, whereas there is no significant difference between the results obtained before and after dialysis (Section 5.4.1). Moreover, the final characterisation of the NPs is more interesting.

5.3.5.1 Foundations of quadratic modelling

During a study on defined area, the choice of experimental conditions to experiment or not is important. Developing an effective experience plan generates strong models. The modelling of models made with the JMP software is based on a quadratic equation 5.1 [84].

$$y = a + b \times FRR + c \times TFR + d \times FRR \times TFR + e \times FRR^2 + f \times TFR^2 [84] \tag{5.1}$$

The JMP software allows, on the basis of this quadratic model, to quantify the main effects, interactions and quadratic effects of the studied factors. The experimental plan serve as an experimental framework to collect data. The data is then used to adjust the quadratic model [84].

Knowledge of experimental design was developed during this master's thesis, and the experimental design chosen for this experiment was therefore not optimal. The experimental design used, described in section 5.3.2, did not allow to correctly approximate all the terms of the quadratic equation. Indeed, this design did not allow a complete quadratic model to be defined, as it can only define the quadratic effect of one of the two variables. Part of the information, if it is present,

could not be modelled. The quadratic effect of the FRR was studied. Graphically, it was the one most likely to have a quadratic effect (Section 5.4.3). The Appendix C.3 describes two optimal designs commonly used for JMP model production [84].

5.3.5.2 Model diagnosis

In order to validate the application conditions of a model, a diagnosis of the model was carried out. Firstly, the R-squared and adjusted R-squared were evaluated. This value should ideally be maximized and is between 0 and 1. R-squared provides information on the amount of variability explained by the model. A R-squared close to one explains a large portion of the data variance (statistical measure of data variability). The predicted and real values, in the case of a high R-squared, are practically the same and inversely for a low R-squared. The adjusted R-squared is similar to R-squared and allows the comparison of one model with another, which is not allowed by the R-squared. Then, the homogeneity of the variance was checked graphically as well as the normality of residuals using a normal quantile plot. The significance of the model was assessed thanks to an analysis of variance. Modelling also makes it possible to detect a potential lack of fit reflecting a problem in the choice of the model. If one of these conditions was not validated, due to a p-value that is too high for example, the model was considered invalid. It was judged as not correctly explaining the data. The different valid models addressed in the rest of this work have been validated according to this diagnosis [84].

Invalid models are theoretically not usable. The various possibilities offered by the model are thus unusable. However, it is interesting to understand why they are invalid. Understanding the behavior of data is therefore limited to graphical interpretation. This graphic interpretation remains useful to compare the conclusions made statistically and mathematically by the valid models [84].

5.3.5.3 Designing models: variants and adaptations by property

A large number of quadratic models were generated for this work. Some were validated while others were invalidated.

Each physicochemical property studied in this experiment was modelled on the basis of the two variables for NPs with and without rapamycin. For the modelling of encapsulation efficiency, only the case of NPs with rapamycin was studied.

In addition to the two-variable models, models incorporating a third variable were produced for each property in order to investigate a possible effect of replicates (N). The effect of replicates corresponds to all the systemic or random variations that can occur between different replicates of

a measurement point of an experiment. There can be many causes, such as the day effect (when replicates are run on different days), the batch effect (when the material used comes from two different batches), the learning effect (when there is learning between the different replicates run), etc. As the experiment was carried out sequentially over several days, this kind of effect could occur. This could explain that one set of values of a replicate differs from the values of the other replicates generating noise in modelling. Modelling and graphic representation make it possible to identify this effect [84].

The replicates were thus considered as a categorical variable dividing the points into three groups for each case (with and without rapamycin). For these models, the quadratic equation 5.1 should contain an additional term designating the main effect of the replicates. The modelling of this third variable should be treated with caution. Initially, only the modelling of the TFR and FRR was of interest. The variability of the data can sometimes generate noise that prevents the correct effects from being perceived. When this third variable is include in the models, the noise is reduced by modelling it, which can distort the model. For this reason, three-variable models will tend to improve the validation of the conditions applications, such as R-squared, for example, without necessarily providing the right information on the impact of the TFR and FRR [84].

Finally, models excluding points defined as outliers were generated to see the impact and variability brought by them on the different models. This data analysis is interesting because it can help to better highlight the effects of the variables. It is also logical that removing the extremes will reduce the model variability and will therefore increase the validation of the application conditions. The different points were defined as outliers graphically and/or via modelling. Outliers were chosen based on the hypothesis that they may disrupt the model and they don't follow the trends. But nothing certifies that they were outliers. The choice of these outliers and the response of the models generated by these choices must thus be treated with caution. The various points defined as outliers will be described for each property later in this work (Section 5.4.3). In some cases, their exclusion allowed to obtain a valid model [84].

5.4 Results and discussions

Precise data on the physicochemical properties obtained for the various products are given in the Appendix C.4.

The condition TFR =593µL/min and FRR=0.4 with rapamycin has only two replicates when measuring EE and the zeta potential.

5.4.1 Impact of dialysis on physicochemical properties of NPs

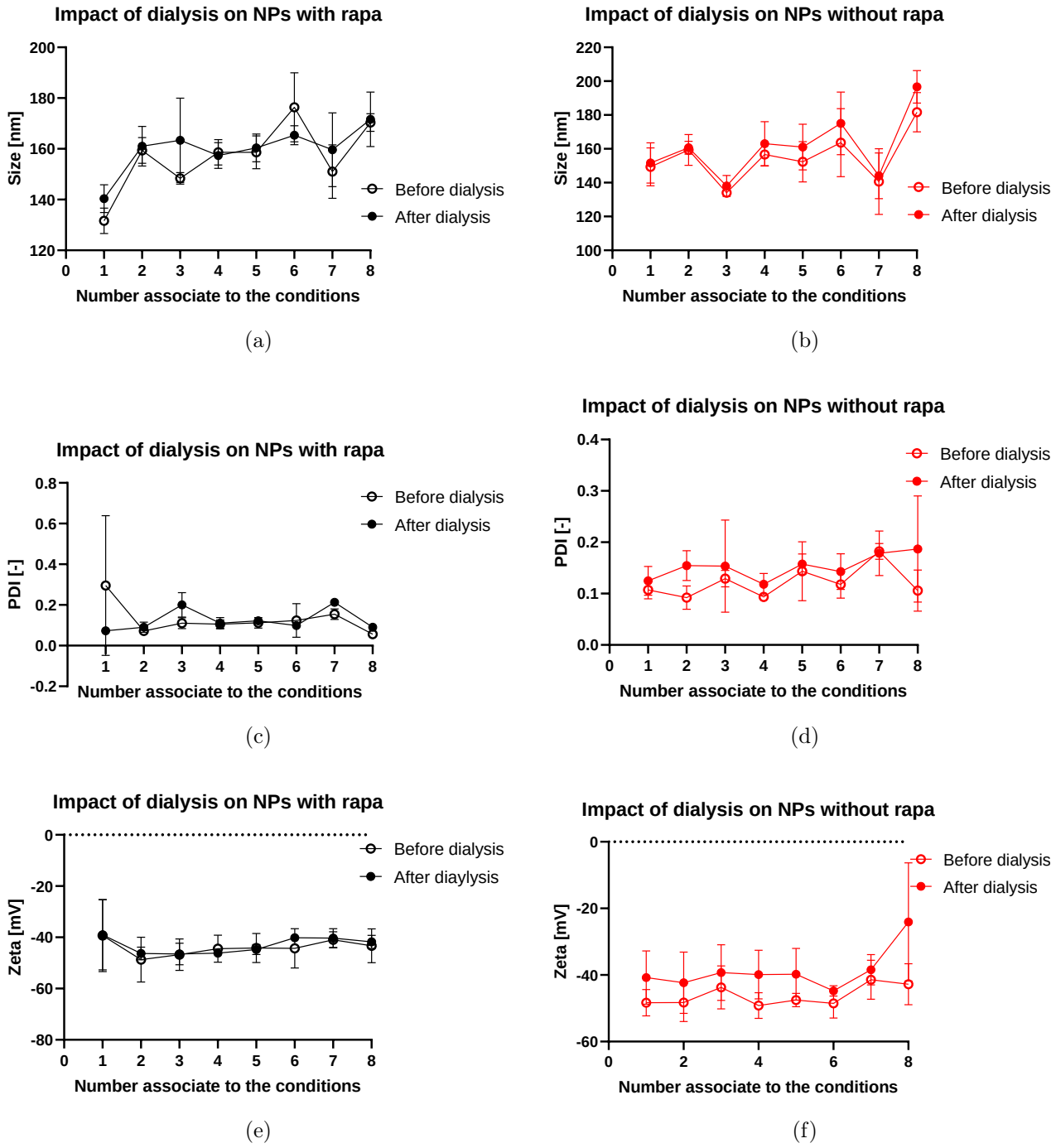

Figure 5.2: **Physicochemicals properties of NPs before and after dialysis with and without rapamycin** (a) Size of NPs with rapamycin (b) Size of NPs without rapamycin (c) PDI of NPs with rapamycin (d) PDI of NPs dialysis without rapamycin (e) Zeta potential of NPs dialysis with rapamycin (f) Zeta potential of NPs without rapamycin

Dialysis only slightly affected the physicochemical properties of the NPs (Figure 5.2). With rapamycin, no overall difference was visible between before and after dialysis (Figure 5.2(a), 5.2(b) and 5.2(c)). The difference observed between before and after are random and not very present. Without rapamycin, a very small difference is visible, with a slight shift towards higher post-dialysis values (Figure 5.2(d), 5.2(e) and 5.2(f)). This applies to all properties. As the difference is very small, it is negligible. For the remainder of this work, only the characterisation after dialysis will therefore be studied. It is also possible to note a large variability in the values obtained.

5.4.2 Comparison with and without rapamycin

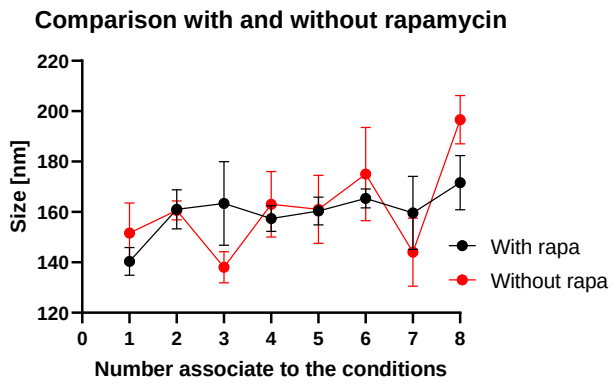

(a)

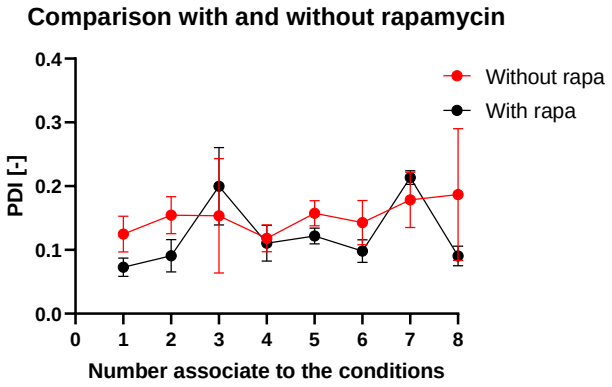

(b)

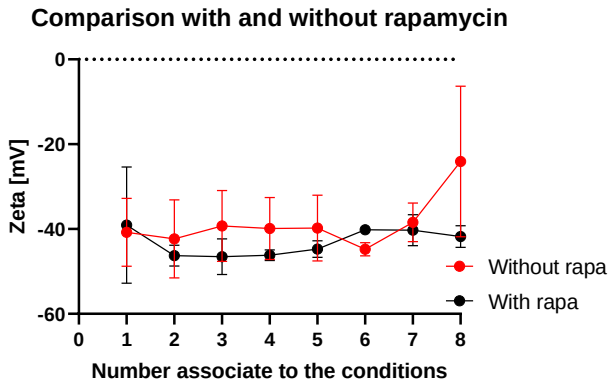

(c)

Figure 5.3: **Physicochemicals properties of NPs after dialysis with and without rapamycin** (a) Size (b) PDI (c) Zeta

The graphs showing the comparison before dialysis can be found in the appendix C.5.

The order of magnitude of the difference between NPs with and without rapamycin is not major and is thus negligible (Figure 5.3). No trend can be seen for NPs with rapamycin compared with

NPs without rapamycin and vice versa. The standard deviations of the different conditions are often large. This shows that the values obtained for the different properties, with and without rapamycin, are fairly variable and the same ranges of values can be obtained in both conditions. Rapamycin has therefore no influence on NP physicochemical properties.

5.4.3 Graphical interpretation of the data on JMP software

The three replicates were defined by different coloured dots in the following graphs and the points defined by a star represent the measurement points considered as outliers. These latter will be discussed again in section 5.3.5.3 on modelling and have undergone a specific treatment. A smoothing line is also visible in blue for each FRR class, showing the trends in TFRs.

5.4.3.1 Size of NPs with rapamycin

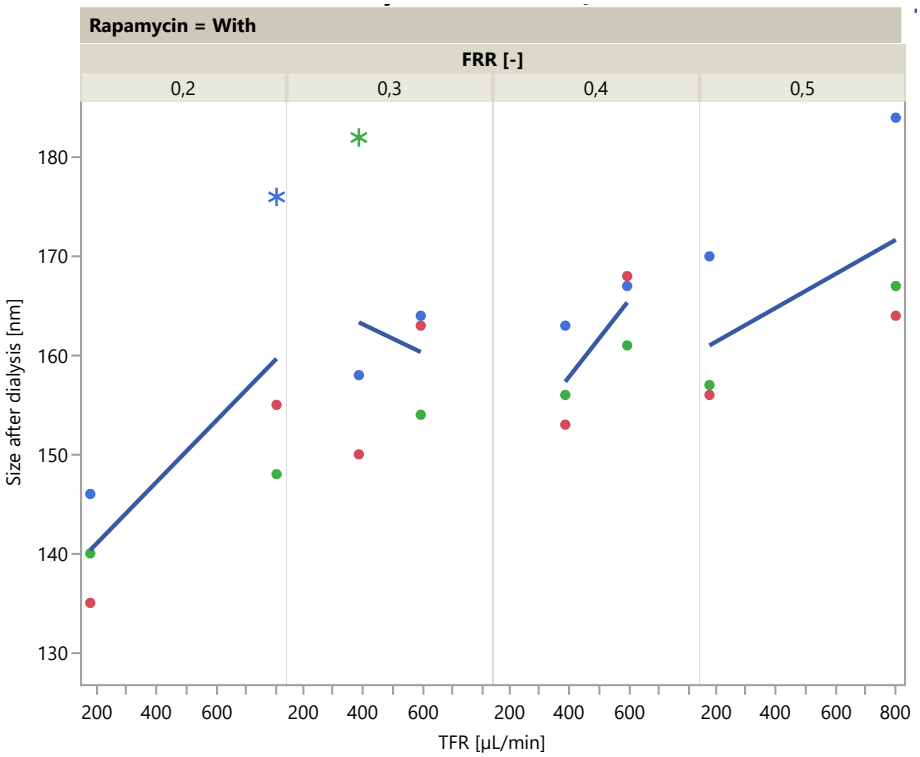

Figure 5.4: Size [nm] after dialysis for NPs with rapamycin for each FRR tested based on TFR

The FRR has an impact on the size of the NPs (Figure 5.4). By decreasing it, the NP size decreases accordingly. This can be seen through the overall trend of points data to increase with ratios across the graph. Then, within each ratio class, except when the FRR is 0.3, it is possible to identify that increased TFR tends to give larger NPs. This is represented in particular by the slope of the trend lines for each FRR. The change in slope for an FRR of 0.3 compared to others can be explained by

the presence of an outlier. In this case, the trend line is not particularly representative. Another outlier was also defined. Both were defined based on a larger measured size than the overall trend of the measurement points. The variability of the measurement points within each group of points representing the same TFR and FRR conditions is not negligible. However, this variability is fairly consistent from one group to another. This homogeneity implies a certain homogeneity of variance and a degree of reliability in the measurements. It enables them to be compared from one measurement point to another. This also reinforces the idea that the different replicates were not affected differently by the experimental conditions. Indeed, none replicate effect can be identified.

5.4.3.2 Size of NPs without rapamycin

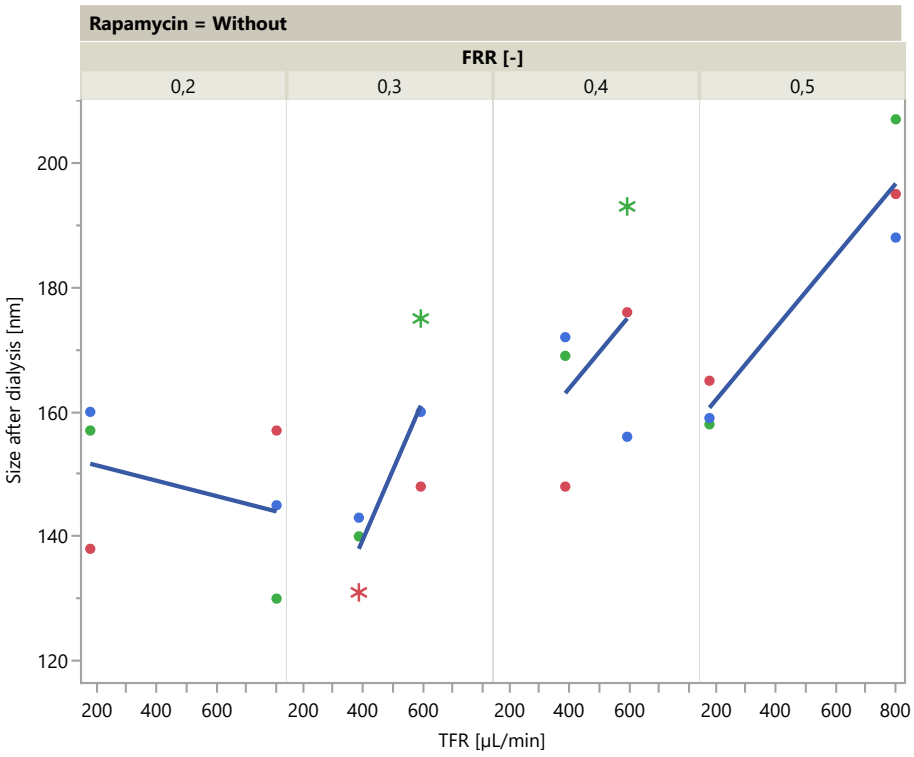

Figure 5.5: Size [nm] after dialysis for NPs without rapamycin for each FRR tested based on TFR

The influence of FRR and TFR on size of NPs without rapamycin is the same as those with rapamycin. That confirms the conclusions reached in the section 5.4.2. In the case without rapamycin, it is the class with an FRR equal to 0.2 rather than 0.3, as in the case with rapamycin, that indicated a different influence of the TFR compared to other FRR classes. It could be that the influence of the TFR diminishes and reverses at very low ratios. The outliers are much less significant and their designation as outliers is debatable. In fact, they are not abnormally large or small. These outliers have been defined for modelling (achieved in a subsequent section (Section 5.4.5.1)). The aim is to see what impact it would have to remove three of the most extreme

points in size modelling. The choice of these three outliers was supported by the fact that, when modelling, these three points are the ones that deviate furthest from the observed value when predicted (Appendix C.6.1). The variability between the replicates is quite consequent although less so than in the case with rapamycin. No effect of the replicates is visible graphically. The same conclusions on variability and on the effect of replicates can be drawn as for the case with rapamycin.

5.4.3.3 PDI of NPs with rapamycin

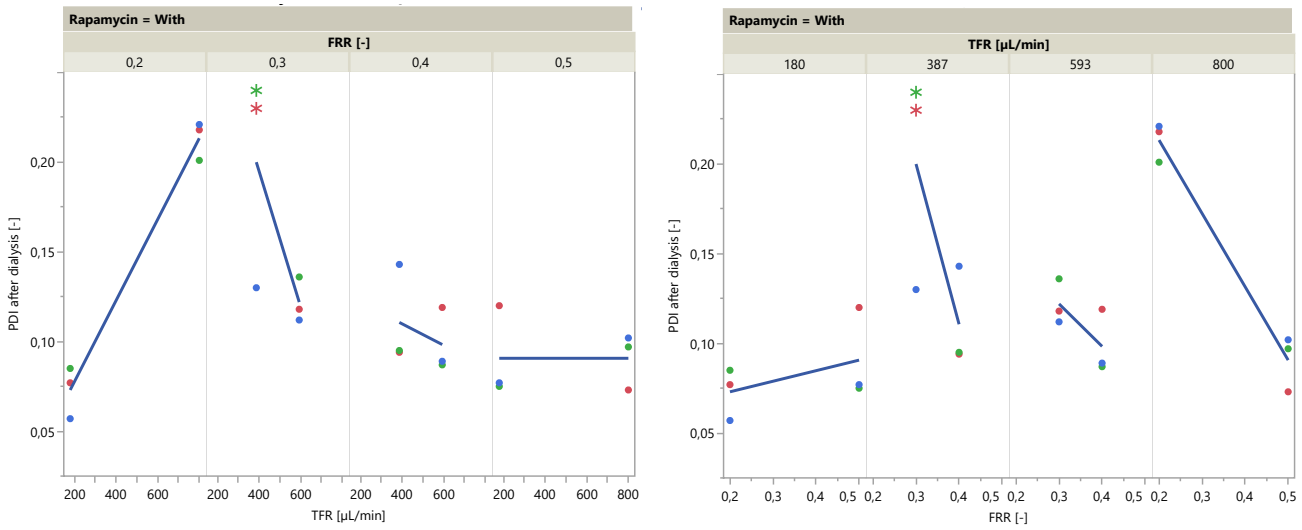

(a) (b)

Figure 5.6: **PDI after dialysis for NPs with rapamycin based on TFR and FRR** (a) for each FRR tested based on TFR (b) for each TFR tested based on FRR

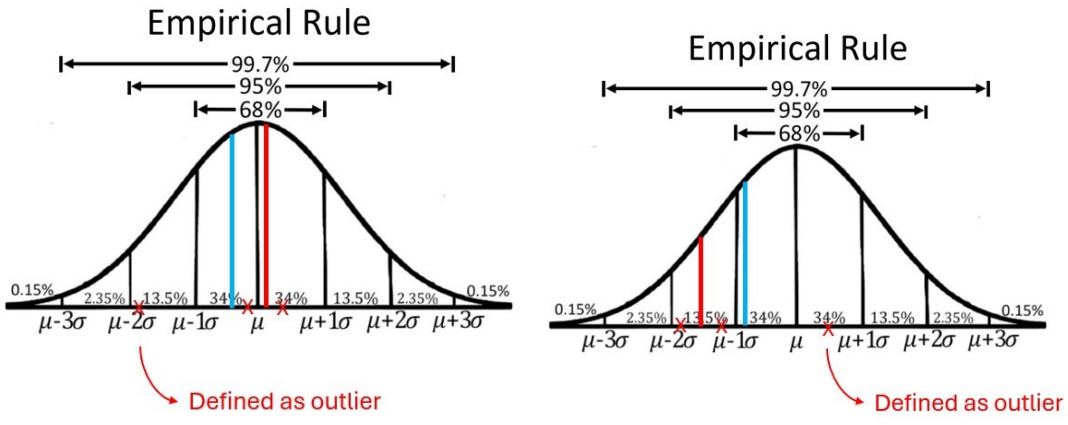

(a) (b)

Figure 5.7: **Explanation about the empirical rule** (a) Well defined outliers (b) Outliers not well defined [85]

The effect of TFR on PDI is highly variable (Figure 5.6(a)). It is different for each FRR. This effect seems to be very important for a ratio of 0.2, with a sharp increase in PDI for a high TFR before reversing abruptly for a ratio of 0.3. The TFR then gradually loses its influence on the PDI as the FRR increases to no longer have influence for a FRR of 0.5. Although this graph gives the impression that the FRR is a categorical variable, it should not be forgotten that it is in fact a continuous variable, just like the TFR. So trends are unlikely to change suddenly. However, it is possible to imagine that the influence of the TFR on the PDI would reach a maximum between a ratio of 0.2 and 0.3. It is certain that the influence of the TFR varies according to the FRR set. Figure 5.6(b), which inverts the TFR and FRR axes, better illustrates the effect of the ratio which, apart from a TFR of 180µL/min, decreases the PDI as it increases. No effect of replicates is visible graphically.

The use of triplicates in the design of experiments is also being questioned. Diagrams will be used to illustrate this section (Figure 5.7(a), 5.7(b)). The values shown in these diagrams are not correct, but serve to illustrate the point. The blue line represents the mean without exclusion of outliers and the red line with exclusion of outliers.

Statistically, the measurement made for a point under certain conditions (example PDI measurement for a FRR=0.3 and a TFR=387) has 68% chance of ending up in the zone defined by the real average value added or decreased from the real standard deviation of this point under these conditions [86]. Using three outliers is not ideal because if one of the replicates falls outside this zone (32% chance for each measurement point), it will seriously distort the calculation and location of the average from the real average (Figure 5.7(a)). In addition, it is difficult to determine whether this is the point that differs from the other two or the other two that best represent the average (Figure 5.7(a) and 5.7(b)). Using five replicates, for example, has a better probability of estimating the real location of this average and the outliers. This calls into question the outliers defined and the average obtained. These values should be treated with caution [84].

For a FRR of 0.2, the low variability between the different replicate measurements refers to a small standard deviation. This small standard deviation supporting the idea that the average estimated by the 3 points is close to the real average. This is consistent with the idea that the estimated TFR impact is correct. For a FRR equal to 0.3, when the TFR is 387, it is possible to observe a great variability between the points. This leads to greater uncertainty about the accuracy of the average value.

The homogeneity of the variability of the replicates between the different points makes it possible to suspect the presence of of one or more outliers. No trend of the FRR, as with the analysis of the size of NPs with rapamycin (Figure 5.4) makes it possible to suspect one point more than another. The two outliers were defined based on a graph of the predicted values compared with the values

observed when producing models (Section on models: Section 5.4.5.2, Appendix with the model: Appendix C.6.2). Other outliers were tested, but the model excluding these outliers gave the best result.

5.4.3.4 PDI of NPs without rapamycin

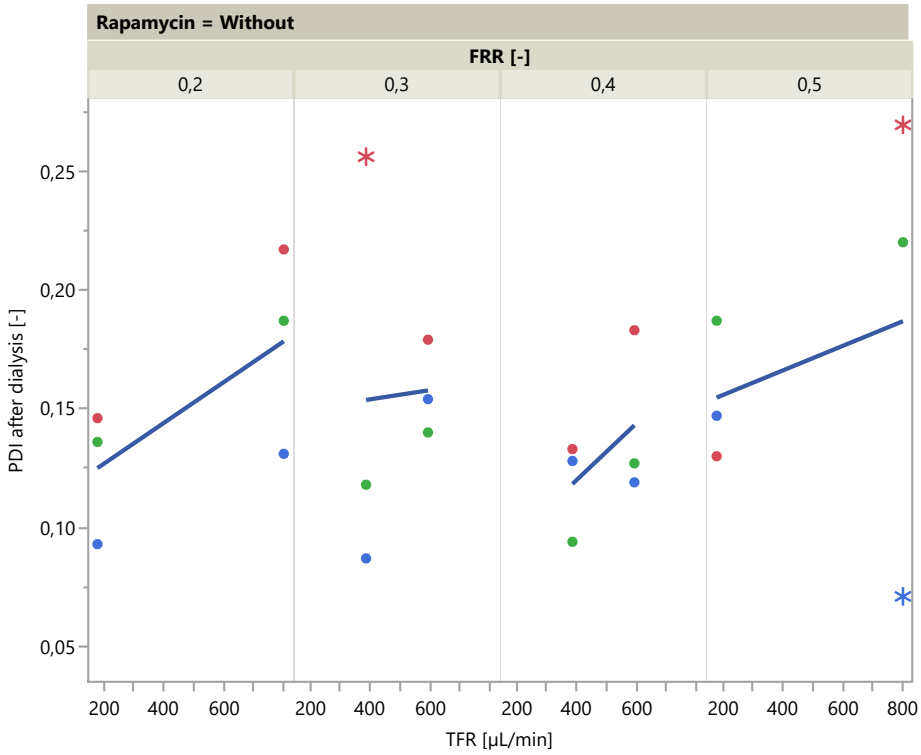

Figure 5.8: PDI after dialysis for NPs without rapamycin for each FRR tested based on TFR

The influence of TFR on PDI in the case without rapamycin is rather clear (Figure 5.8). It is preferable to decrease the TFR to obtain lower PDI values. The FRR seems to have no specific influence on the PDI. A high degree of variability between the different points generates a lot of noise, which could prevent information from being correctly observed. This variability is particularly high for a FRR of 0.5 and a TFR of 800µL/min which is a measurement point at the boundary of the domain and also for a FRR of 0.3 and a TFR of 387µL/min. Three outliers were defined, presenting a more extreme value in groups of replicates with high variability. This choice is comforted during the modelling (Section 5.4.5.2), allowing to improve the models.

It is possible to observe a slight effect of replicates, with higher PDI values for red replicates and lower for blue replicates. As explained in Section 5.3.5.3, several natural explanations can explain the presence of an effect of replicates. An adjustment could be made to take account this effect to better approximate the data. As the protocol was the same for all the replicates, this effect of

replicates is probably due to sequential work. It is not possible to determine which values are the reference values. To do this properly, other comparative data to serve as reference data and to highlight this effect and the adjustment to be made would be needed.

5.4.3.5 Zeta potential of NPs with rapamycin

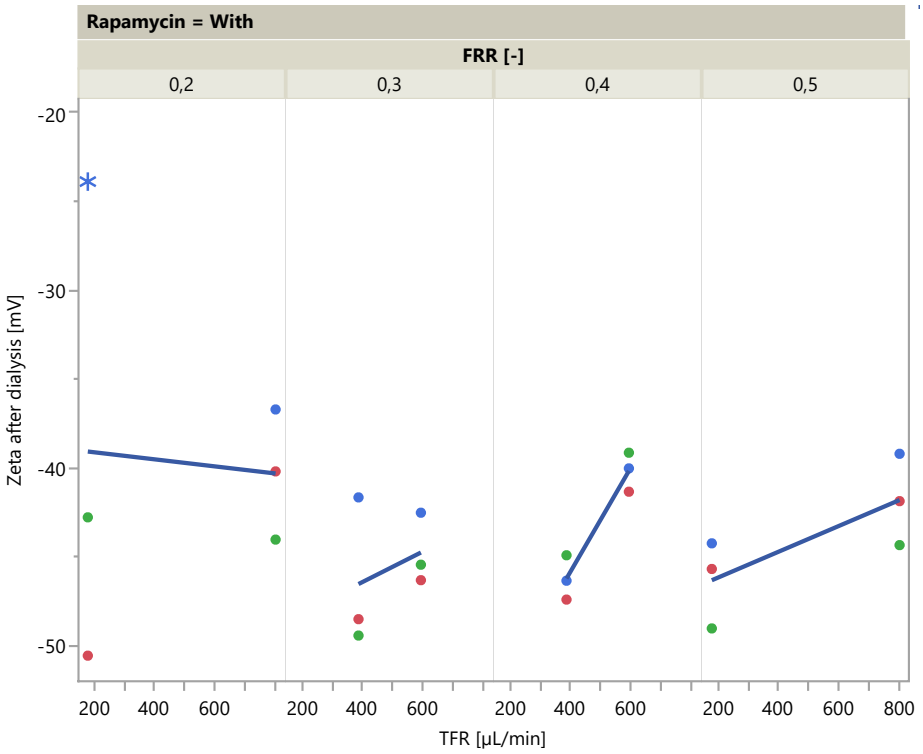

Figure 5.9: Zeta [mV] after dialysis for NPs with rapamycin for each FRR tested based on TFR

The FRR has no impact on the zeta potential (Figure 5.9). The TFR increases the zeta potential by a few millivolts by decreasing. This latter trend would be reinforced if the outliers were removed. The variability of the replicates seems more acceptable or even very satisfying for a ratio of 0.4. The variability for a TFR of 180µL/min and a FRR of 0.2, conditions with the outliers, is high. The others are generally weaker, although two of the three conditions still show significant variability. This questions the possibility that the limits are exceeded for such conditions and that a domain restriction would allow better control over variability. An effect of the replicates could possibly be detected with the points in blue having higher values. However, in the case of an FRR of 0.4 or 0.5, the values of the different replicates are relatively similar. A possible adjustment could be made if the effect of the replicates is confirmed.

5.4.3.6 Zeta potential of NPs without rapamycin

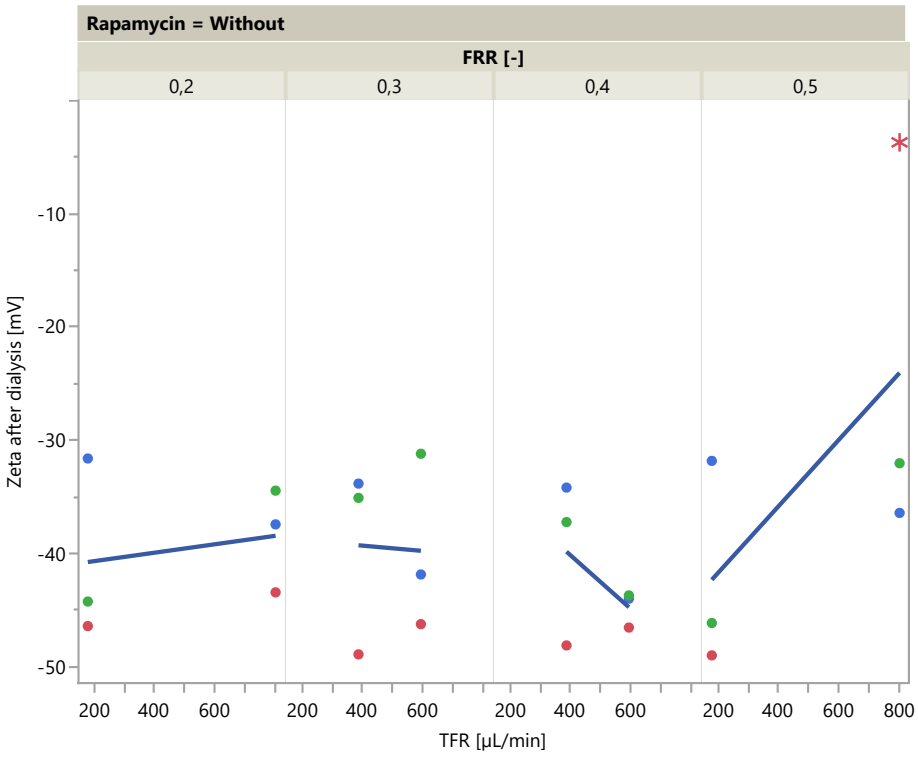

Figure 5.10: Zeta [mV] after dialysis for NPs without rapamycin for each FRR tested based on TFR

An effect of the replicates is clearly visible in the study of NPs without rapamycin (Figure 5.10). With the exception of one measurement point, the replicates in red are shifted downwards. No impact of the FRR is visible. The effect of the TFR is difficult to perceive and variable from one FRR class to another. At low ratios, the TFR seems to have no effect, but for higher TFRs, the impact seems to be more significant and variable. Modelling can be particularly useful for assessing the impact of the TFR and FRR in this case. The variability between replicates was fairly uniform, except for the replicates where an outlier was identified. This is worth around 15 mV and more, which is not negligible. The consequences of good and poor variability have already been discussed in Section 5.4.3.1.

5.4.3.7 EE of NPs

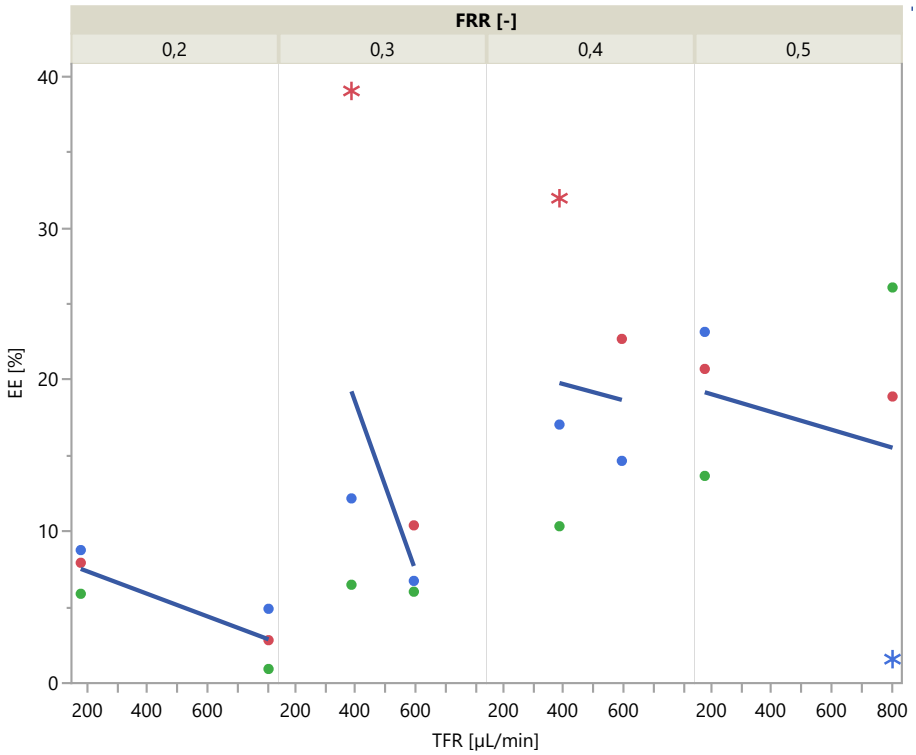

Figure 5.11: EE [%] after dialysis for NPs without rapamycin for each FRR tested based on TFR

Increasing the FRR increases EE (Figure 5.11). The TFR also influences the EE, to a lesser extent, by reducing it as it increases. Three outliers were identified, however only two were necessary during the modelling (without outliers with a TFR of 387µL/min and FRR of 0.4) (Section 5.4.5.4). An effect of the replicates could be visible with measurement points in green often inferior to the others. This effect, if it exists, is very slight

5.4.4 Outliers common to several properties

Each measurement point defined as an outlier for one property was compared with those defined for another property in order to identify any similarities between the different outliers defined for each property.

In the case with rapamycin, two measurement points were defined as outliers for two different properties. One of the replicates, with a TFR of 387µL/min and a ratio of 0.3, is an outlier for PDI and EE. Another replicate under the same conditions is an outlier for size and PDI. Without rapamycin, one of the replicates for a TFR of 800µL/min and an FRR of 0.5 is an outlier for both

the PDI and the zeta potential. All the other outliers are different from one property to another.

This leads to suspect that these three measurement points may be unreliable. The assumption that these are not good productions and therefore they distort the results can be made. To a greater extent, this combination of variables could tend to generate outliers especially for the condition TFR=387µL/min and FRR=0.3 which generated two outliers. However, certain factors mitigate against these hypotheses. First, the values for the other properties are correct. Secondly, these outliers only concern certain replicates of the same condition, and not all three replicates. Finally, outliers have been defined as such but nothing certifies that they are outliers.

5.4.5 Modelling: Effect tests

Effect Tests

Source	Nparm	DF	Sum of Squares	F Ratio	Prob > F
FRR [-]	1	1	3763,2000	22,2957	0,0002*
TFR [µL/min]	1	1	1078,6635	6,3907	0,0217*
FRR [-]*TFR [µL/min]	1	1	1335,0236	7,9096	0,0120*
FRR [-]*FRR [-]	1	1	96,0000	0,5688	0,4611
N	2	2	324,2500	0,9605	0,4025

Figure 5.12: Effect tests, modelling of size after dialysis without rapamycin with extreme points

Once the conditions for applying a model have been validated, the model can be used. Thanks to effect tests provided in the model results, the presence or absence of an effect of the variables on the property studied can be identified (Figure 5.12). Effect tests specifies whether the effect of the variable is a main effect, a quadratic effect or whether it is due to the interaction between the two variables. As explained in Section 5.3.5.1, the design of the experiment allows us to assess the possible quadratic effect of only one of the two variables [84].

The effect of the variable is significant for a p-value of less than 5%. To give an example, the effect tests obtained when modelling the size without rapamycin with outliers, revealed that the FRR and the TFR have a main effect as well as an effect through their interaction (Figure 5.12) [84].

Table 5.2: Effect significance and model validity for NPs with rapamycin

With Rapamycin									
	Size		PDI		Zeta			EE	
Outliers	With	Without	With	Without	With	Without	Without + effect of replicates	With	Without
FRR	S	S	S	S	NS	NS	NS	S	S
TFR	S	S	S	S	NS	S	S	NS	NS
FRR*TFR	NS	NS	S	S	NS	NS	NS	NS	NS
FRR^2	NS	S	NS	NS	NS	NS	NS	NS	NS
replicate effect	NS	S	NS	NS	S	NS	NS	NS	NS
Validity	Yes	Yes	No	Yes	No	No	Yes	No	Yes

Table 5.3: Effect significance and model validity for NPs without rapamycin

Without Rapamycin							
	Size		PDI		Zeta		
Outliers	With	Without	With	Without	With	Without	Without + replicate effect
FRR	S	S	NS	NS	NS	NS	NS
TFR	S	S	NS	S	NS	NS	NS
FRR*TFR	S	S	NS	NS	NS	NS	NS
FRR^2	NS	NS	NS	S	NS	NS	NS
Replicates	NS	NS	S	NS	NS	S	S
Validity	Yes	Yes	No	Yes	No	No	Yes

All the responses from the effect tests on the variables (orange row) as well as the precision of whether or not the conditions of application of the model are validated (blue row) for the different models are shown in Table 5.2 and Table 5.3. Table 5.2 is for the NPs with rapamycin and Table 5.3 is for the NPs without rapamycin. These tables show the significance (S) or the non-significance (NS) of the different effects of the variables for each physicochemical property studied. For each property, models with and without outliers were also produced to study the impact of outliers on the significance of the variables and the validity of the models (yellow row). The outliers used are those defined by stars in each graph analysed in Section 5.4.3. A row has also been dedicated to the significance of the replicate effect (purple row).

The models incorporating this third variable did not change the validation or the significance of the two others variable except for the zeta case. Indeed, without modelling the effect of replicates, the models produced were invalid. Therefore only zeta require an extra column for the model with the replicate effects. The significance of the effects of the other variables is thus identical with or without modelling the effect of the replicates.

The information in Tables 5.2 and 5.3 will be discussed in the following subsections dedicated to each property. Given the number of models produced, only the most interesting will be discussed.

5.4.5.1 Size modelling

The basic modelling, without removing the outliers and without adding the third variable for the size, was already satisfactory and valid. The integration of this third variable into the modelling did not show much added value. Only the modelling with all the points as well as without the outliers will be discussed. Their respective models and their validation parameters are included in the Appendix C.6.1.

Basic model

The application conditions for this model have been validated.

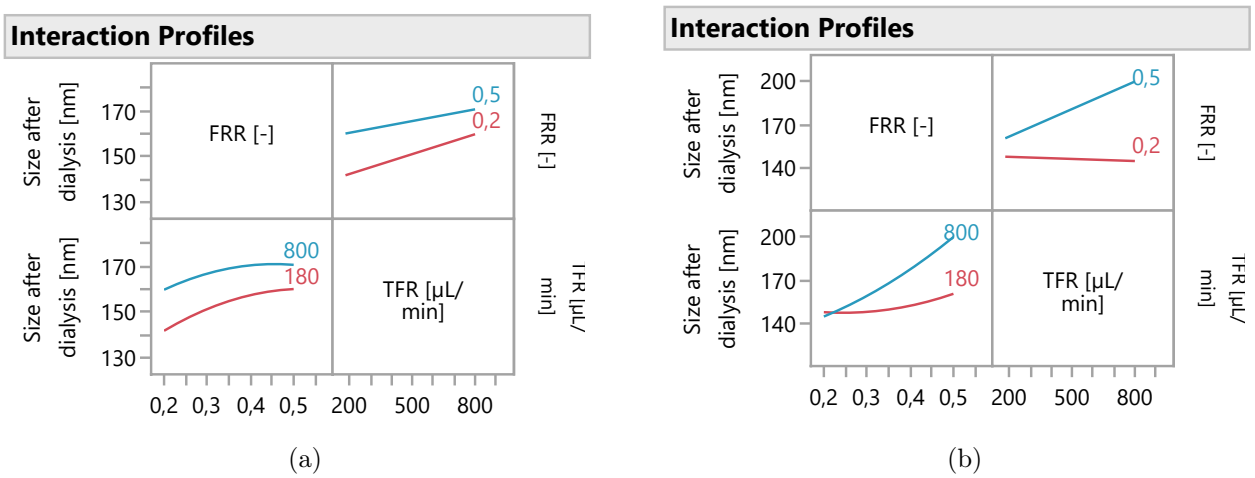

Figure 5.13: **Interaction profiles of the size NPs of the basic model** (a) With rapamycin (b) without rapamycin

The graphical analysis (Section : 5.4.3) of TFR and FRR effects are confirmed (Tables 5.2 and 5.3 and Figures 5.13(a) and 5.13(b)). In the case without rapamycin, the modelling makes it possible to highlight the effect of the two variables via their interaction. (Tables 5.3 and Figure 5.13(b)). Depending on the FRR chosen, the effect of the TFR is not not the same. For a high FRR value (0.5), it is preferable to minimise the TFR used to minimise the size of the NPs. But for a low FRR (0.2), varying the TFR has no influence on the size of the NPs.

The R-squared and adjusted R-squared are for the model with and without rapamycin respectively 0.45, 0.34 and 0.6, 0.46. The meaning of R-squared and adjusted R-squared is explained in Section 5.3.5.2. The high variability prevents to correctly predict the sizes but the model is usable to observe the trends.

Improved model

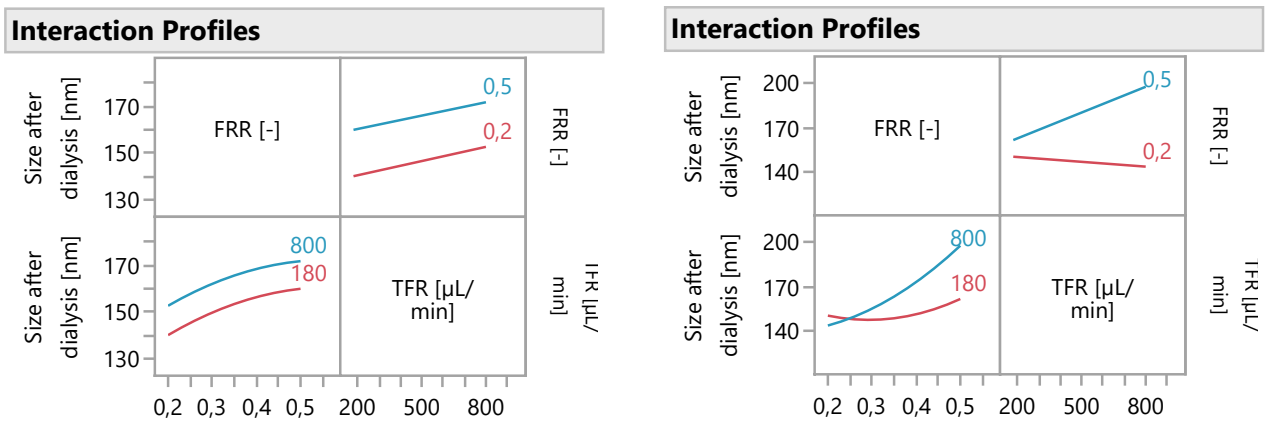

(a) (b)

Figure 5.14: **Interaction profiles of the size of NPs of the improved model** (a) With rapamycin (b) without rapamycin

The interaction profiles of the modelling without outliers (Figure 5.14(a) and 5.14(b)) being very similar to those with outliers. A quadratic effect of the ratio is detected, in the case with rapamycin (Table 5.2). This effect, even if it was not detected in the basic model, could already be assumed by the curvature of the interaction profile as a function of the FRR and is accentuated in the model without outliers.

The R-squared and adjusted R-squared go up to 0.72 and 0.66 for with rapamycin and up to 0.76 and 0.71 for without rapamycin which is good progress.

5.4.5.2 PDI modelling

The initial modelling, without the effect of replicates and considering outliers, generated invalid model in both cases. In the case with rapamycin, a lack of fit was detected and in the case without rapamycin, the model is not significant (p-val<5% in the analysis of variance).

The exclusion of the two defined outliers (Figure 5.6(a)) is sufficient to obtain a valid model for NPs with rapamycin. The inclusion of the effect of replicates makes no sense from a graphical point of view and results in a model that is valid but less efficient than without this effect. In the case without rapamycin, although excluding the three outliers produces a valid model, the inclusion of the third variable, which is slightly visible graphically (Figure 5.8), increases the significance of the model. This makes sense because this effect was suspected graphically.

The initial model and the most optimal model in both cases are presented in Appendix C.6.2. As the base model is invalid, it is unusable and will not be presented.

Improved model

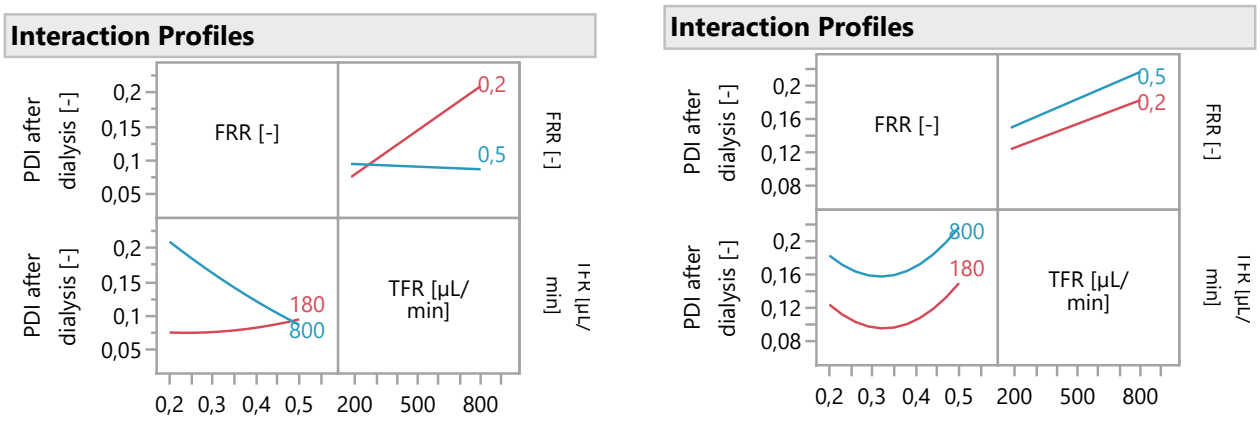

(a) (b)

Figure 5.15: **Interaction profiles of the PDI of NPs of the improved model** (a) With rapamycin (b) without rapamycin

The effect of the TFR and FRR on the PDI and their interaction is significant for NPs with rapamycin (Table 5.2). In the interaction profiles, this is clearly visible with the straight lines (main effect)(Figure 5.15(a)). These lines for a low FRR and a high FRR have a different slope but intersect at one point, reflecting the interaction between the FRR and the TFR. Indeed, depending on the TFR fixed, the impact of FRR chosen on the PDI varies.
Graphically, the effects of the variables were difficult to understand. Thanks to the interaction profiles and by cross-referencing these with the graphs produced in Section 5.4.3.3 and 5.4.3.4, it is now easier to understand the complexity of the variables.

For a very low TFR, it is preferable to set a low FRR to minimise the PDI, but the trend quickly reverses and around 250-300µL/min it is preferable to set a higher FRR. For the TFR, the interaction profile recommends a low TFR except for a very high FRR of 0.5 where the TFR no longer has any impact (almost horizontal line for an FRR of 0.5, so the effect of the FRR = 0.5 on the TFR is negligible (Figure 5.15(a))). Graphically, this is only true at the extreme of the research area according to the FRR axis, and intermediate FRRs such as 0.3 and 0.4 recommend higher TFRs to reduce the PDI (Figure 5.6(a)). Graphically, removing the outliers, it can be seen that this trend is only weakly confirmed for a TFR of 180 and 387µL/min and stops for higher TFRs (Figure 5.6(b)). There is therefore a statistical and graphical contradiction.

For rapamycin free NPs, a quadratic effect of the FRR and a main effect of the TFR were identified (Table 5.3 and Figure 5.15(b). It allows to better identify the quadratic effect, which was difficult

to observe graphically due to the high variability of the measurements and the weakness of this effect (Figure 5.8). It is thus preferable to use intermediate FRR to reduce the PDI.

The R-squared and adjusted R-squared are 0.84 and 0.80 for with rapamycin and is to 0.68 and 0.54 for without rapamycin.

5.4.5.3 Zeta modelling

As with PDI, the conditions applications for basic model for both with and without rapamycin are not valid. The reason for these invalidities is due to a non-significant model (p-val<5% in the analysis of variance). Adding the replicate effect to the modelling makes sense, as it is graphically visible (Figures 5.9 and 5.10). It is therefore logical that the modelling of this third variable should have an impact on the validation of the models. Moreover, excluding outliers only is not enough to obtain a valid model (and conversely with the effect of replicates only). Consequently, the modelling is improved by defining the different replicates as a third categorical variable and excluding outliers from the modelling. The basic and improved models are available in the Appendix C.6.3.

Improved model

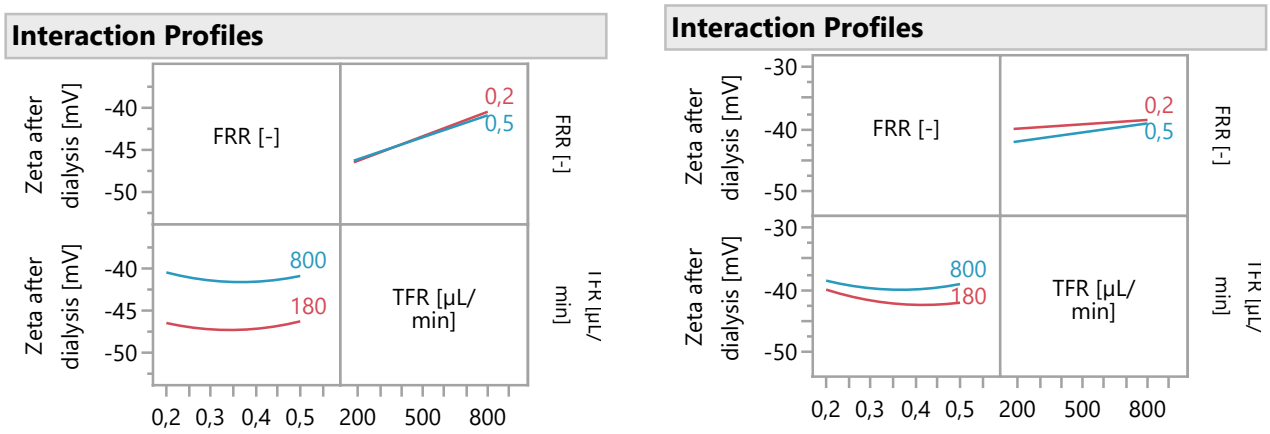

Figure 5.16: **Interaction profiles of the zeta potential of NPs of the improved model** (a) With rapamycin (b) without rapamycin

Only TFR has an impact (main effect) on the zeta potentiel for NPs containing rapamycin (Table 5.2 and Figure 5.16(a)). The modelling perfectly confirms the trends seen graphically (Figure 5.9).

For the case without rapamycin, no effect is detected (Table 5.3 and Figure 5.16(a)). In the interaction profiles, the difference between the two extreme FRR and TFR is minimal. Graphically, the TFR has no effect on potential zeta for a ratio of 0.2 and 0.3 and then becomes quite variable

above a FRR of 0.3 (Figure 5.10). This effect was complicated to interpret. Since the effect of the replicates is strong, it is possible that it dominates the explanation of the variability of the data. The effect of other variables with weaker effects may thus be masked. However, it is also likely that the other variables simply have no effect.

The R-squared and adjusted R-squared is 0.56 and 0.4 for with rapamycin and is to 0.57 and 0.4 for without rapamycin which are low values.

5.4.5.4 EE modelling

The modelling of all the measurement points also faces a problem of too low significance which invalidates the model. Different models were then tested, excluding two or three outliers (mentionned Section 5.4.3.7), adding or not the effect of replicates. All of these tested models are valid. The model with the best condition of application is the model that excludes the three outliers and includes the replicates as a variable. This model as well as the initial model can be found in the Appendix C.6.4.

Improved model

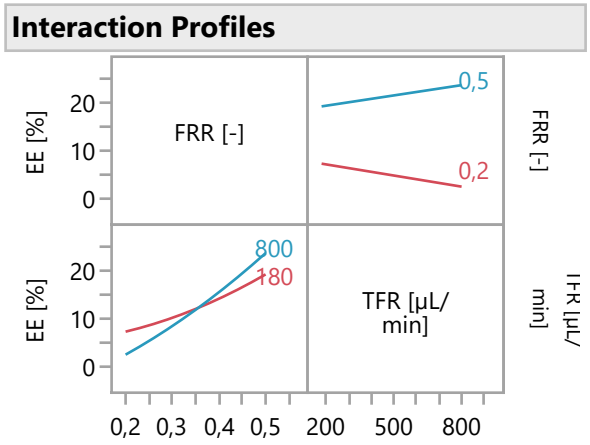

Figure 5.17: Interaction profiles of the EE of NPs of the improved model

Overall, the responses from the different valid models were identical. Only the R-squared as well as the p-value of certain effects are more significant for some, but remains present for others. The significance of the interaction of the two variables is close to a p-value of 5%, the significance threshold. The interaction becomes very weakly significant only in the modelling excluding the three outliers and integrating the effect of the replicates. This effect is therefore not certain since it is not significant in the majority of models but could be possible. (It is then not included in the Table 5.2). Figure 5.17 shows the interaction profile of this model. The interaction profiles of the

other models are almost identical, and the same trends emerge.

A strong effect of the FRR is visible (Table 5.2 and Figure 5.17). This effect was already visible graphically (Figure 5.11). The graph also shows a possible slight effect of TFR not visible through modelling. This can be explained by the fact that the modelling removed three outliers. The R-squared and adjusted R-squared are for this model respectively 0.86 and 0.79.

5.4.6 Predictive models

The models produced allow predictions to be made. These make it possible to provide isocurves of the physicochemical properties whose target values can be fixed, for example. An example of an isocurve is presented in the Appendix C.6.5. These make it possible to give, on the basis of a target value of a physicochemical property, all the possible combinations of variables.

However, given the high variability of the data in the graphs and models presented in the previous sections, the predictions are not reliable. The number of replicates and measurement points is also too small to provide enough data to develop a robust predictive model. Much more data would be needed to establish a predictive model. Furthermore, the experimental design does not allow a complete quadratic model. So part of the information, if present, cannot be modeled.

5.4.7 Comparison with the literature and summary of effects

No study using the same polymers, drug and microfluidic machine was found in the literature. The expectations formulated on the basis of the literature therefore come from articles whose experimental conditions are as close as possible to those used in this work.

In comparison with the literature, the sizes, PDIs and zeta values obtained are satisfactory [39][40][87][88][89]. In fact, the values are in the same order of magnitude as those found in the literature for microfluidic systems. Sizes often vary between approximately 100 and 250 nm. Further studies, involving other polymers and drugs (in different concentrations), other microfluidic systems and surfactants, etc. have shown that it is possible to achieve NPs between 50 and 100nm or even reaching around 600nm and more. PDI values are also regularly between 0 and 0.2, with some conditions showing PDI above 0.2. The zeta potential is strongly influenced by the constituent materials [90]. The values obtained are fully consistent with the literature [39][40][87][88][89].

The literature on EE values is a little more controversial [39][40]. Some articles claim that microfluidic systems can provide EE values, without the use of surfactant, between 10 and 30%, depending on the variables set, while others claim that certain peaks at 40% can be measured. Every articles agree that the use of surfactant increases EE, which can now be as high as 50%.

The values obtained can thus be considered low. This idea is reinforced by the fact that Dolomite describes this microfluidic system as having an EE of up to 99% [75]. The variability obtained for the various physicochemical properties is also too high compared to what can be found in the literature [39][40][37][53][54][91][92].

For the following tables, this legend will be used (Table 5.4).

Table 5.4: Legend of Tables

Symbol	Signification
$\nearrow$	Increase
$\searrow$	Decrease
$\sim$	Stable, no effect
$\bowtie$	Variable, max or min

Table 5.5: Summary of the effects of TFR and FRR on physicochemical properties for NPs with rapamycin

	FRR	TFR
Size $\searrow$	$\searrow$	$\searrow$
PDI $\searrow$	If TFR $\searrow$ then $\searrow$ or $\nearrow$	If FRR $\searrow$ then $\nearrow$ or $\searrow$
Zeta $\nearrow$	$\sim$	$\searrow$
EE $\nearrow$	$\nearrow$	$\searrow$

Table 5.6: Summary of the effects of TFR and FRR on physicochemical properties for rapamycin-free NPs

	FRR	TFR
Size $\searrow$	$\searrow$	$\searrow$
PDI $\searrow$	$\sim$	$\searrow$
Zeta $\nearrow$	$\bowtie$	$\sim$

Table 5.7: Summary of the effects of TFR and FRR on physicochemical properties for NPs containing drugs based on RG 502H polymer, as reported in the literature

	FRR	TFR
Size $\searrow$	$\sim$	$\nearrow$
PDI $\searrow$	$\searrow$	$\searrow$
EE	$\sim$	$\searrow$

Table 5.8: Summary of the effects of TFR and FRR on physicochemical properties for NPs containing drugs based on several articles

	FRR	TFR
Size ↘	↗	↗
PDI ↘	↘	∼ or ↗
Zeta ↗	∼ or ⋈	∼ or ⋈
EE	⋈	↗

Here is summary tables of the effects of the two variables (Tables 5.5 and 5.6). The trends obtained graphically and via modelling have been compared. These tables allow a better comparison with the literature. For ease of comparison, the trends observed in the literature have also been summarised in the case of NPs containing a drug (Tables 5.7 and 5.8). These trends are highly variable from one article to another and vary greatly depending on the experimental conditions used, which are not identical to those used in this work. One of the tables shows the results from the most similar experiment, using the same polymer as for this experiment, the RG 502H (Table 5.7) [39]. The other table represents a summary of the effects found in the literature for different microfluidic systems, using different substances for the NPs (Table 5.8) [40][87][88][89]. For the sake of clarity, the effects of the variables have been summarised as far as possible. It should be kept in mind that these trends can be highly variable.

The effects of the variables on size are quite clear in the literature. The effect obtained during this work is contradictory with what is found. In the literature, to minimise the size of the NPs, it is better to use a high TFR and a high FRR (or no influence of the FRR) (Tables 5.7 and 5.8). The results obtained in this work indicate the opposite (Tables 5.5).

In the literature, the influence of the TFR and FRR on the PDI is highly variable. In this work it is also the property for which the effects of the variables were the most difficult to perceive. Since the two variables interact, variations in one influence the other. It is thus difficult to describe trends. In the literature, it is preferable to use a low FRR to minimise PDI values (Tables 5.7 and 5.8). The results obtained confirm this only for low TFR values (below 200-250µL/min, Section 5.4.5.2) (Tables 5.5). The effect of the TFR on the PDI is a little less clear-cut and differs from article to article (Tables 5.7 and 5.8). The results show that it is preferable to use a high FRR for a low TFR, but that when the TFR increases, the FRR must be rapidly reduced (Table 5.7). The most favourable condition for obtaining the lowest possible PDI is to set the FRR at 0.5 and the TFR at 180µL/min (Tables 5.15(a)).

The effect of FRR on zeta (Tables 5.5) is in line with what is expected based on the literature (Table 5.8), but a slight effect of TFR is detected (Tables 5.5) on zeta that is not generally found in the literature (Table 5.8). Without rapamycin, this effect is not seen (Tables 5.6), which is

consistent with the literature (Table 5.8).

Finally, the effect of TFR on EE (Tables 5.5) is consistent with what was observed in the article with the closest experimental conditions (Table 5.7). However, the effect of the FRR on EE obtained in this work (Tables 5.5) is contradictory to what can be found in the literature (Tables 5.7 and 5.8).

5.4.8 Conclusion

An assumption that enables to remain critical in the face of deviations from expectations and observed variability is the choice of the experimental design. Indeed, since this work is the first done on Dolomite microfluidics system in the ADDB laboratory of UCLouvain, no information base was available. The domain has been defined largely according to the limits offered by the machine. A too large area, going out of optimal conditions of production could therefore prevent from observing the right trends.

Moreover, since the knowledge of experimental design was developed during this latest experiment with JMP, a non-optimal plan was defined. As explained in Section 5.4.6 and C.3, more optimal designs would allow full quadratic modelling and thus ensure that all the information has been modelled.

In addition to a better experimental design, a larger number of measurement points and replicates could reduce the variability of the data, improving the modelling. However, it is necessary to remain realistic in the choice of the number of measurement points and replicates. Experiments carried out with, for example, five replicates would allow a more accurate estimate of the model parameters (for example, the average of replicates). An accumulation of data, as experiments are carried out on this microfluidic system, would make it possible to improve the prediction of predictive models. More data would counterbalance current variability to better detect information.

Other hypotheses can be made regarding to the origin of the large variability obtained between the different replicates of the same combination of conditions. It can come from the microfluidic system used and the way it has been used, the way in which the NPs are preserved and harvested after production and the temperature during the production of the NPs [93]. Using a surfactant can help decrease this variability [65].

The variability of the replicates is not homogeneous for each combination of variables for one property. This heterogeneity is also different from one physicochemical property to another. In other words, there is no trend to define which combinations of variables achieve low variability for all properties. It is possible to determine certain conditions common to two properties reflecting

low variability (such as an FRR of 0.2 for the PDI with rapamycin (Figure 5.6(a)) and the EE (Figure 5.11)) or conversely an high variability. This can question the limits of the field. Indeed, it is possible to notice that the variability is highest in the case without rapamycin for PDI (Figure 5.8) and zeta potential (Figure 5.10) and in the case with rapamycin for EE (Figure 5.11) when the FRR and TFR are set at 0.5 and 800µL/min. Similary, variability is also high for the case of zeta potenital with rapamycin (Figure 5.9) at 0.2 and 180µL/min. It might be interesting to carry out an experiment on a smaller area with measurement points closer together to compare the results obtained.

Chapter 6

Conclusion

6.1 Putting the objectives into context

The aim of this master thesis was therefore to explore a new microfluidic system at UCLouvain designed for the production of NPs. The use of a microfluidic system offers a number of advantages over more conventional production methods (less batch-to-batch variability, continuous flow production, etc). This production system is thus better suited to producing industrialised NPs. It is with this in mind that this thesis was oriented.

As the machine was new, the aim of this master thesis was to explore it as far as possible. The guideline used, which is the long-term objective of this master thesis, is to develop a system capable of returning variables to be fixed in order to obtain an optimised NPs. It would first have to be developed for a specific polymer and drug, then extended to other polymers and drugs.

But to start, the first objective was to succeed in producing NPs. Once this had been achieved, the next objective was to obtain data for several conditions in order to check that NPs production still worked when the two variables were changed and also to obtain a database for future reflections. This allowed the following objectives to be defined. The first was to examine the rate of precipitation in the chip. Indeed, some conditions produce more precipitation which hinders the continuous production of NPs. It was therefore necessary to present this precipitation and define the most favourable conditions regarding to this precipitation.

The second objective was to make a first step towards this predictive model, trying to achieve it and also to identify the influence of TFR and FRR on the production of NPs according to the different physicochemical properties. This objective has been partially achieved. The different trends of the effects of variables have been identified but the predictive model obtained is not reliable. However, it has provided valuable insights for the achievement of this functional predictive model.

6.2 Improvement path and perspectives

6.2.1 Improving the predictive model

A number of areas for improvement have already been highlighted in Section 5.4.8, which discusses the conclusion of the data modelling experiment. These are included in this conclusion. Several points can be rethought to obtain a predictive model that fits the data well.

Among these, the use of a more appropriate experimental design would enable a good comparison between the different data points as well as providing sufficient information for predictive modelling. The current experimental design does not allow a complete quadratic model to be generated, which is necessary to ensure that all the information has been modelled. The use of a complete factorial design with 3 levels, as described in Appendix C.3 would be more suitable.

In addition, the high variability in the dataset and the number of replicates currently used mean that it is not possible to establish a quality model that fits the data well. There are several possible solutions.

Increasing the number of replicates would allow a more accurate estimate of the model parameters to be made. In addition, it will be easier to certify which point is an outlier and thus destabilises the predictive model. This was explained in Section 5.4.3.3. Similarly, using a larger number of data points would improve the accuracy of the model. Storing measurements over time can be a solution for increasing the amount of data, but care must be taken to avoid the day effect.

Moreover, the area under study remains large. As explain in Section 5.4.8, since the aim is to obtain an efficient predictive model, restructuring the domain towards a smaller area with less variability could be of interest. This field can therefore be defined according to two objectives: "Produce NPs with optimised physicochemical properties and with low variability between productions". This would also make it possible to compare the trends in the effects of the variables observed with those obtained in this master thesis.

Questions may arise about the protocol used. The variability of the measurements could be due to the method of collection or storage of the NPs, the temperature during production or simply the microfluidic system itself [93]. The integration of a surfactant in the protocol, according to the literature, can also reduce variability [65].

6.2.2 New perspectives

The methodology used to calculate EE may be subject to inaccuracies. The current calculation is based on the volumes and concentrations used. The volume is not constant, it can vary depending on the experimental conditions (evaporation of solvent for example). By incorporating a lyophilation step into the protocol, it is possible to base EE calculations on mass, which is constant and also measured with great precision.

It would also be interesting to test other chip models with other designs. This could have an impact on the different outcomes. A comparison between the results would thus be interesting and the use of another chip could also have an impact on the variability of the measurements.

Finally, a more distant perspective of this master thesis would be to extend the production to other polymers and other encapsulated drugs.

Appendix A

Reliable and comparative data acquisition

A.1 Zetasizer Ultra and Zeta view parameters and protocols

For the Zetasizer Ultra from Malvern, the samples analysed were obtained by dilution of generally 20µL sometimes 40µL of NPs in 1mL milliQ water. This depends on the intensity of the perceived signal (and the shape of the correlogram). The following parameters have been set.

For size and PDI, dilution was carried out in DTS0012 cells. The temperature has been set at 25°C. The equilibration time was set at 10 sec. The analysis model used was the multiple narrow modes. Measurements were performed three times for each replicate and the mean value as well as the standard deviation were retained. The remaining parameters have been selected by default.

To measure zeta, the sample was transferred to DTS1070 cells using a 1mL syringe. This syringe was rinsed twice with milliQ water between each use. Three measurements were also performed for each replicate. The pause between each repetition has been set at 10 seconds. The model used was auto mode. The equilibration time has also been set at 10 seconds. The remaining parameters have been left as default.

For the concentration measurements, the ZetaView was rinsed manually using a 20mL syringe of milliQ water. Calibration was then carried out using polystyrene 100nm (PS100) at a dilution of 1:250,000. Approximately 800-900µL of PS100 were injected using a 1mL syringe. Once calibration has been successfully completed, the ZetaView was rinsed again with 20mL of milliQ water. The temperature was set at 24°C. The sensitivity (laser power) was set at 75% and the shutter (exposure time) at 100. The sample was diluted between 1:20,000 and 1:40,000 depending on the number of detected NPs. 1mL of the sample was injected into the ZetaView. Between each analysis, the ZetaView was rinsed with 20mL of milliQ.

A.2 Tables of physicochemical properties of NPs

Table A.1: Physicochemical properties (Size and PDI) of NPs of RG 502H 0.5%

FRR [-]	TFR [µL/min]	N1 Size [nm]	N2 Size [nm]	N3 Size [nm]	N1 PDI [-]	N2 PDI [-]	N3 PDI [-]
0,143	40	145+/-1,74	144+/-1,05	156+/-2,13	0,086+/-1,74	0,084+/-0,017	0,096+/-0,017
0,167	50	156+/-1,8	157+/-1,34	169+/-2,42	0,092+/-0,011	0,097+/-0,006	0,055+/-0,021
0,2	60	166+/-2,18	169+/-0,98	183+/-0,50	0,043+/-0,035	0,060+/-0,014	0,060+/-0,033
0,25	70	190+/-3,8	191+/-1,06	175+/-1,54	0,07+/-0,026	0,067+/-0,017	0,059+/-0,018
0,333	80	227+/-2,68	211+/-3	251+/-3,03	0,104+/-0,019	0,07+/-0,033	0,122+/-0,006

Table A.2: Physicochemical properties (Zeta potential) of NPs of RG 502H 0.5%

FRR [-]	TFR [µL/min]	N1 zeta [mV]	N2 zeta [mV]	N3 zeta [mV]
0,143	40	-45,22 +/- 0,85	-49,83+/-1,674	-43,96+/-0,600
0,167	50	-48,53+/-0,68	-48,46+/-0,879	-42,07+/-0,685
0,2	60	-45,66+/-1,241	-53,58+/-0,68	-44,25+/-0,215
0,25	70	-47,09+/-0,13	-45,99+/-2,525	-48,8+/-0,573
0,333	80	-45,68+/-0,63	-48,42+/-0,964	-47,92+/-0,663

Table A.3: Physicochemical properties (concentration) of NPs of RG 502H 0.5%

FRR [-]	TFR [L/min]	N1 concentration [particles/mL]	N2 concentration [particles/mL]	N3 concentration [particles/mL]
0,143	40	1,46e+012	2,32e+012	1,84e+012
0.167	50	2,08e+012	1,6e+012	1,84e+012
0.2	60	1,52e+012	1,48e+012	2,08e+012
0.25	70	1,52e+012	2,36e+012	1,92e+012
0.333	80	1,48e+012	1,64e+012	1,32e+012

Table A.4: Physicochemical properties (Size and PDI) of NPs of RG 752S 0.5%

FRR [-]	TFR [µL/min]	N1 Size [nm]	N2 Size [nm]	N3 Size [nm]	N1 PDI [-]	N2 PDI [-]	N3 PDI [-]
0,143	40	191+/-4,31	190+/-8,38	195+/-3,37	0,123+/-0,024	0,071+/-0,037	0,078+/-0,023
0,167	50	280+/-3,01	208+/-2,34	214+/-2,69	0,142+/-0,030	0,142+/-0,074	0,143+/-0,045
0,2	60	224+/-4,09	219+/-1,16	225+/-1,15	0,091+/-0,04	0,077+/-0,007	0,089+/-0,012
0,25	70	294+/-10,56	274+/-2,73	258+/-2,78	0,157+/-0,037	0,137+/-0,019	0,117+/-0,009
0,333	80	389+/-74,25	364+/-2,04	350+/-11,37	0,277+/-0,152	0,131+/-0,014	0,136+/-0,016

Table A.5: Physicochemical properties (Zeta potential) of NPs of RG 752S 0.5%

FRR [-]	TFR [µL/min]	N1 zeta [mV]	N2 zeta [mV]	N3 zeta [mV]
0,143	40	-44,19+/-1,47	-50,15+/-0,274	-45,84+/-1,778
0,167	50	-58,62+/-1,52	-42,47+/-1,48	-46,59+/-0,994
0,2	60	-53,21+/-0,60	-37,46+/-2,78	-44,55+/-0,304
0,25	70	-51,93+/-0,239	-45,02+/-0,216	-40,44+/-0,384
0,333	80	-46,12+/-0,017	-44,43+/-0,198	-40,98+/-0,097

Table A.6: Physicochemical properties (Concentration) of NPs of RG 752S 0.5%

FRR [-]	TFR [L/min]	N1 concentration [particles/mL]	N2 concentration [particles/mL]
0,143	40	9,6e+011	8,1e+011
0.167	50	5,6e+011	5,1e+011
0.2	60	6e+011	1,1e+012
0.25	70	8,4e+011	6,8e+011
0.333	80	9e+011	3,8e+011

Appendix B

Impact of TFR and FRR on polymer precipitation in the chip channel during NPs production

B.1 Calibration curve of Resomer RG 502H 0.5% in acetone

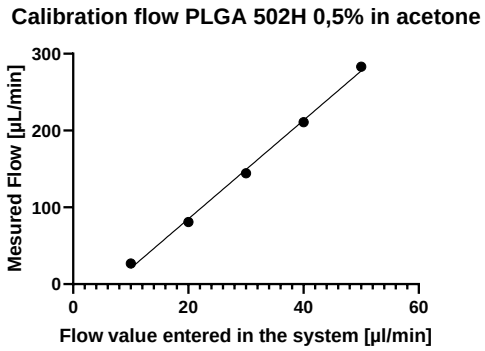

Figure B.1: Calibration curve of Resomer RG 502H 0.5% in acetone

B.2 Tables of physicochemical properties of NPs

Table B.1: Size [nm] of NPs of RG 502H 0.5%

FRR [-]\TFR[µL/min]	30	180	340	490	650	800
0,143	227+/-1,37	137+/-0,21	162+/-1,90	143+/-0,73	139+/-9,4	145+/-1,39
0,2	199+/-1,26	143+/-0,48	139+/-2,88	143+/-1,52	147+/-1,82	151+/-1,26
0,333	213+/-1,97	154+/-0,02	144+/-1,36	153+/-1,21	163+/-2,9	166+/-3,88
0,4	205+/-2,93	162+/-0.44	154+/-1,13	160+/-1,32	168+/-1,07	155+/-1,18
0,5	212+/-0,71	181+/-2.8	174+/-0,33	176+/-0,74	176+/-1,02	156+/-1,36

Table B.2: PDI of NPs of RG 502H 0.5%

FRR [-]\TFR[µL/min]	30	180	340	490	650	800
0,143	0,24+/-0,009	0,149+/-2,28	0,23+/-0,009	0,14+/-0,005	0,19+/-0,053	0,20+/-0,010
0,2	0,26+/-0,055	0,35+/-0,04	0,124+/-0,009	0,11+/-0,027	0,14+/-0,011	0,16+/-0,009
0,333	0,49+/-0,14	0,10+/0,025	0,082+/-0,019	0,10+/-0,001	0,087+/-0,014	0,11+/-0,002
0,4	0,48+/-0,19	0,068+/-0,016	0,096+/-0,008	0,086+/-0,021	0,082+/-0,024	0,14+/-0,017
0,5	0,52+/-0,1	0,064+/-0,004	0,073+/-0,014	0,056+/-0,008	0,046+/-0,008	0,14+/-0,019

Table B.3: Precipitation score of NPs of RG 502H 0.5%

FRR [-]\TFR[µL/min]	30	180	340	490	650	800
0,143	2	4	3	3,5	4	3
0,2	2	3	3	2	2	2
0,333	2,5	1	1,5	1	1	1
0,4	2,5	1,5	1	1	1	1
0,5	3	1	1	1	1	1

B.3 Parameters

For the IDW method, the value of the theta parameter for size, PDI and precipitation score has been optimised to 5, 2.5 and 1.5 respectively.

For the construction of linear models in the second method, four parameters must be set. The y-intercept, the type of model used, the start of the threshold or plateau, and the value of the first point. The mathematical function used, also called variogram models, was the spherical model. This model is often used and is defined by the formula B.3.[81]

$$\gamma(h) = \begin{cases} c\left(\frac{3h}{2a} - \frac{h^3}{2a^3}\right) & \text{si } h \leq a \\ c & \text{si } h > a \end{cases} \quad [94] \tag{B.1}$$

The y-intercepts for size, PDI and precipitation were set at 356, 0.0007 and 0.44 respectively. They correspond to the value of the variance of the residuals. The residuals were calculated by subtracting the trend. The start of the plateau was set at 0.25, 0.2 and 0.28 respectively. The value of the first point was set at 43, 0.00024 and 0.21.

B.4 Linear models

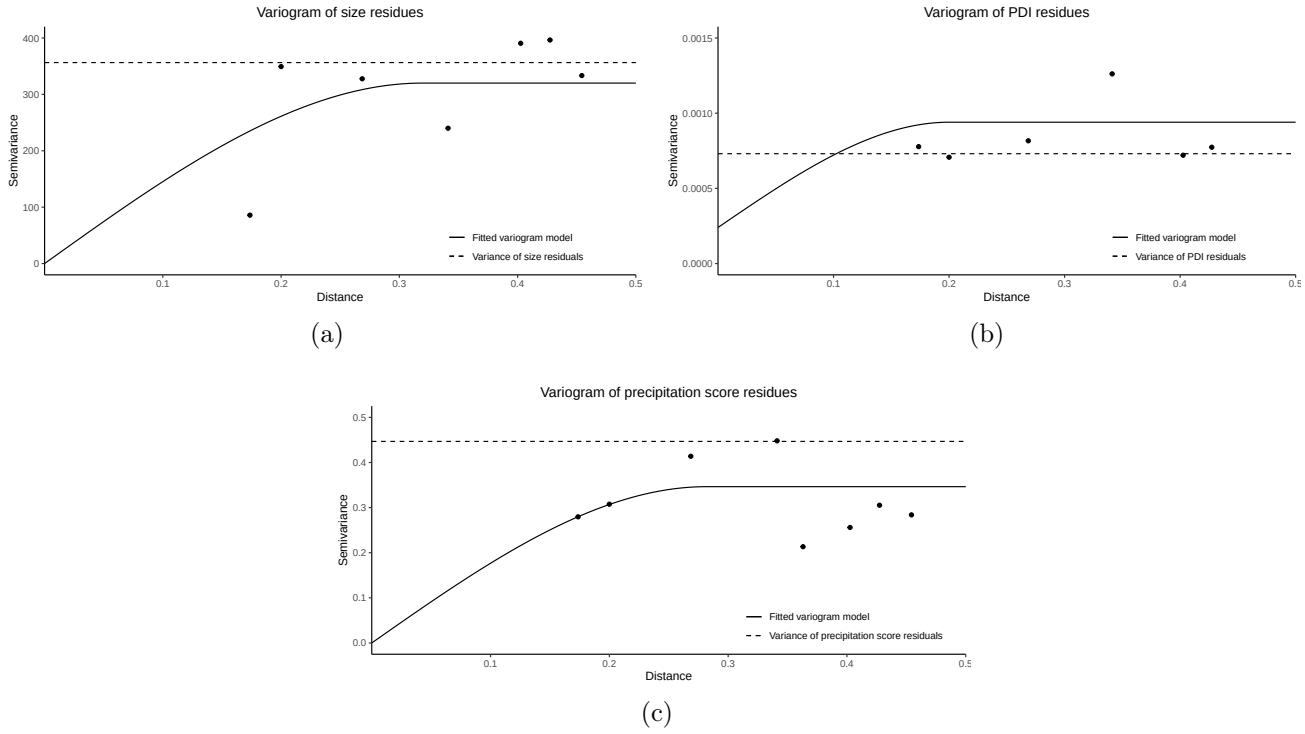

Figure B.2: **Linear models of the semi-variance of physicochemicals properties used for Kriging predictions to predict the point of the field of study** (a) Variogram of size residues (b) Variogram of PDI residues (c) Variogram of precipitation score residues

The various variograms are not stationary of order 2. In fact, they do not tend towards the variance and the semivariance does not depend solely on the distance, the points are fairly scattered.

Appendix C

Drug Encapsulation, Statistical Analysis and Modelling

C.1 Pluronic acid

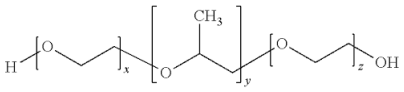

Figure C.1: Pluronic acid Structural Formula

Acid pluronic or poloxamere is a copolymer composed of three blocks, as shown in figure ... . It is characterized by the presence of a hydrophobic central block, polypropylene glycol (PPG)(or polypropylene oxide(PPO)), surrounded by two hydrophilic blocks, polyethylene glycol (PEG) (or polyethylene oxide(PEO)). This structure gives it amphiphilic properties. Acid pluronic can therefore increase the solubility of hydrophobic compounds in water. Some poloxamers can also form gels, useful for drug delivery for example. Due to its properties, it is widely used in the industrial, medical, cosmetic and pharmaceutical fields.[95][96]

Pluronic F-127 is a specific type of pluronic acid. Its molecular weight is 12600 g/mol. The F refers to "Flakes". Pluronic acids can be defined by 3 letters, F (Flakes), P (paste) and L (Liquid). The next two numbers (12) refer to the molecular weight of the PPO block. The last number refers to the weight fraction of the PEO block (7 for 70%). Pluronic F-127 have a very high proportion of PEG, which makes this pluronic acid very soluble in water.[97][98]

C.2 Calculation of EE, HPLC-UV parameters and protocol

The following protocol was drawn up on the basis of research carried out by one of the laboratory's researchers from the research laboratory in ADDB at UCLouvain. The NPs sample was diluted by a factor of ten in acetonitrile (ACN). ACN was used to break up the NPs and enable the HPLC-UV to measure the amount of rapamycin.

The following parameters have been set. The mobile phase used was 100% ACN. Sampling lasted seven minutes. The maximum pressure was set at 350 bar for safety reasons. The wavelengths used for HPLC-UV were 254 and 277nm. 254nm is an intense absorption band for many compounds and 277nm was used because rapamycin has a maximum absorption peak at this wavelength. The retention time was 2.9 minutes. The total flow of ACN was set at 1µL/min.

The EE was calculated on the basis of volumes and concentrations. The following methodology was used. Rapamycin calibration curves were analysed from 1.5625 to 100µg/mL. The received area value was translated into concentration via the calibration line. The concentration, weighted by its dilution factor, was multiplied by the volume measured after dialysis. In this way, the mass of rapamycin measured by HPLC-UV could be calculated. Then, the volume generated by the organic flow was calculated on the basis of the respective time of each production and the flow rate of this stream. By multiplying this volume by the rapamycin concentration of the solution used, the initial mass of rapamycin introduced could be calculated. The EE was then calculated on the basis of the amount of rapamycin measured by HPLC-UV compared with the amount of rapamycin initially introduced.

C.3 Optimal experimental design

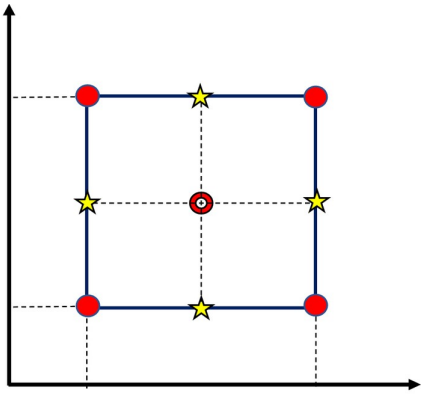

Figure C.2: Factorial design with a central point and complete factorial plan with three levels [99]

The factorial design with a central point requires the use of minimum five points. These are points are "the four factorial points" and the central point. The four factorial points correspond to the four corners of the study domain (In red in Figure C.2, the central point being represented by the red circle). To provide more power to the model, it is usual to repeat the experiment from the point to the center several times. The factorial design with a central point provides the coefficients of the first five terms of the quadratic equation .

The complete factorial plan with three levels, based on nine points, is one of the experimental plan by excellence. Indeed, it completes the previous plan by adding four additional points, namely intermediate points between the minimum and maximum variables (Star points in Figure C.2). These points are located between the minimum and maximum levels for each variables, perpendicular to the central point. This model allows to obtain all the coefficients of the quadratic equation and to optimize the interactions between the different variables.

C.4 Table of the physicochemical properties

Table C.1: Size of the NPs with rapamycin for three replicates

Number	FRR [-]	TFR [µL/min]	N1 Size before dialysis [nm]	N1 Size after dialysis [nm]	N2 Size before dialysis [nm]	N2 Size after dialysis [nm]	N3 Size before dialysis [nm]	N3 Size after dialysis [nm]
1	0,2	180	127	135	131	140	137	146
2	0,5	180	158	156	155	157	165	170
3	0,3	387	147	150	147	182	151	158
4	0,4	387	154	153	164	156	158	163
5	0,3	593	165	163	152	154	159	164
6	0,4	593	167	168	170	161	192	167
7	0,2	800	147	155	143	148	163	176
8	0,5	800	167	164	170	167	174	184

Table C.2: Size of the NPs without rapamycin for three replicates

Number	FRR [-]	TFR [µL/min]	N1 Size before dialysis [nm]	N1 Size after dialysis [nm]	N2 Size before dialysis [nm]	N2 Size after dialysis [nm]	N3 Size before dialysis [nm]	N3 Size after dialysis [nm]
1	0,2	180	137	138	159	157	152	160
2	0,5	180	169	165	151	158	158	159
3	0,3	387	133	131	135	140	134	143
4	0,4	387	149	148	159	169	162	172
5	0,3	593	144	148	166	175	147	160
6	0,4	593	158	176	186	193	147	156
7	0,2	800	162	157	124	130	136	145
8	0,5	800	171	195	194	207	180	188

Table C.3: Zeta potential of the NPs with rapamycin for three replicates

Number	FRR [-]	TFR [µL/min]	N1 Zeta before dialysis [mV]	N1 Zeta after dialysis [mV]	N2 Zeta before dialysis [mV]	N2 Zeta after dialysis [mV]	N3 Zeta before dialysis [mV]	N3 Zeta after dialysis [mV]
1	0,2	180	-23,21	-50,53	-49,27	-42,76	-45,44	-23,9
2	0,5	180	-38,73	-45,66	-55,22	-49	-52,19	-44,22
3	0,3	387	-41,57	-48,48	-53,51	-49,4	-45,14	-41,64
4	0,4	387	-45,17	-47,38	-49,31	-44,89	-38,87	-46,32
5	0,3	593	-38,23	-46,29	-49,5	-45,42	-44,85	-42,5
6	0,4	593	-35,49	-41,32	-49,74	-39,13	-47,59	-40,01
7	0,2	800	-37,44	-40,18	-43,45	-44,01	-42,11	-36,7
8	0,5	800	-36,02	-41,85	-48,89	-44,32	-45,01	-39,19

Table C.4: Zeta potential of the NPs without rapamycin for three replicates

Number	FRR [-]	TFR [µL/min]	N1 Zeta before dialysis [mV]	N1 Zeta after dialysis [mV]	N2 Zeta before dialysis [mV]	N2 Zeta after dialysis [mV]	N3 Zeta before dialysis [mV]	N3 Zeta after dialysis [mV]
1	0,2	180	-43,98	-46,43	-51,75	-44,26	-49,27	-31,62
2	0,5	180	-44,23	-49,02	/	-46,16	-52,32	-31,83
3	0,3	387	-51,2	-48,93	-39,95	-35,1	-39,97	-33,84
4	0,4	387	-53,41	-48,14	-45,8	-37,24	-48,27	-34,19
5	0,3	593	-46,57	-46,26	-49,85	-31,2	-46,15	-41,87
6	0,4	593	-52,72	-46,56	-43,92	-43,72	-48,95	-44,01
7	0,2	800	-40,7	-43,45	-35,99	-34,46	-47,59	-37,44
8	0,5	800	-47,69	-3,682	-35,87	-32,04	-44,8	-36,43

Table C.5: PDI of the NPs with rapamycin for three replicates

Number	FRR [-]	TFR [µL/min]	N1 PDI before dialysis [-]	N1 PDI after dialysis [-]	N2 PDI before dialysis [mV]	N2 PDI after dialysis [mV]	N3 PDI before dialysis [mV]	N3 PDI after dialysis [mV]
1	0,2	180	0,0993	0,077	0,692	0,085	0,094	0,057
2	0,5	180	0,058	0,12	0,092	0,075	0,066	0,077
3	0,3	387	0,141	0,23	0,095	0,24	0,094	0,13
4	0,4	387	0,126	0,094	0,085	0,095	0,105	0,143
5	0,3	593	0,108	0,118	0,089	0,136	0,14	0,112
6	0,4	593	0,086	0,119	0,066	0,087	0,218	0,089
7	0,2	800	0,183	0,218	0,147	0,201	0,133	0,221
8	0,5	800	0,044	0,073	0,074	0,097	0,051	0,102

Table C.6: PDI of the NPs without rapamycin for three replicates

Number	FRR [-]	TFR [µL/min]	N1 PDI before dialysis [-]	N1 PDI after dialysis [-]	N2 PDI before dialysis [mV]	N2 PDI after dialysis [mV]	N3 PDI before dialysis [mV]	N3 PDI after dialysis [mV]
1	0,2	180	0,088	0,146	0,112	0,136	0,122	0,093
2	0,5	180	0,066	0,13	0,106	0,187	0,105	0,147
3	0,3	387	0,128	0,256	0,146	0,118	0,114	0,087
4	0,4	387	0,089	0,133	0,102	0,094	0,089	0,128
5	0,3	593	0,208	0,179	0,097	0,14	0,126	0,154
6	0,4	593	0,087	0,183	0,1334	0,127	0,133	0,119
7	0,2	800	0,19	0,217	0,192	0,187	0,164	0,131
8	0,5	800	0,089	0,2694	0,152	0,22	0,077	0,071

Table C.7: EE of the NPs for three replicates

Number	FRR [-]	TFR [µL/min]	N1 EE [%]	N2 EE [%]	N3 EE [%]
1	0,2	180	7,94	5,89	8,77
2	0,5	180	20,72	13,66	23,16
3	0,3	387	39,05	6,49	12,18
4	0,4	387	31,97	10,34	17,05
5	0,3	593	10,40	6,03	6,74
6	0,4	593	22,7	/	14,66
7	0,2	800	2,83	0,93	4,9
8	0,5	800	18,9	26,09	1,58

C.5 Comparison with and without rapamycin

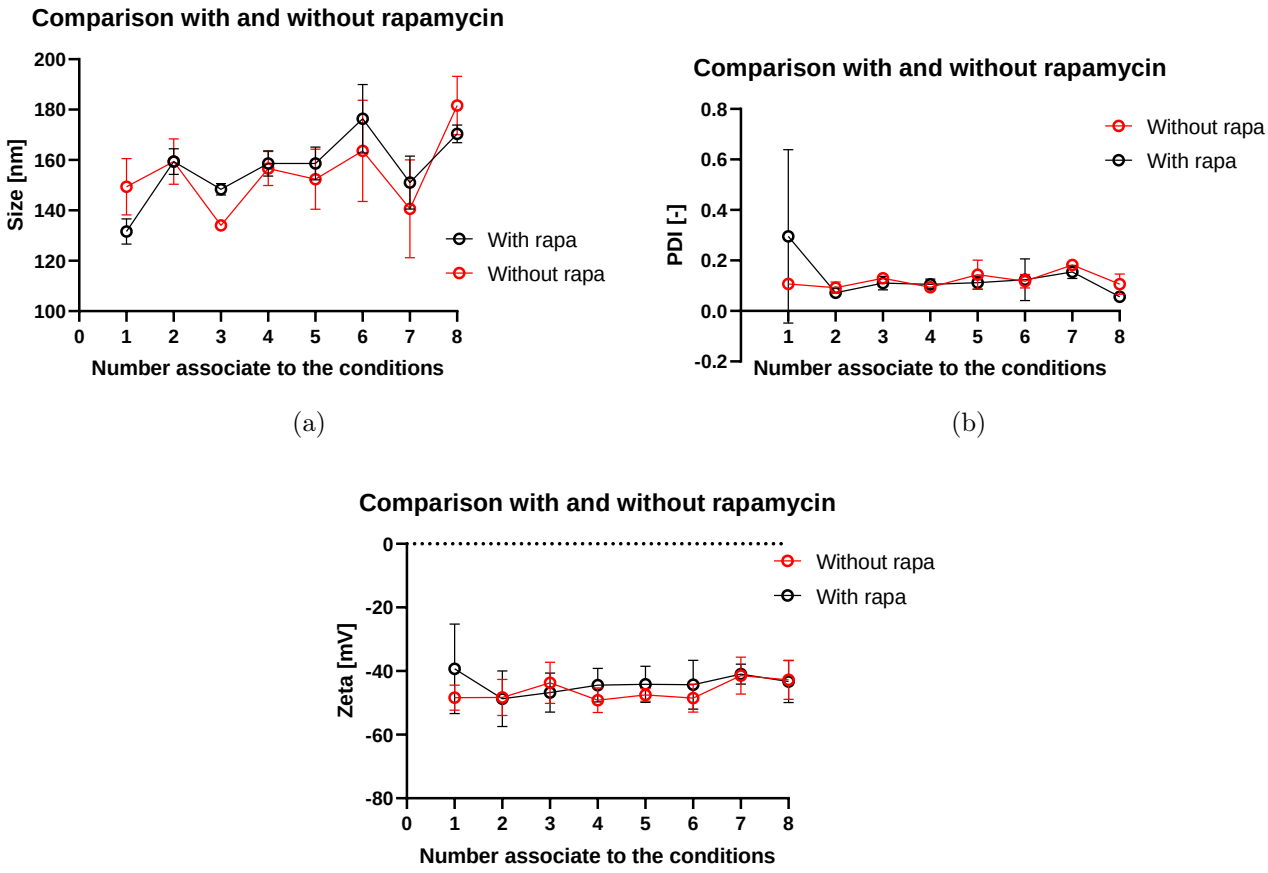

Figure C.3: **Physicochemical properties of NPs with and without rapamycin before dialysis** (a) Size (b) PDI (c) Zeta

C.6 JMP modelling

C.6.1 Models of NPs size

C.6.1.1 Basic model of NPs size

Response Size after dialysis [nm] Rapamycin=With

Whole Model

Actual by Predicted Plot

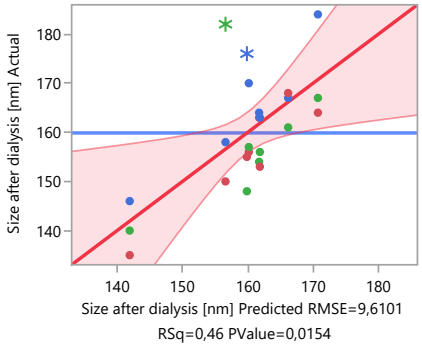

Effect Summary

Source	Logworth	PValue
FRR [-]	1,908	0,01235
TFR [µL/min]	1,855	0,01396
FRR [-]*FRR [-]	0,404	0,39470
TFR [µL/min]*FRR [-]	0,290	0,51270

Lack Of Fit

Source	DF	Sum of Squares	Mean Square	F Ratio
Lack Of Fit	3	218,0557	72,6852	0,7568
Pure Error	16	1536,6667	96,0417	**Prob > F**
Total Error	19	1754,7224		0,5345
				Max RSq
				0,5270

Residual by Predicted Plot

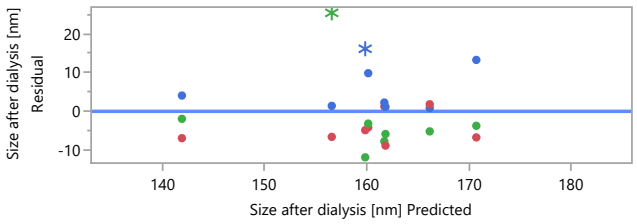

Summary of Fit

RSquare	0,459857
RSquare Adj	0,346143
Root Mean Square Error	9,610089
Mean of Response	159,875
Observations (or Sum Wgts)	24

Analysis of Variance

Source	DF	Sum of Squares	Mean Square	F Ratio
Model	4	1493,9026	373,476	4,0440
Error	19	1754,7224	92,354	**Prob > F**
C. Total	23	3248,6250		0,0154*

Figure C.4: Basic model of size NPs

Response Size after dialysis [nm] Rapamycin=With

Whole Model

Parameter Estimates

Term	Estimate	Std Error	t Ratio	Prob>|t|
Intercept	133,76797	8,055341	16,61	<,0001*
FRR [-]	48,5	17,54554	2,76	0,0123*
TFR [µL/min]	0,0229948	0,008493	2,71	0,0140*
(TFR [µL/min]-490)*(FRR [-]-0,35)	-0,03956	0,059298	-0,67	0,5127
(FRR [-]-0,35)*(FRR [-]-0,35)	-170,8333	196,1651	-0,87	0,3947

Effect Tests

Source	Nparm	DF	Sum of Squares	F Ratio	Prob > F
FRR [-]	1	1	705,67500	7,6410	0,0123*
TFR [µL/min]	1	1	677,08130	7,3314	0,0140*
TFR [µL/min]*FRR [-]	1	1	41,10466	0,4451	0,5127
FRR [-]*FRR [-]	1	1	70,04167	0,7584	0,3947

Residual Normal Quantile Plot

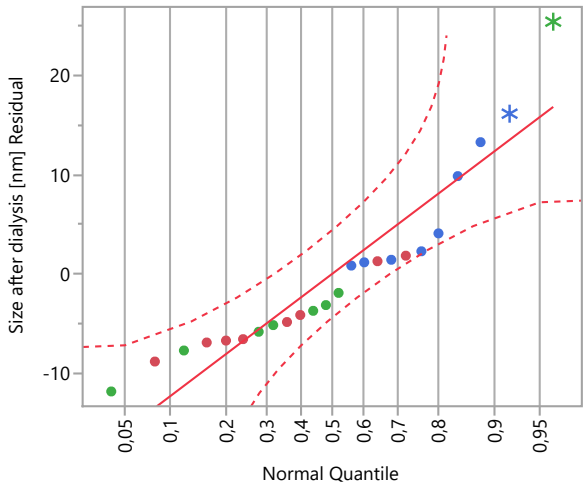

FRR [-]

Leverage Plot

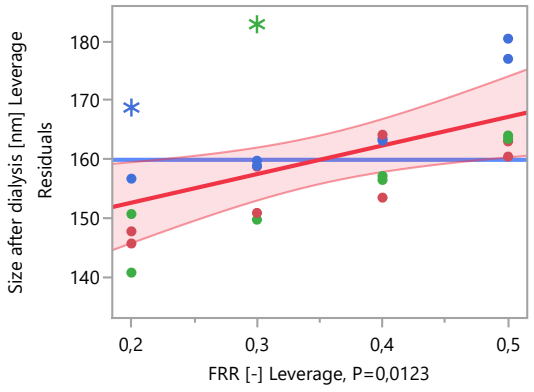

TFR [µL/min]

Leverage Plot

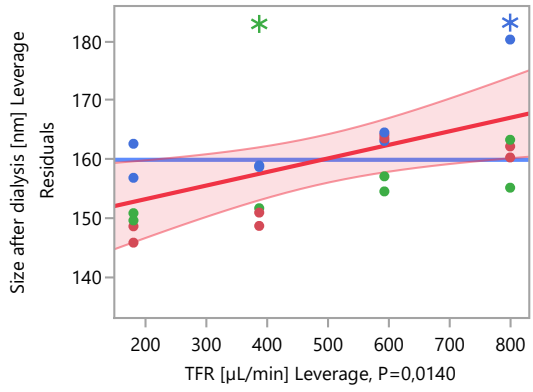

Figure C.5: Basic model of size NPs (cont.)

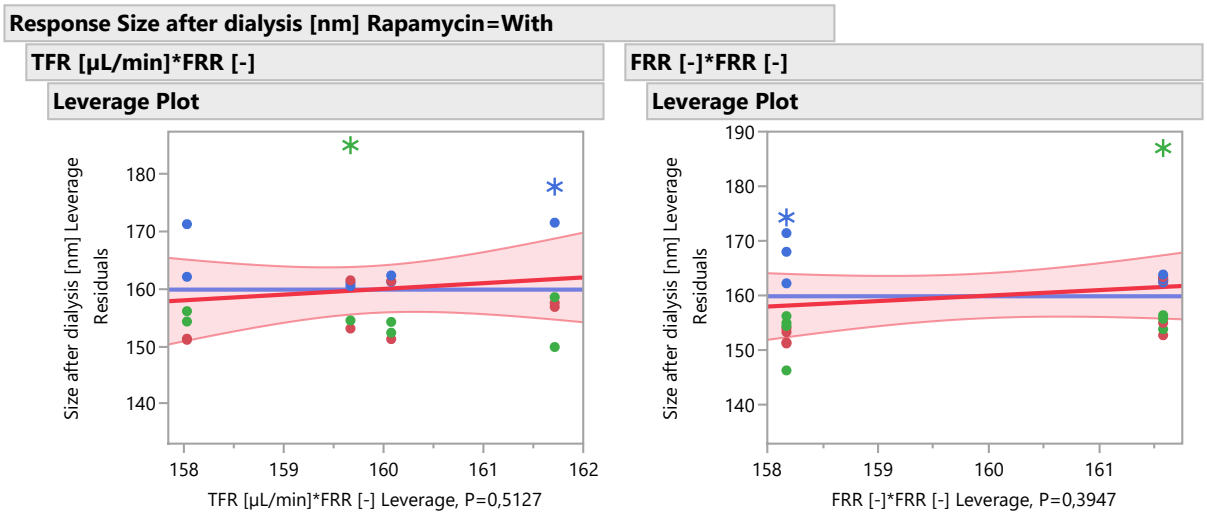

Figure C.6: Basic model of size NPs (cont.)

Response Size after dialysis [nm] Rapamycin=Without

Whole Model

Actual by Predicted Plot

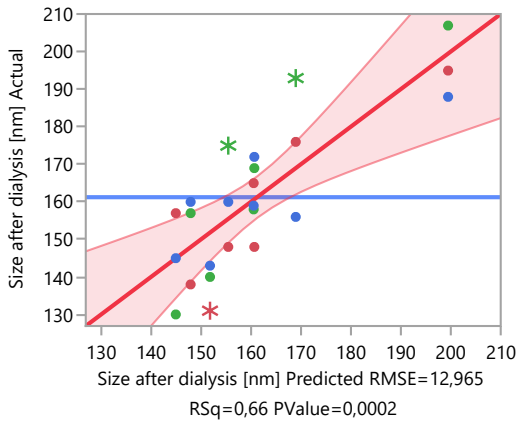

Effect Summary

Source	Logworth	PValue
FRR [-]	3,838	0,00015
TFR [µL/min]*FRR [-]	1,959	0,01098
TFR [µL/min]	1,693	0,02027 ^
FRR [-]*FRR [-]	0,338	0,45907

Lack Of Fit

Source	DF	Sum of Squares	Mean Square	F Ratio
Lack Of Fit	3	857,6129	285,871	1,9580
Pure Error	16	2336,0000	146,000	**Prob > F**
Total Error	19	3193,6129		0,1610
				Max RSq
				0,7532

Residual by Predicted Plot

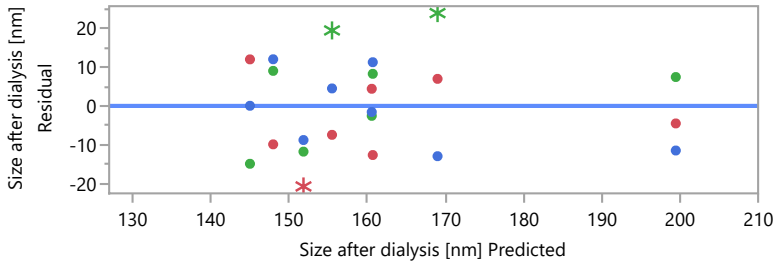

Summary of Fit

RSquare	0,662641
RSquare Adj	0,591618
Root Mean Square Error	12,96476
Mean of Response	161,25
Observations (or Sum Wgts)	24

Analysis of Variance

Source	DF	Sum of Squares	Mean Square	F Ratio
Model	4	6272,8871	1568,22	9,3299
Error	19	3193,6129	168,08	**Prob > F**
C. Total	23	9466,5000		0,0002*

Figure C.7: Basic model of size NPs (cont.)

Response Size after dialysis [nm] Rapamycin=Without

Whole Model

Analysis of Variance

Source	DF	Squares	Prob > F

Parameter Estimates

Term	Estimate	Std Error	t Ratio	Prob>|t|
Intercept	105,32842	10,86728	9,69	<,0001*
FRR [-]	112	23,6703	4,73	0,0001*
TFR [µL/min]	0,0290236	0,011457	2,53	0,0203*
(TFR [µL/min]-490)*(FRR [-]-0,35)	0,2254517	0,079997	2,82	0,0110*
(FRR [-]-0,35)*(FRR [-]-0,35)	200	264,642	0,76	0,4591

Effect Tests

Source	Nparm	DF	Sum of Squares	F Ratio	Prob > F
FRR [-]	1	1	3763,2000	22,3887	0,0001*
TFR [µL/min]	1	1	1078,6635	6,4174	0,0203*
TFR [µL/min]*FRR [-]	1	1	1335,0236	7,9426	0,0110*
FRR [-]*FRR [-]	1	1	96,0000	0,5711	0,4591

Residual Normal Quantile Plot

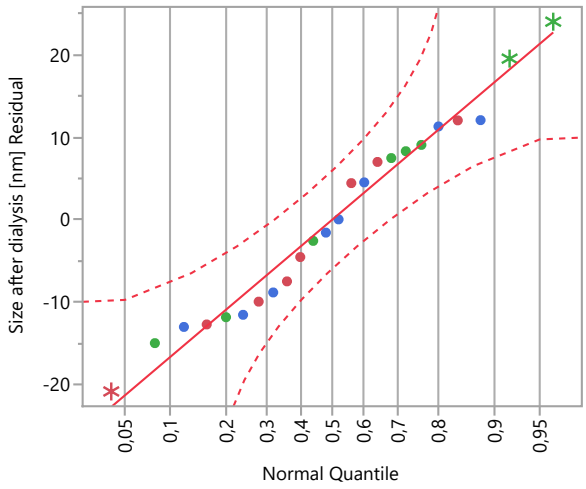

FRR [-]

Leverage Plot

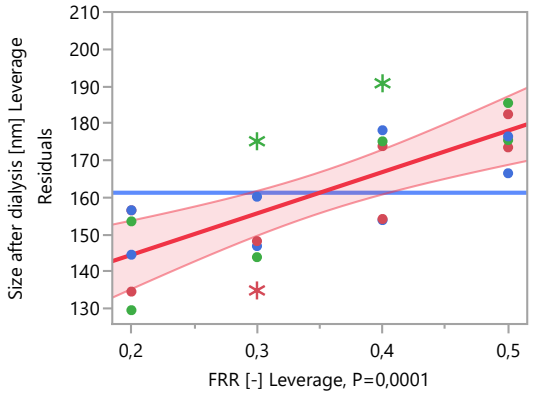

TFR [µL/min]

Leverage Plot

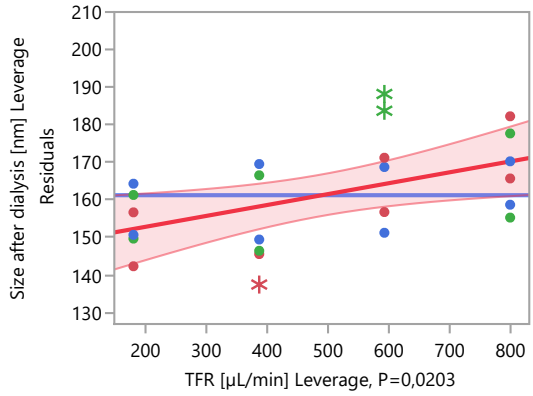

Figure C.8: Basic model of size NPs (cont.)

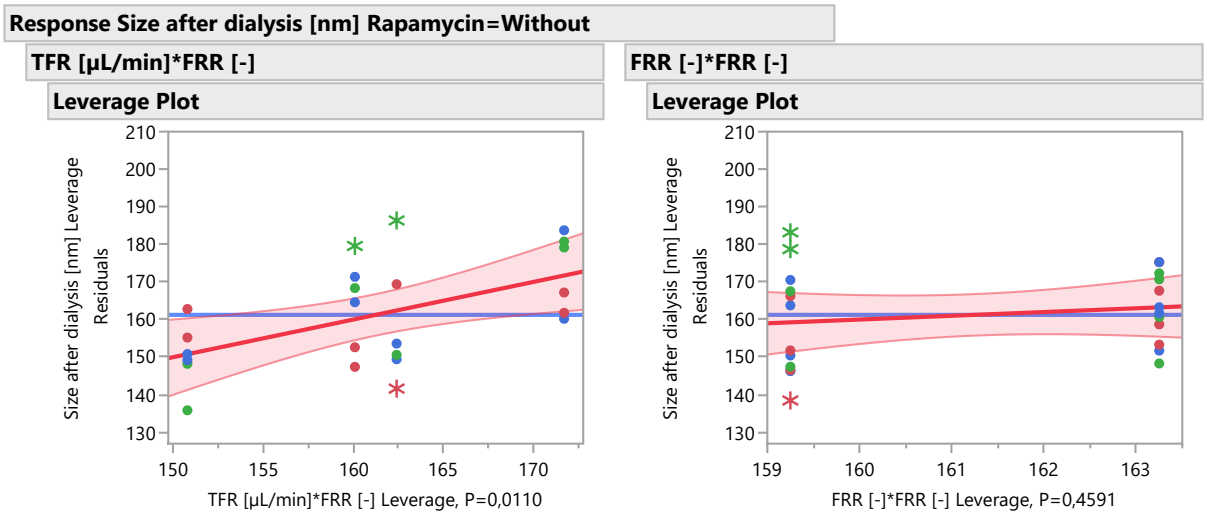

Figure C.9: Basic model of size NPs (cont.)

C.6.1.2 Improved model of NPs size

Response Size after dialysis [nm] Rapamycin=With

Whole Model

Actual by Predicted Plot

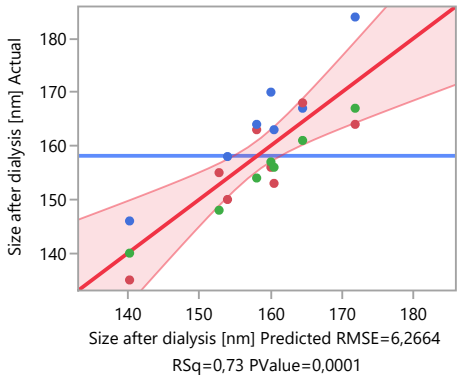

Effect Summary

Source	Logworth	PValue
FRR [-]	4,046	0,00009
TFR [µL/min]	2,430	0,00372
FRR [-]*FRR [-]	0,555	0,27852
TFR [µL/min]*FRR [-]	0,034	0,92419

Lack Of Fit

Source	DF	Sum of Squares	Mean Square	F Ratio
Lack Of Fit	3	53,71876	17,9063	0,4084
Pure Error	14	613,83333	43,8452	**Prob > F**
Total Error	17	667,55210		0,7494
				Max RSq
				0,7477

Residual by Predicted Plot

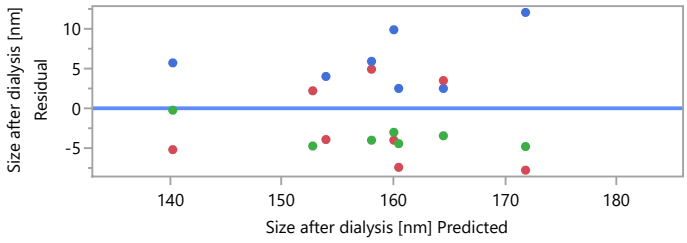

Summary of Fit

RSquare	0,72558
RSquare Adj	0,66101
Root Mean Square Error	6,2664
Mean of Response	158,1364
Observations (or Sum Wgts)	22

Analysis of Variance

Source	DF	Sum of Squares	Mean Square	F Ratio
Model	4	1765,0388	441,260	11,2372
Error	17	667,5521	39,268	**Prob > F**
C. Total	21	2432,5909		0,0001*

Figure C.10: Improved model of size NPs

Response Size after dialysis [nm] Rapamycin=With

Whole Model

Parameter Estimates

Term	Estimate	Std Error	t Ratio	Prob>|t|
Intercept	128,30864	5,745178	22,33	<,0001*
FRR [-]	62,076521	12,18439	5,09	<,0001*
TFR [µL/min]	0,0195934	0,005832	3,36	0,0037*
(TFR [µL/min]-480,591)*(FRR [-]-0,35909)	-0,003955	0,040951	-0,10	0,9242
(FRR [-]-0,35909)*(FRR [-]-0,35909)	-150,7584	134,6715	-1,12	0,2785

Effect Tests

Source	Nparm	DF	Sum of Squares	F Ratio	Prob > F
FRR [-]	1	1	1019,2563	25,9566	<,0001*
TFR [µL/min]	1	1	443,2317	11,2874	0,0037*
TFR [µL/min]*FRR [-]	1	1	0,3663	0,0093	0,9242
FRR [-]*FRR [-]	1	1	49,2094	1,2532	0,2785

Residual Normal Quantile Plot

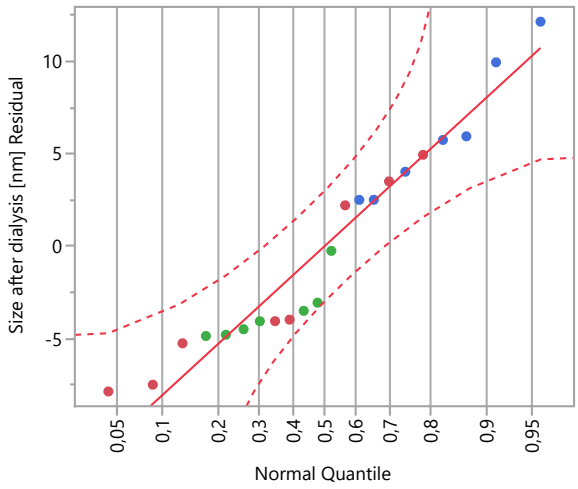

FRR [-]

Leverage Plot

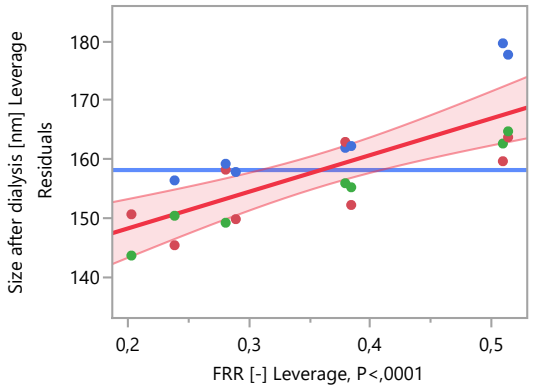

TFR [µL/min]

Leverage Plot

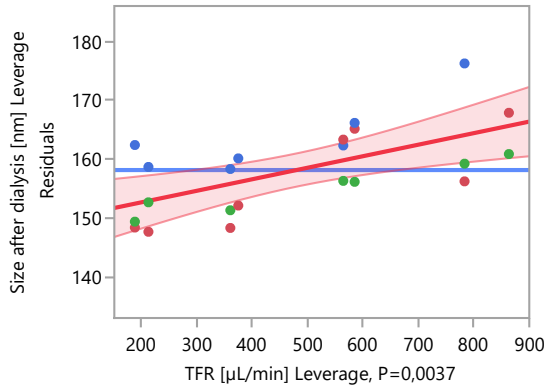

Figure C.11: Improved model of size NPs (cont.)

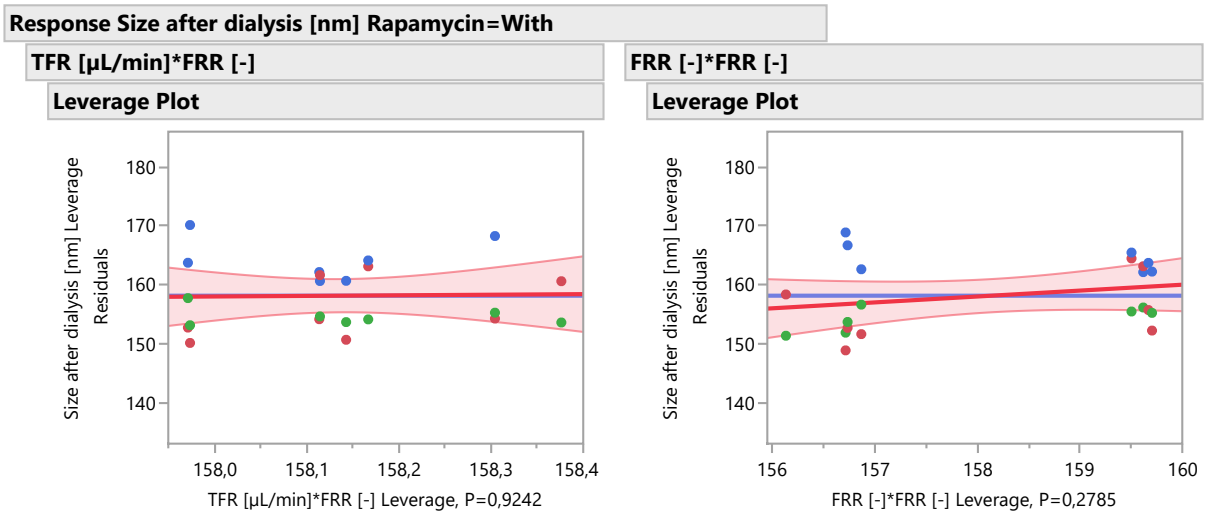

Figure C.12: Improved model of size NPs (cont.)

Response Size after dialysis [nm] Rapamycin=Without

Whole Model

Actual by Predicted Plot

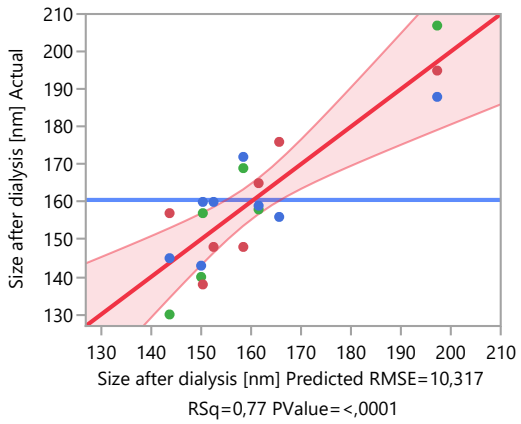

Effect Summary

Source	Logworth	PValue
FRR [-]	4,455	0,00004
TFR [µL/min]*FRR [-]	2,601	0,00250
TFR [µL/min]	1,715	0,01929 ^
FRR [-]*FRR [-]	0,773	0,16870

Lack Of Fit

Source	DF	Sum of Squares	Mean Square	F Ratio
Lack Of Fit	3	220,3880	73,463	0,6442
Pure Error	13	1482,5000	114,038	**Prob > F**
Total Error	16	1702,8880		0,6002
				Max RSq
				0,7981

Residual by Predicted Plot

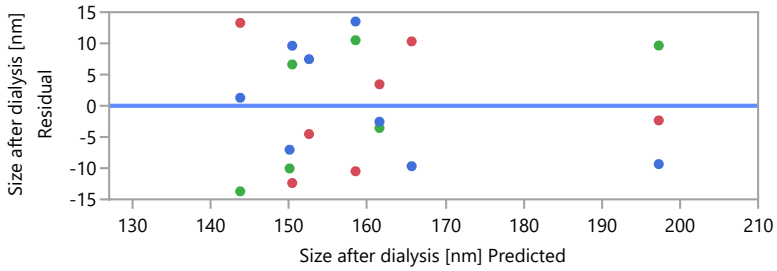

Summary of Fit

RSquare	0,768101
RSquare Adj	0,710127
Root Mean Square Error	10,31652
Mean of Response	160,5238
Observations (or Sum Wgts)	21

Analysis of Variance

Source	DF	Sum of Squares	Mean Square	F Ratio
Model	4	5640,3501	1410,09	13,2489
Error	16	1702,8880	106,43	**Prob > F**
C. Total	20	7343,2381		<,0001*

Figure C.13: Improved model of size NPs (cont.)

Response Size after dialysis [nm] Rapamycin=Without

Whole Model

Analysis of Variance

Source	DF	Squares	Prob > F

Parameter Estimates

Term	Estimate	Std Error	t Ratio	Prob>|t|
Intercept	106,13235	9,154868	11,59	<,0001*
FRR [-]	108,46109	19,14253	5,67	<,0001*
TFR [µL/min]	0,0240307	0,009238	2,60	0,0193*
(TFR [µL/min]-485,095)*(FRR [-]-0,35238)	0,2282352	0,063757	3,58	0,0025*
(FRR [-]-0,35238)*(FRR [-]-0,35238)	328,09061	227,5871	1,44	0,1687

Effect Tests

Source	Nparm	DF	Sum of Squares	F Ratio	Prob > F
FRR [-]	1	1	3416,7680	32,1033	<,0001*
TFR [µL/min]	1	1	720,2206	6,7671	0,0193*
TFR [µL/min]*FRR [-]	1	1	1363,8759	12,8147	0,0025*
FRR [-]*FRR [-]	1	1	221,1864	2,0782	0,1687

Residual Normal Quantile Plot

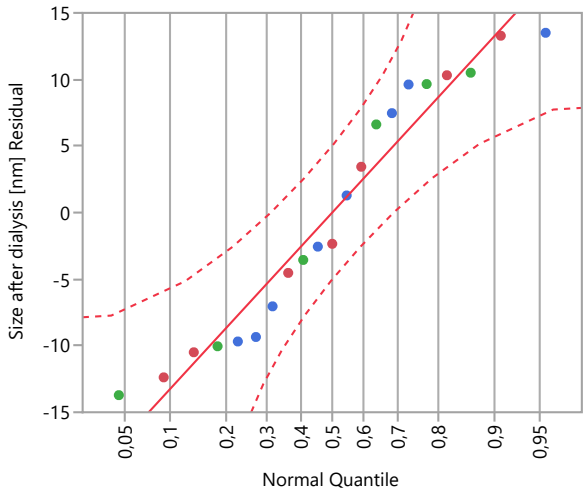

FRR [-]

Leverage Plot

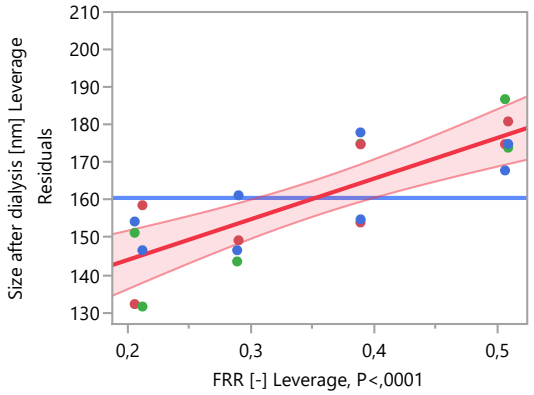

TFR [µL/min]

Leverage Plot

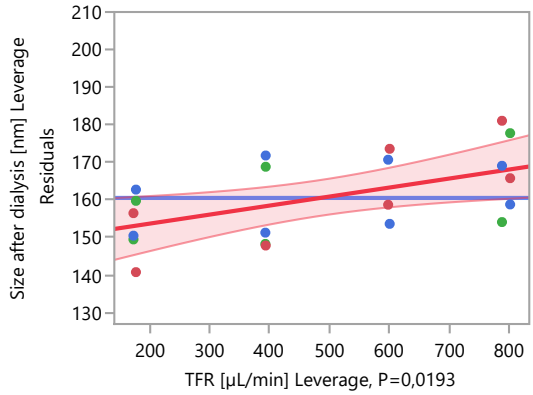

Figure C.14: Improved model of size NPs (cont.)

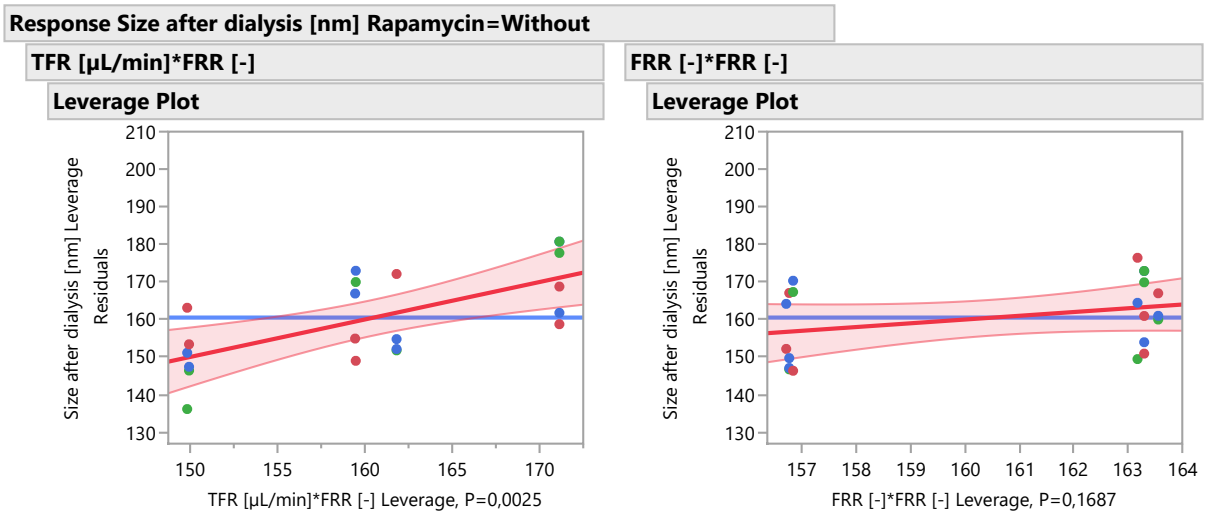

Figure C.15: Improved model of size NPs (cont.)

C.6.2 Models of NPs PDI

C.6.2.1 Basic model of NPs PDI

Response PDI after dialysis [-] Rapamycin=With

Whole Model

Actual by Predicted Plot

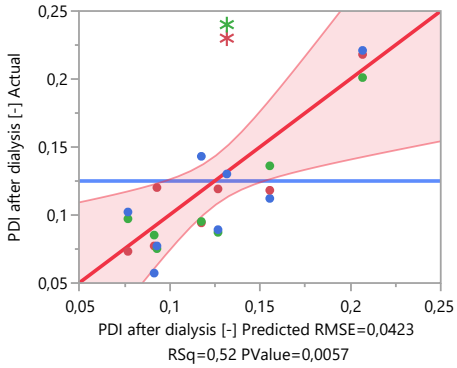

Effect Summary

Source	Logworth	PValue
FRR [-]	1,914	0,01218
FRR [-]*TFR [µL/min]	1,855	0,01397
TFR [µL/min]	1,344	0,04527 ^
FRR [-]*FRR [-]	0,431	0,37078

Lack Of Fit

Source	DF	Sum of Squares	Mean Square	F Ratio
Lack Of Fit	3	0,02166281	0,007221	9,3586
Pure Error	16	0,01234533	0,000772	Prob > F
Total Error	19	0,03400815		0,0008*
				Max RSq
				0,8251

Residual by Predicted Plot

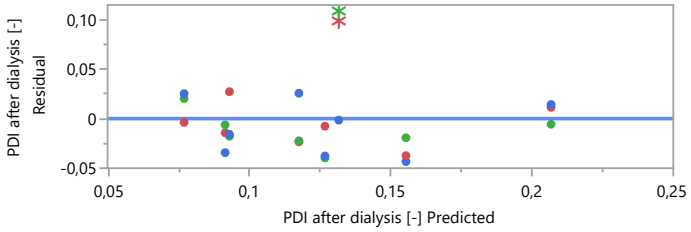

Summary of Fit

RSquare	0,518225
RSquare Adj	0,416799
Root Mean Square Error	0,042307
Mean of Response	0,124833
Observations (or Sum Wgts)	24

Analysis of Variance

Source	DF	Sum of Squares	Mean Square	F Ratio
Model	4	0,03658119	0,009145	5,1094
Error	19	0,03400815	0,001790	Prob > F
C. Total	23	0,07058933		0,0057*

Figure C.16: Basic model of NPs PDI

Response PDI after dialysis [-] Rapamycin=With

Whole Model

Parameter Estimates

Term	Estimate	Std Error	t Ratio	Prob>|t|
Intercept	0,1703693	0,035463	4,80	0,0001*
FRR [-]	-0,214	0,077242	-2,77	0,0122*
TFR [µL/min]	8,0122e-5	3,739e-5	2,14	0,0453*
(FRR [-]-0,35)*(TFR [µL/min]-490)	-0,000707	0,000261	-2,71	0,0140*
(FRR [-]-0,35)*(FRR [-]-0,35)	-0,791667	0,863593	-0,92	0,3708

Effect Tests

Source	Nparm	DF	Sum of Squares	F Ratio	Prob > F
FRR [-]	1	1	0,01373880	7,6757	0,0122*
TFR [µL/min]	1	1	0,00822029	4,5926	0,0453*
FRR [-]*TFR [µL/min]	1	1	0,01311793	7,3289	0,0140*
FRR [-]*FRR [-]	1	1	0,00150417	0,8404	0,3708

Residual Normal Quantile Plot

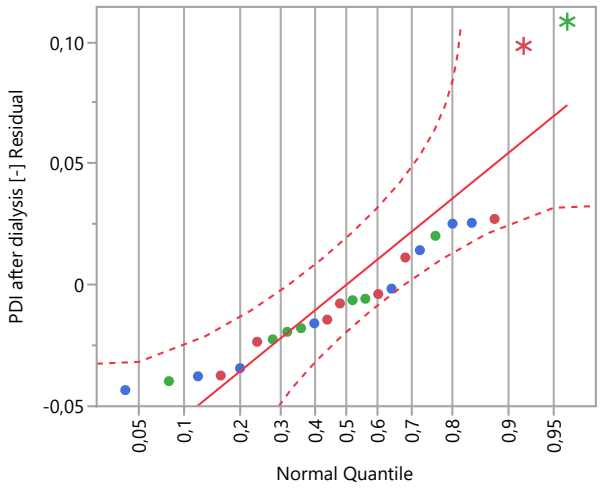

FRR [-]

Leverage Plot

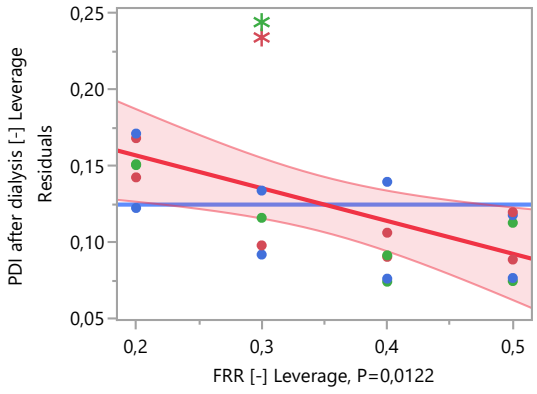

TFR [µL/min]

Leverage Plot

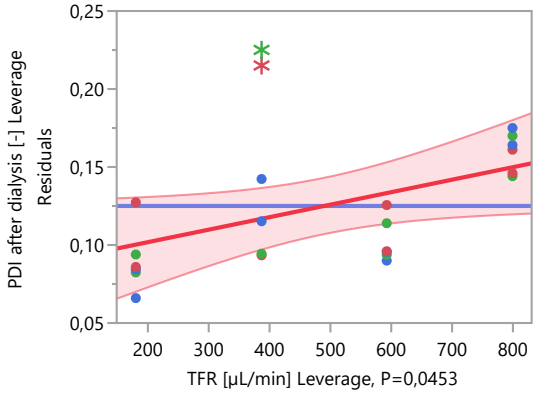

Figure C.17: Basic model of NPs PDI (cont.)

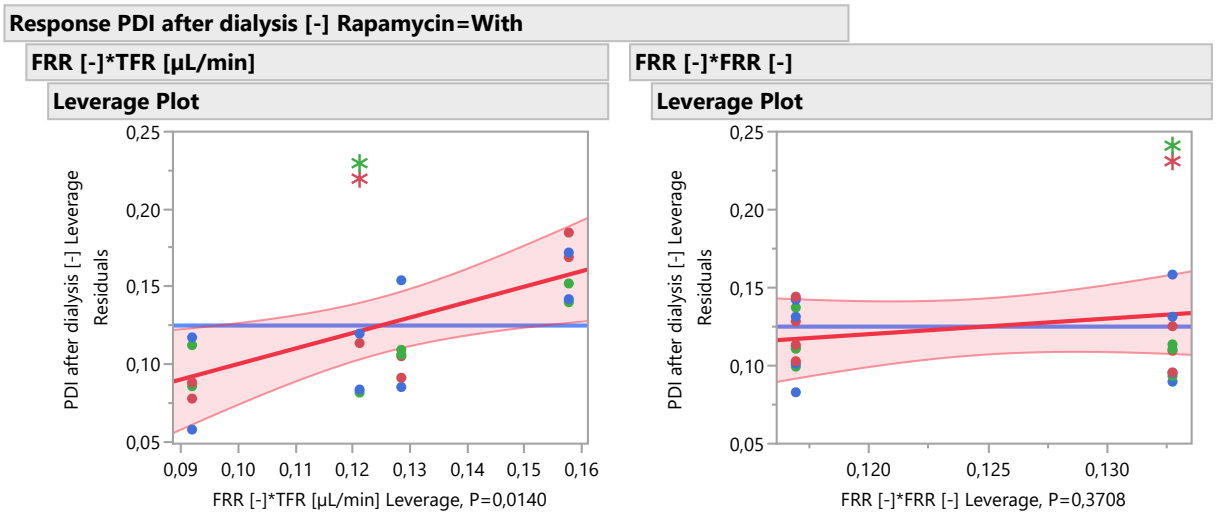

Figure C.18: Basic model of NPs PDI (cont.)

Response PDI after dialysis [-] Rapamycin=Without

Whole Model

Actual by Predicted Plot

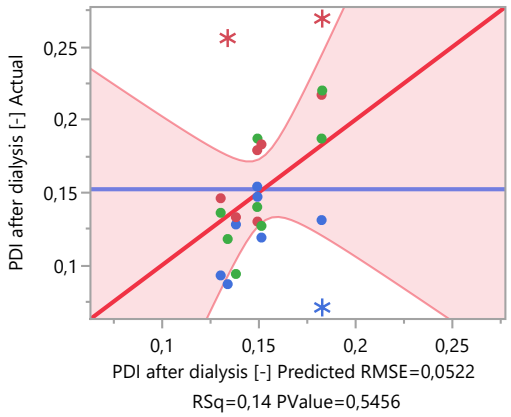

Effect Summary

Source	Logworth	PValue
TFR [µL/min]	0,820	0,15127
FRR [-]*FRR [-]	0,389	0,40806
FRR [-]	0,131	0,73922 ^
FRR [-]*TFR [µL/min]	0,120	0,75861

Lack Of Fit

Source	DF	Sum of Squares	Mean Square	F Ratio
Lack Of Fit	3	0,00304705	0,001016	0,3334
Pure Error	16	0,04874597	0,003047	Prob > F
Total Error	19	0,05179302		0,8014
				Max RSq
				0,1931

Residual by Predicted Plot

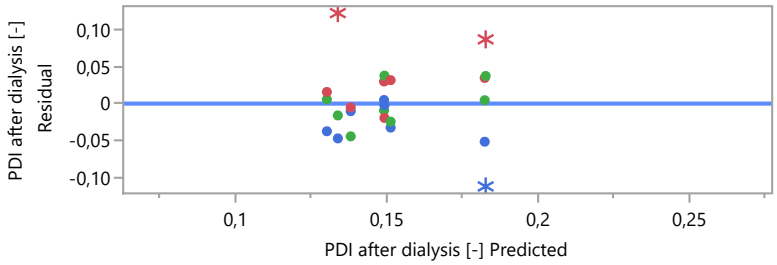

Summary of Fit

RSquare	0,142712
RSquare Adj	-0,03777
Root Mean Square Error	0,052211
Mean of Response	0,152183
Observations (or Sum Wgts)	24

Analysis of Variance

Source	DF	Sum of Squares	Mean Square	F Ratio
Model	4	0,00862193	0,002155	0,7907
Error	19	0,05179302	0,002726	Prob > F
C. Total	23	0,06041495		0,5456

Figure C.19: Basic model of NPs PDI (cont.)

Response PDI after dialysis [-] Rapamycin=Without

Whole Model

Analysis of Variance

Source	DF	Squares	Prob > F

Parameter Estimates

Term	Estimate	Std Error	t Ratio	Prob>|t|
Intercept	0,0958375	0,043764	2,19	0,0412*
FRR [-]	0,0322	0,095323	0,34	0,7392
TFR [µL/min]	6,899e-5	4,614e-5	1,50	0,1513
(FRR [-]-0,35)*(TFR [µL/min]-490)	-0,0001	0,000322	-0,31	0,7586
(FRR [-]-0,35)*(FRR [-]-0,35)	0,9016667	1,065745	0,85	0,4081

Effect Tests

Source	Nparm	DF	Sum of Squares	F Ratio	Prob > F
FRR [-]	1	1	0,00031105	0,1141	0,7392
TFR [µL/min]	1	1	0,00609470	2,2358	0,1513
FRR [-]*TFR [µL/min]	1	1	0,00026497	0,0972	0,7586
FRR [-]*FRR [-]	1	1	0,00195121	0,7158	0,4081

Residual Normal Quantile Plot

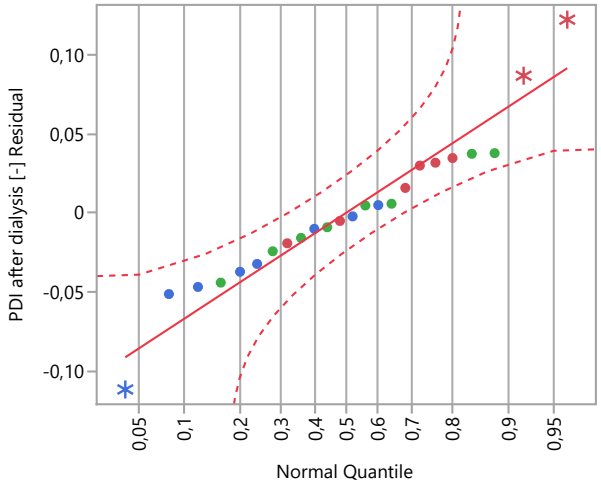

FRR [-]

Leverage Plot

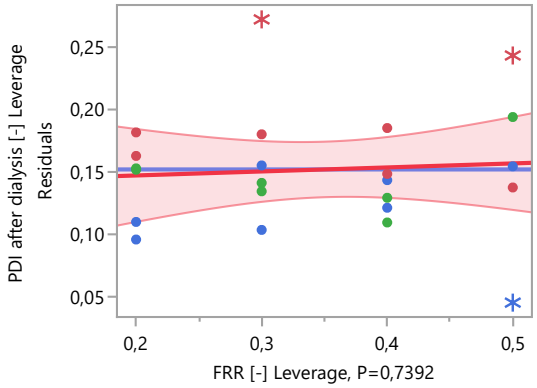

TFR [µL/min]

Leverage Plot

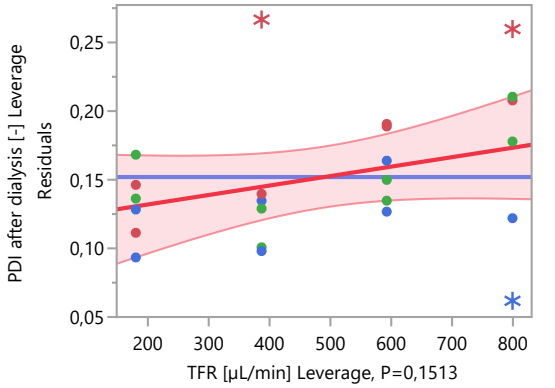

Figure C.20: Basic model of NPs PDI (cont.)

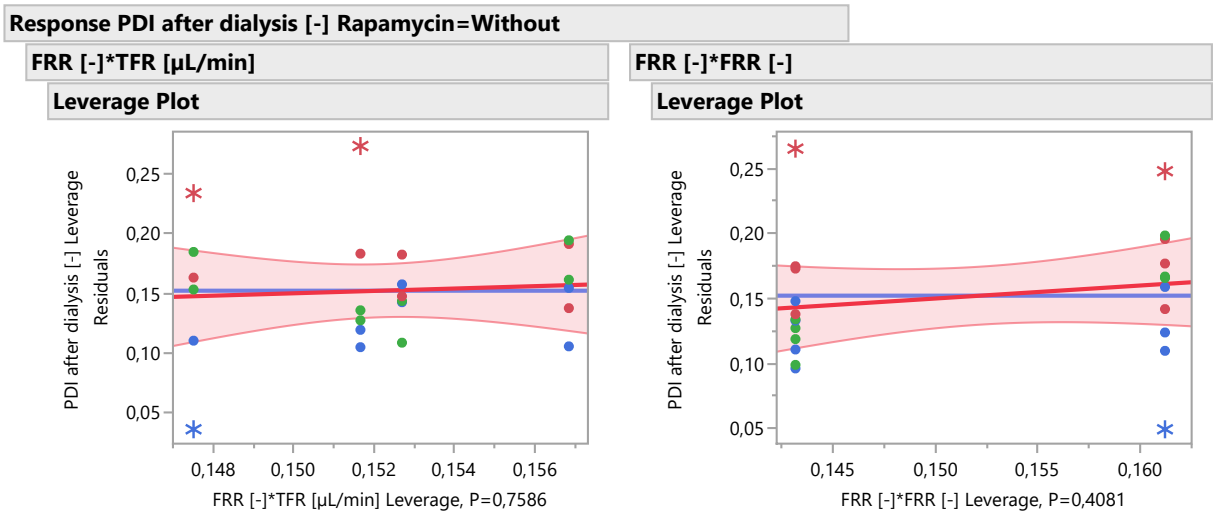

Figure C.21: Basic model of NPs PDI (cont.)

C.6.2.2 Improved model of NPs PDI

Response PDI after dialysis [-] Rapamycin=With

Whole Model

Actual by Predicted Plot

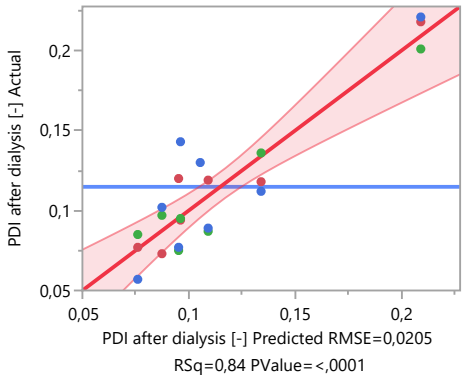

Effect Summary

Source	Logworth	PValue
FRR [-]*TFR [µL/min]	4,828	0,00001
TFR [µL/min]	4,255	0,00006 ^
FRR [-]	3,582	0,00026 ^
FRR [-]*FRR [-]	0,283	0,52061

Lack Of Fit

Source	DF	Sum of Squares	Mean Square	F Ratio
Lack Of Fit	3	0,00219767	0,000733	2,0738
Pure Error	14	0,00494533	0,000353	**Prob > F**
Total Error	17	0,00714300		0,1498
				Max RSq
				0,8878

Residual by Predicted Plot

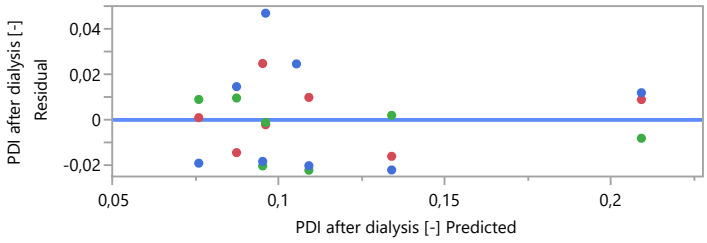

Summary of Fit

RSquare	0,837877
RSquare Adj	0,799731
Root Mean Square Error	0,020498
Mean of Response	0,114818
Observations (or Sum Wgts)	22

Analysis of Variance

Source	DF	Sum of Squares	Mean Square	F Ratio
Model	4	0,03691627	0,009229	21,9647
Error	17	0,00714300	0,000420	**Prob > F**
C. Total	21	0,04405927		<,0001*

Figure C.22: Improved model of NPs PDI

Response PDI after dialysis [-] Rapamycin=With

Whole Model

Parameter Estimates

Term	Estimate	Std Error	t Ratio	Prob>|t|
Intercept	0,1240062	0,018848	6,58	<,0001*
FRR [-]	-0,175266	0,038206	-4,59	0,0003*
TFR [µL/min]	9,753e-5	1,831e-5	5,33	<,0001*
(FRR [-]-0,35455)*(TFR [µL/min]-499,364)	-0,000758	0,000127	-5,98	<,0001*
(FRR [-]-0,35455)*(FRR [-]-0,35455)	0,2884518	0,439721	0,66	0,5206

Effect Tests

Source	Nparm	DF	Sum of Squares	F Ratio	Prob > F
FRR [-]	1	1	0,00884213	21,0438	0,0003*
TFR [µL/min]	1	1	0,01192621	28,3838	<,0001*
FRR [-]*TFR [µL/min]	1	1	0,01503470	35,7818	<,0001*
FRR [-]*FRR [-]	1	1	0,00018081	0,4303	0,5206

Residual Normal Quantile Plot

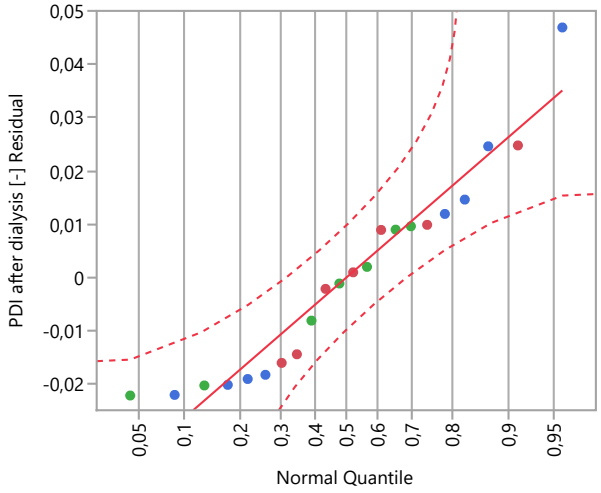

FRR [-]

Leverage Plot

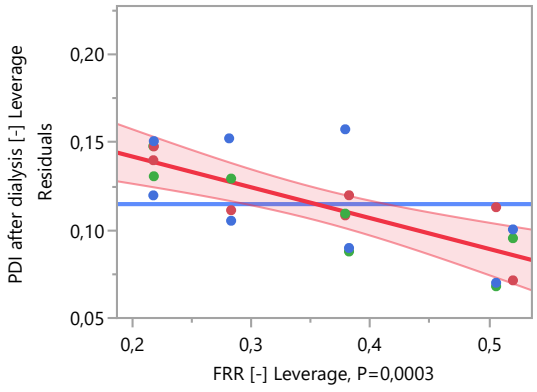

TFR [µL/min]

Leverage Plot

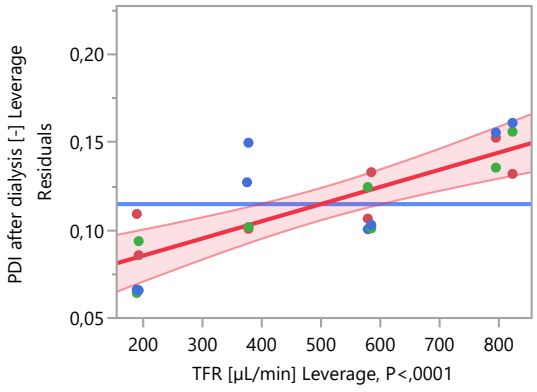

Figure C.23: Improved model of NPs PDI (cont.)

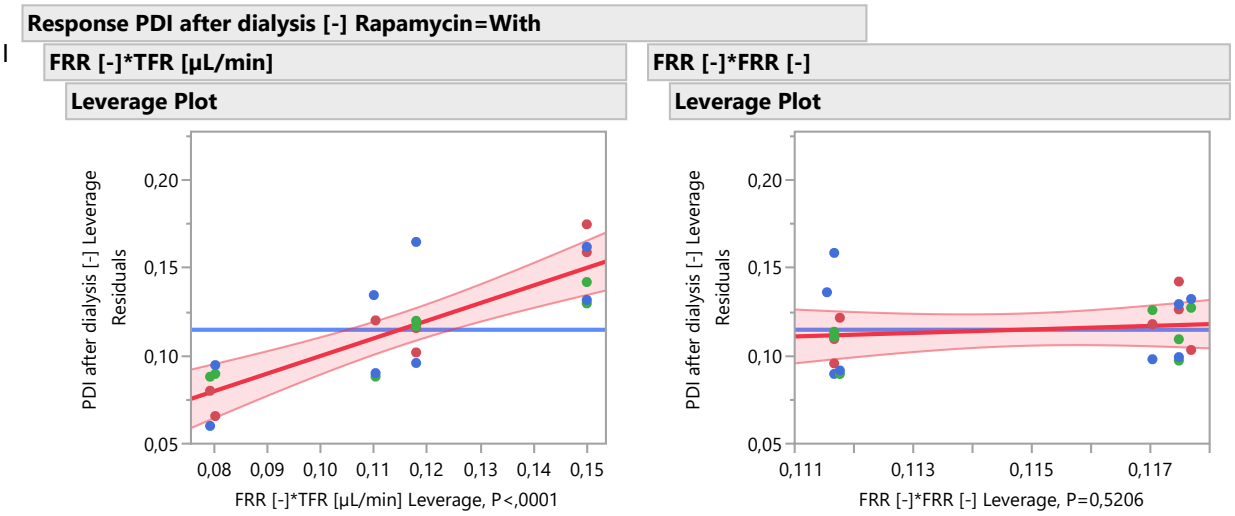

Figure C.24: Improved model of NPs PDI (cont.)

Response PDI after dialysis [-] Rapamycin=Without

Whole Model

Actual by Predicted Plot

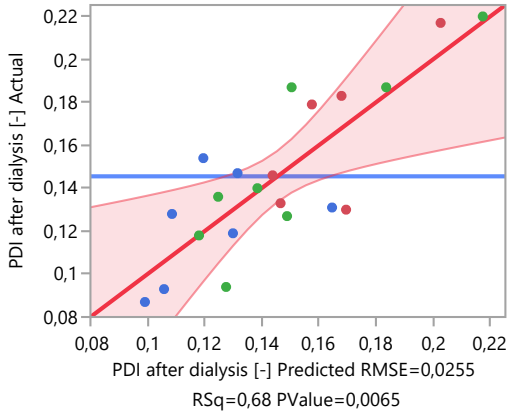

Effect Summary

Source	Logworth	PValue
TFR [µL/min]	2,689	0,00205
FRR [-]*FRR [-]	2,017	0,00962
N	1,256	0,05549
FRR [-]	0,501	0,31571 ^
FRR [-]*TFR [µL/min]	0,084	0,82440

Residual by Predicted Plot

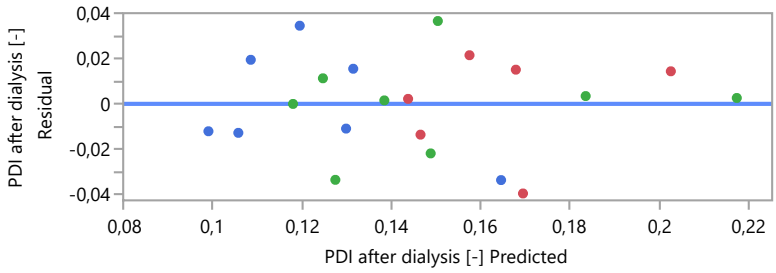

Summary of Fit

RSquare	0,679521
RSquare Adj	0,542173
Root Mean Square Error	0,025486
Mean of Response	0,145524
Observations (or Sum Wgts)	21

Analysis of Variance

Source	DF	Sum of Squares	Mean Square	F Ratio
Model	6	0,01928157	0,003214	4,9474
Error	14	0,00909367	0,000650	**Prob > F**
C. Total	20	0,02837524		0,0065*

Parameter Estimates

Term	Estimate	Std Error	t Ratio	Prob>|t|
Intercept	0,0596158	0,026296	2,27	0,0397*
FRR [-]	0,0555657	0,053399	1,04	0,3157
TFR [µL/min]	0,0001009	2,673e-5	3,78	0,0020*
(FRR [-]-0,3381)*(TFR [µL/min]-465,381)	0,0000436	0,000193	0,23	0,8244
(FRR [-]-0,3381)*(FRR [-]-0,3381)	1,7909542	0,597738	3,00	0,0096*
N[1]	0,0190285	0,008255	2,30	0,0370*

Figure C.25: Improved model of NPs PDI (cont.)

Response PDI after dialysis [-] Rapamycin=Without

Whole Model

Parameter Estimates

Term	Estimate	Std Error	t Ratio	Prob>|t|
N[2]	-4,28e-5	0,007881	-0,01	0,9957

Effect Tests

Source	Nparm	DF	Sum of Squares	F Ratio	Prob > F
FRR [-]	1	1	0,00070333	1,0828	0,3157
TFR [µL/min]	1	1	0,00925750	14,2522	0,0020*
FRR [-]*TFR [µL/min]	1	1	0,00003320	0,0511	0,8244
FRR [-]*FRR [-]	1	1	0,00583120	8,9773	0,0096*
N	2	2	0,00465115	3,5803	0,0555

Residual Normal Quantile Plot

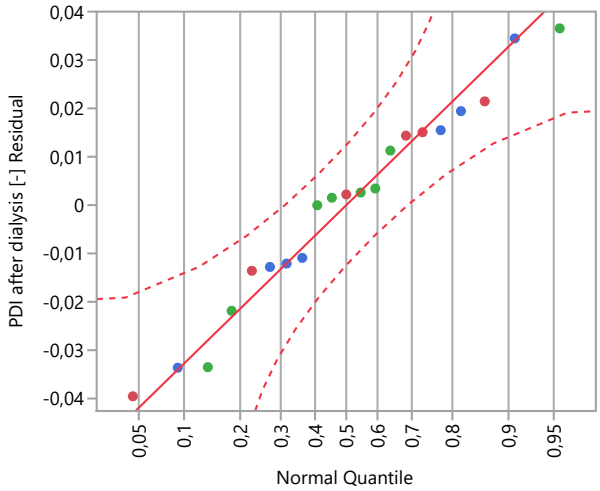

FRR [-]

Leverage Plot

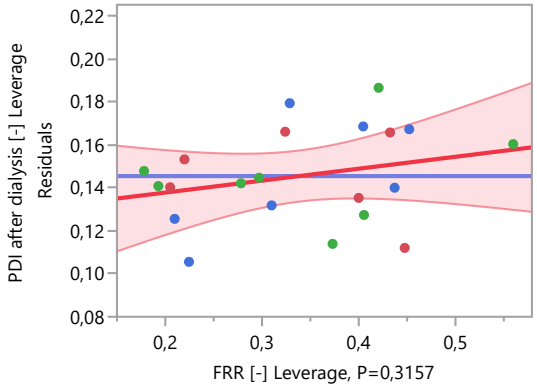

TFR [µL/min]

Leverage Plot

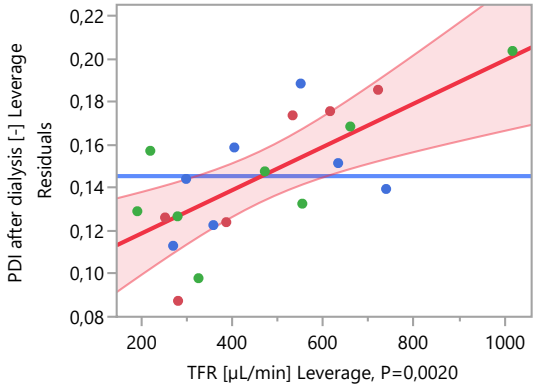

Figure C.26: Improved model of NPs PDI (cont.)

Response PDI after dialysis [-] Rapamycin=Without

FRR [-]*TFR [µL/min]

Leverage Plot

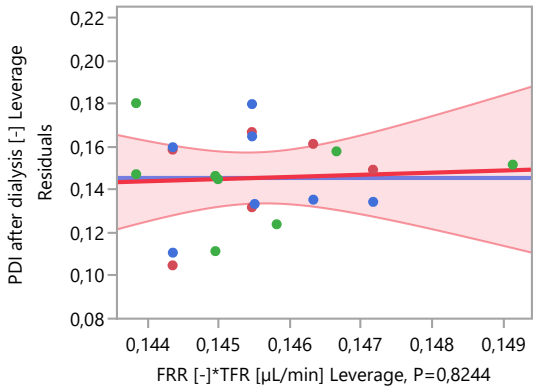

FRR [-]*FRR [-]

Leverage Plot

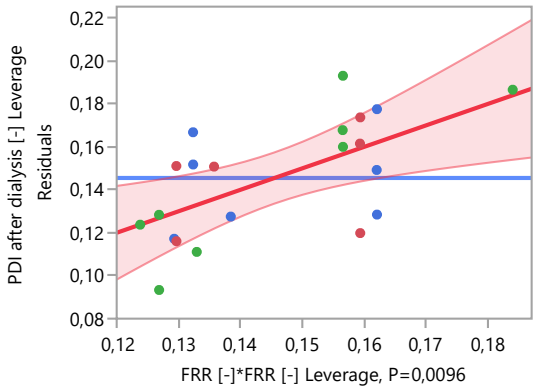

N

Leverage Plot

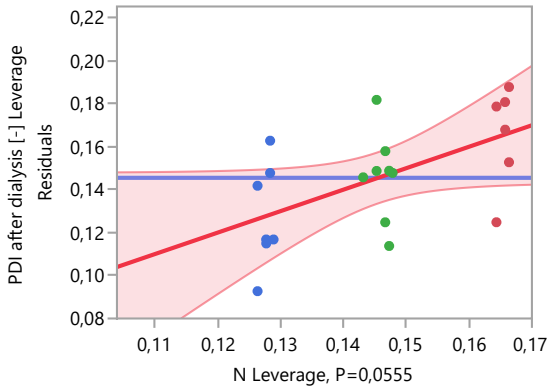

Least Squares Means Table

Level	Least Sq Mean	Std Error	Mean
1	0,14439672	0,01256748	0,164667
2	0,12532544	0,01191996	0,151125
3	0,10638256	0,01143245	0,122714

Figure C.27: Improved model of NPs PDI (cont.)

C.6.3 Models of NPs zeta potential

C.6.3.1 Basic model of NPs zeta potential

Response Zeta after dialysis [mV] Rapamycin=With

Whole Model

Actual by Predicted Plot

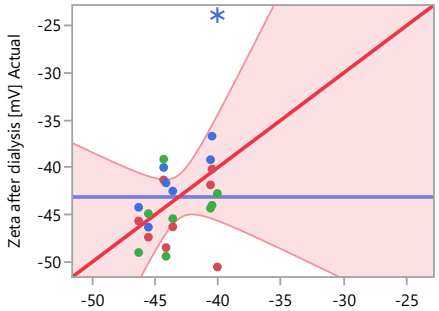

Effect Summary

Source	Logworth	PValue
FRR [-]*FRR [-]	0,576	0,26542
FRR [-]	0,529	0,29589 ^
FRR [-]*TFR [µL/min]	0,474	0,33602
TFR [µL/min]	0,415	0,38446 ^

Lack Of Fit

Source	DF	Sum of Squares	Mean Square	F Ratio
Lack Of Fit	3	81,42463	27,1415	0,9116
Pure Error	16	476,38933	29,7743	Prob > F
Total Error	19	557,81396		0,4574
				Max RSq
				0,3018

Residual by Predicted Plot

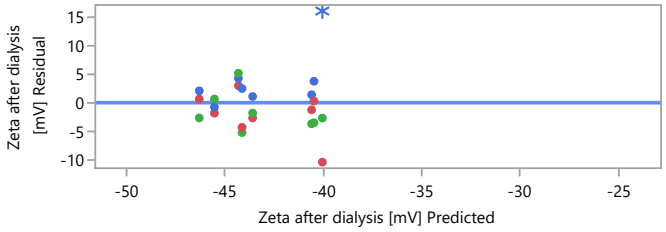

Summary of Fit

RSquare	0,182408
RSquare Adj	0,010283
Root Mean Square Error	5,41836
Mean of Response	-43,1292
Observations (or Sum Wgts)	24

Analysis of Variance

Source	DF	Sum of Squares	Mean Square	F Ratio
Model	4	124,45042	31,1126	1,0597
Error	19	557,81396	29,3586	Prob > F
C. Total	23	682,26438		0,4034

Figure C.28: Basic model of NPs zeta potential

Response Zeta after dialysis [mV] Rapamycin=With

Whole Model

Parameter Estimates

Term	Estimate	Std Error	t Ratio	Prob>|t|
Intercept	-43,08272	4,541762	-9,49	<,0001*
FRR [-]	-10,63333	9,892527	-1,07	0,2959
TFR [µL/min]	0,0042628	0,004788	0,89	0,3845
(FRR [-]-0,35)*(TFR [µL/min]-490)	0,033	0,033433	0,99	0,3360
(FRR [-]-0,35)*(FRR [-]-0,35)	126,91667	110,6018	1,15	0,2654

Effect Tests

Source	Nparm	DF	Sum of Squares	F Ratio	Prob > F
FRR [-]	1	1	33,920333	1,1554	0,2959
TFR [µL/min]	1	1	23,268453	0,7926	0,3845
FRR [-]*TFR [µL/min]	1	1	28,602819	0,9743	0,3360
FRR [-]*FRR [-]	1	1	38,658817	1,3168	0,2654

Residual Normal Quantile Plot

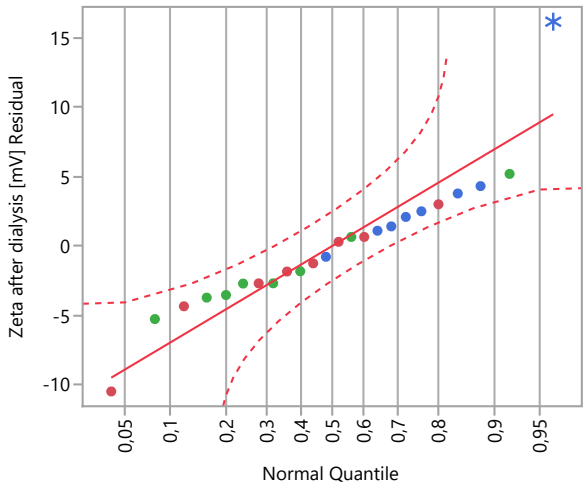

FRR [-]

Leverage Plot

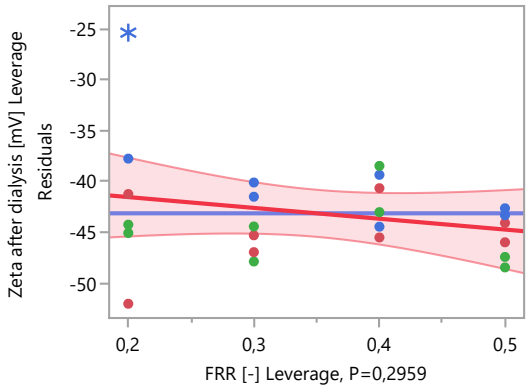

TFR [µL/min]

Leverage Plot

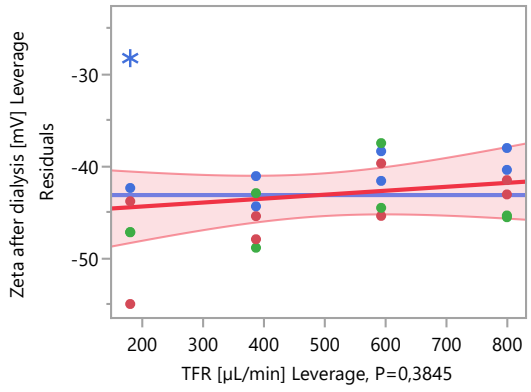

Figure C.29: Basic model of NPs zeta potential (cont.)

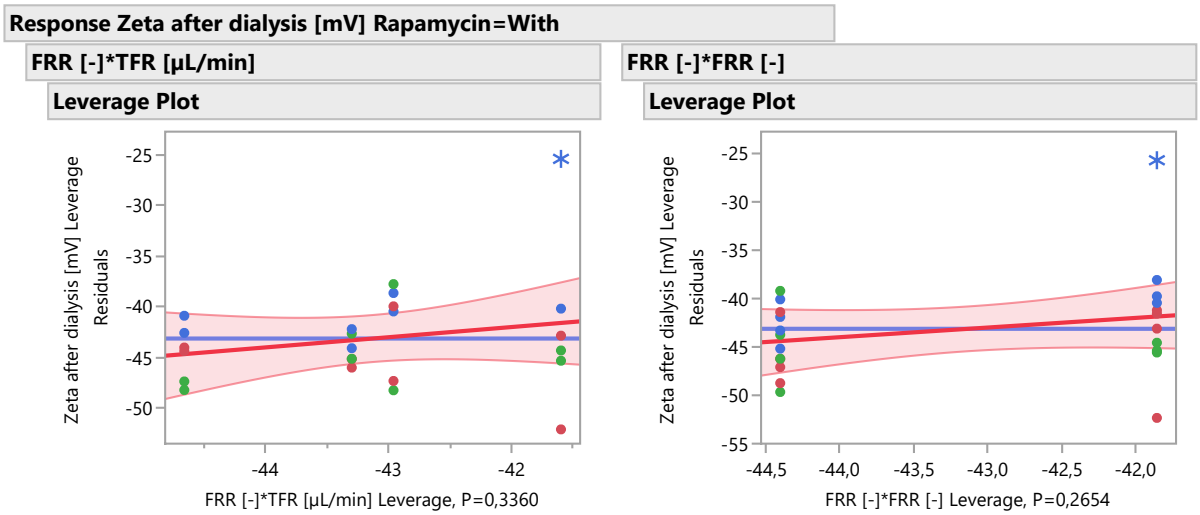

Figure C.30: Basic model of NPs zeta potential (cont.)

Response Zeta after dialysis [mV] Rapamycin=Without

Whole Model

Actual by Predicted Plot

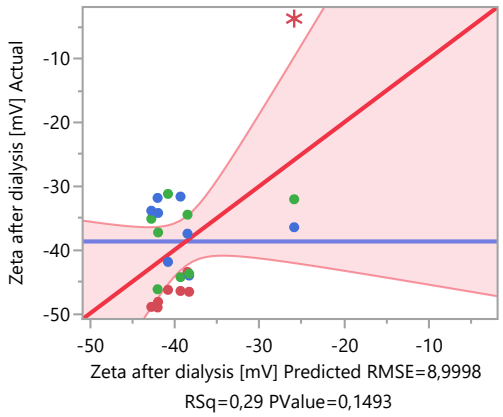

Effect Summary

Source	Logworth	PValue
TFR [µL/min]	0,991	0,10204
FRR [-]*TFR [µL/min]	0,809	0,15521
FRR [-]*FRR [-]	0,631	0,23365
FRR [-]	0,483	0,32870 ^

Lack Of Fit

Source	DF	Sum of Squares	Mean Square	F Ratio
Lack Of Fit	3	194,7988	64,9329	0,7729
Pure Error	16	1344,1320	84,0082	**Prob > F**
Total Error	19	1538,9308		0,5259
				Max RSq
				0,3776

Residual by Predicted Plot

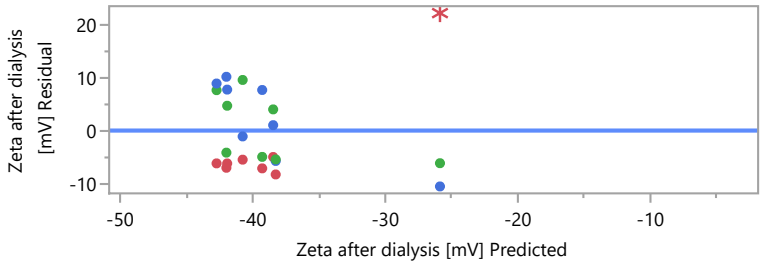

Summary of Fit

RSquare	0,287351
RSquare Adj	0,13732
Root Mean Square Error	8,999798
Mean of Response	-38,6618
Observations (or Sum Wgts)	24

Analysis of Variance

Source	DF	Sum of Squares	Mean Square	F Ratio
Model	4	620,5208	155,130	1,9153
Error	19	1538,9308	80,996	**Prob > F**
C. Total	23	2159,4516		0,1493

Figure C.31: Basic model of NPs zeta potential (cont.)

Response Zeta after dialysis [mV] Rapamycin=Without

Whole Model

Analysis of Variance

Source	DF	Squares	Prob > F

Parameter Estimates

Term	Estimate	Std Error	t Ratio	Prob>|t|
Intercept	-53,94739	7,543784	-7,15	<,0001*
FRR [-]	16,472333	16,43131	1,00	0,3287
TFR [µL/min]	0,0136641	0,007953	1,72	0,1020
(FRR [-]-0,35)*(TFR [µL/min]-490)	0,0821986	0,055532	1,48	0,1552
(FRR [-]-0,35)*(FRR [-]-0,35)	225,99167	183,7076	1,23	0,2336

Effect Tests

Source	Nparm	DF	Sum of Squares	F Ratio	Prob > F
FRR [-]	1	1	81,40133	1,0050	0,3287
TFR [µL/min]	1	1	239,08200	2,9518	0,1020
FRR [-]*TFR [µL/min]	1	1	177,46411	2,1910	0,1552
FRR [-]*FRR [-]	1	1	122,57336	1,5133	0,2336

Residual Normal Quantile Plot

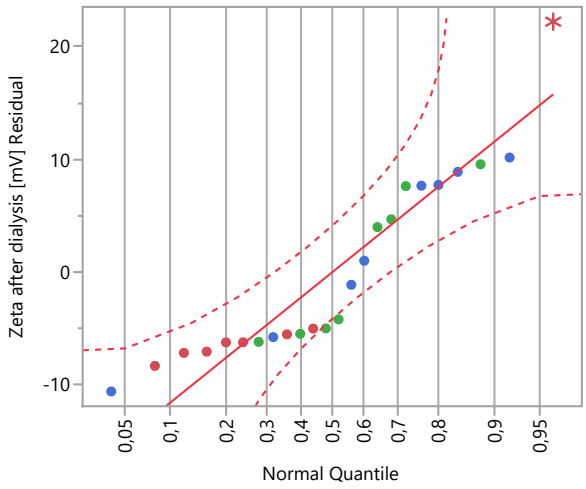

FRR [-]

Leverage Plot

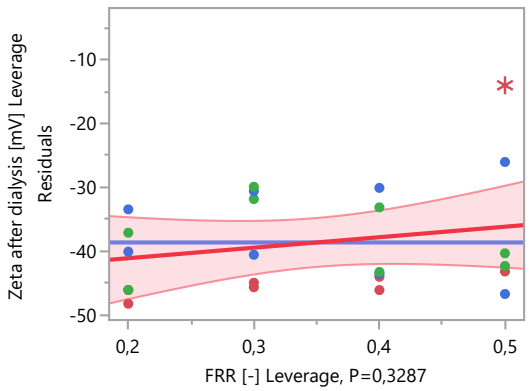

TFR [µL/min]

Leverage Plot

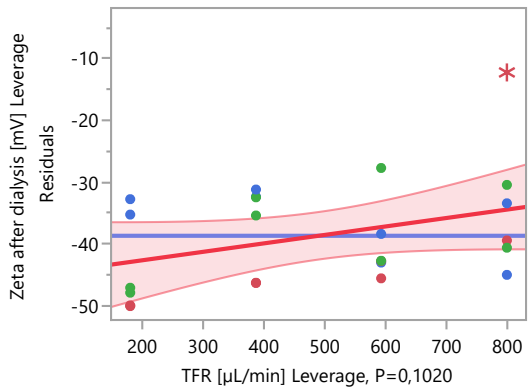

Figure C.32: Basic model of NPs zeta potential (cont.)

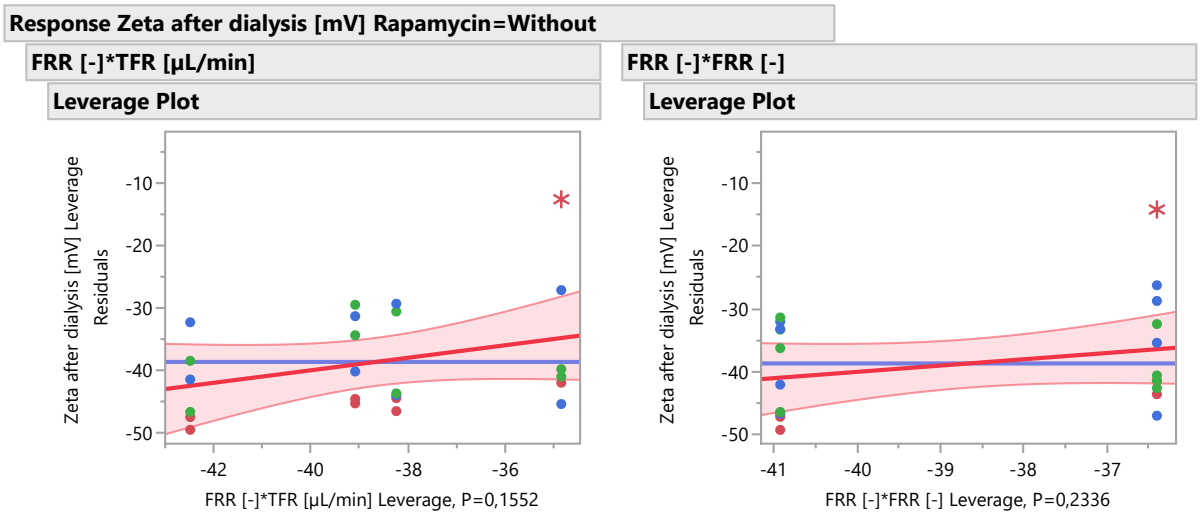

Figure C.33: Basic model of NPs zeta potential (cont.)

C.6.3.2 Improved model of NPs zeta potential

Response Zeta after dialysis [mV] Rapamycin=With

Whole Model

Actual by Predicted Plot

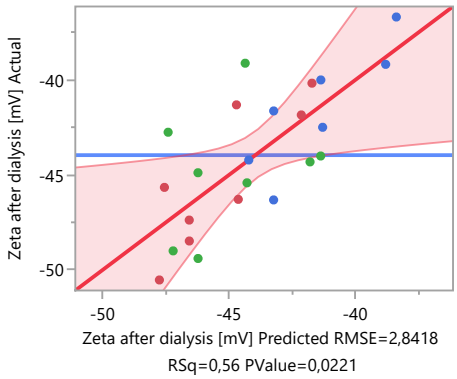

Effect Summary

Source	Logworth	PValue
TFR [µL/min]	2,503	0,00314
N	1,085	0,08227
FRR [-]*FRR [-]	0,301	0,49988
FRR [-]*TFR [µL/min]	0,065	0,86081
FRR [-]	0,008	0,98238 ^

Residual by Predicted Plot

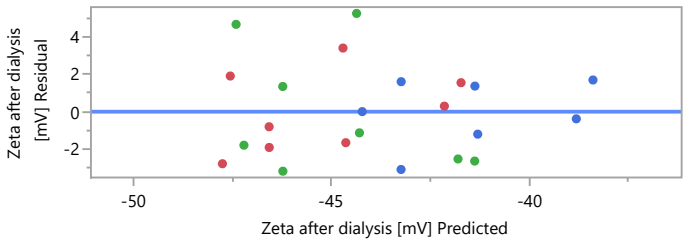

Summary of Fit

RSquare	0,564093
RSquare Adj	0,400628
Root Mean Square Error	2,841815
Mean of Response	-43,9652
Observations (or Sum Wgts)	23

Analysis of Variance

Source	DF	Sum of Squares	Mean Square	F Ratio
Model	6	167,21238	27,8687	3,4508
Error	16	129,21459	8,0759	Prob > F
C. Total	22	296,42697		0,0221*

Parameter Estimates

Term	Estimate	Std Error	t Ratio	Prob>|t|
Intercept	-49,0588	2,644201	-18,55	<,0001*
FRR [-]	0,1227688	5,471638	0,02	0,9824
TFR [µL/min]	0,0092092	0,002652	3,47	0,0031*
(FRR [-]-0,35652)*(TFR [µL/min]-503,478)	-0,003332	0,018697	-0,18	0,8608
(FRR [-]-0,35652)*(FRR [-]-0,35652)	41,40927	59,98556	0,69	0,4999

Figure C.34: Improved model of NPs zeta potential

Response Zeta after dialysis [mV] Rapamycin=With

Whole Model

Parameter Estimates

Term	Estimate	Std Error	t Ratio	Prob>|t|
N[1]	-1,227009	0,83446	-1,47	0,1608
N[2]	-0,882009	0,83446	-1,06	0,3062

Effect Tests

Source	Nparm	DF	Sum of Squares	F Ratio	Prob > F
FRR [-]	1	1	0,004066	0,0005	0,9824
TFR [µL/min]	1	1	97,369646	12,0568	0,0031*
FRR [-]*TFR [µL/min]	1	1	0,256433	0,0318	0,8608
FRR [-]*FRR [-]	1	1	3,848516	0,4765	0,4999
N	2	2	47,351556	2,9317	0,0823

Residual Normal Quantile Plot

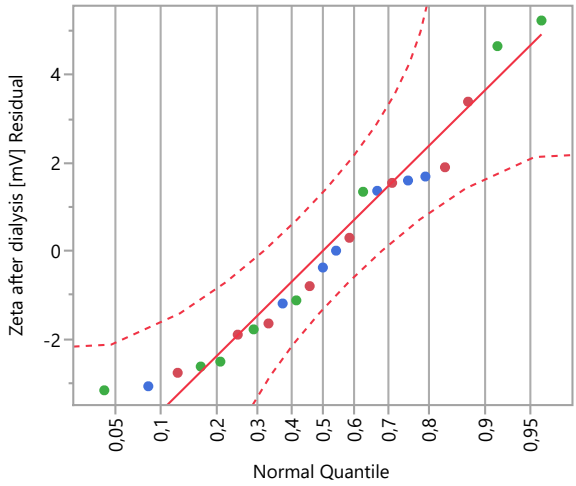

FRR [-]

Leverage Plot

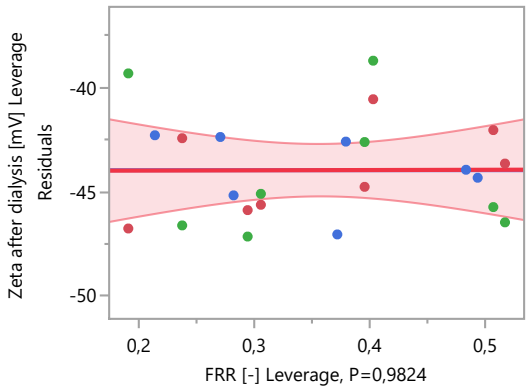

TFR [µL/min]

Leverage Plot

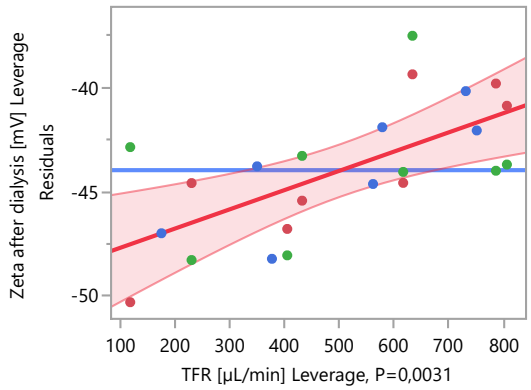

Figure C.35: Improved model of NPs zeta potential (cont.)

Response Zeta after dialysis [mV] Rapamycin=With

FRR [-]*TFR [µL/min]

Leverage Plot

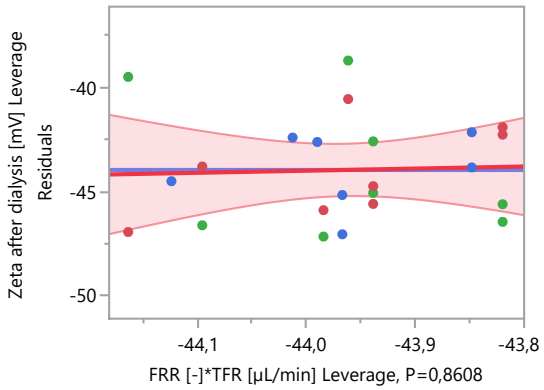

FRR [-]*FRR [-]

Leverage Plot

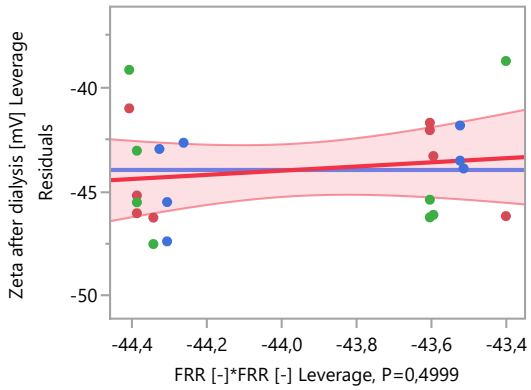

N

Leverage Plot

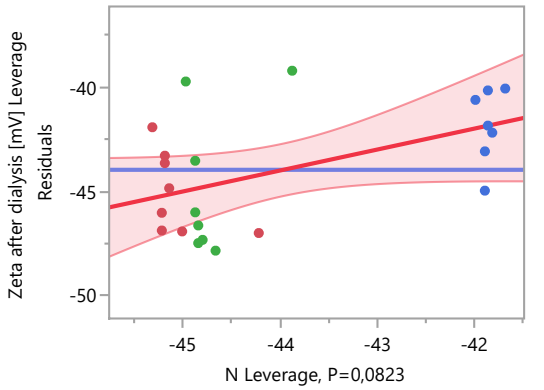

Least Squares Means Table

Level	Least Sq Mean	Std Error	Mean
1	-45,60541	1,2568296	-45,211
2	-45,26041	1,2568296	-44,866
3	-42,26938	1,2624647	-41,511

Figure C.36: Improved model of NPs zeta potential (cont.)

Response Zeta after dialysis [mV] Rapamycin=Without

Whole Model

Actual by Predicted Plot

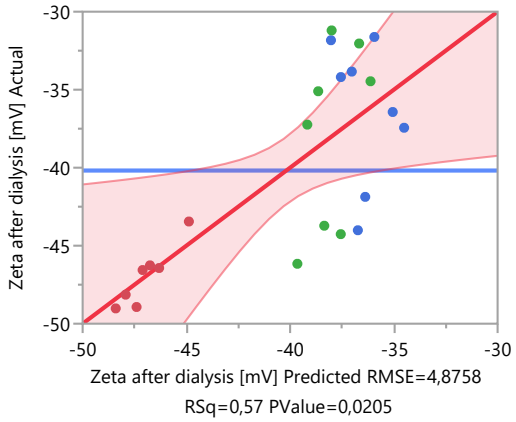

Effect Summary

Source	Logworth	PValue
N	2,666	0,00216
TFR [µL/min]	0,344	0,45256
FRR [-]	0,231	0,58790
FRR [-]*FRR [-]	0,208	0,61996
FRR [-]*TFR [µL/min]	0,097	0,79937

Residual by Predicted Plot

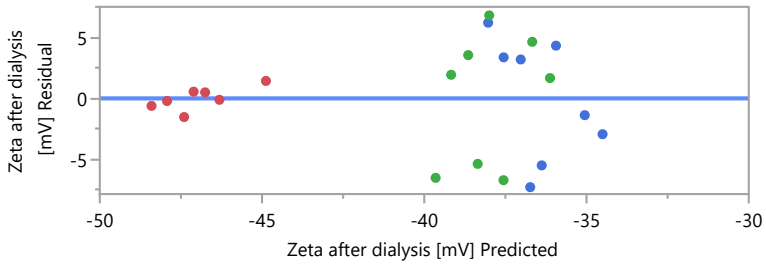

Summary of Fit

RSquare	0,569061
RSquare Adj	0,407459
Root Mean Square Error	4,87581
Mean of Response	-40,1826
Observations (or Sum Wgts)	23

Analysis of Variance

Source	DF	Sum of Squares	Mean Square	F Ratio
Model	6	502,29304	83,7155	3,5214
Error	16	380,37640	23,7735	Prob > F
C. Total	22	882,66944		0,0205*

Parameter Estimates

Term	Estimate	Std Error	t Ratio	Prob>|t|
Intercept	-40,95442	4,330604	-9,46	<,0001*
FRR [-]	-5,191601	9,387898	-0,55	0,5879
TFR [µL/min]	0,0035036	0,00455	0,77	0,4526
(FRR [-]-0,34348)*(TFR [µL/min]-476,522)	0,0082904	0,03208	0,26	0,7994
(FRR [-]-0,34348)*(FRR [-]-0,34348)	52,047372	102,9195	0,51	0,6200

Figure C.37: Improved model of NPs zeta potential (cont.)

Response Zeta after dialysis [mV] Rapamycin=Without

Whole Model

Parameter Estimates

Term	Estimate	Std Error	t Ratio	Prob>|t|
N[1]	-6,376136	1,501947	-4,25	0,0006*
N[2]	2,378693	1,431714	1,66	0,1161

Effect Tests

Source	Nparm	DF	Sum of Squares	F Ratio	Prob > F
FRR [-]	1	1	7,27042	0,3058	0,5879
TFR [µL/min]	1	1	14,09296	0,5928	0,4526
FRR [-]*TFR [µL/min]	1	1	1,58773	0,0668	0,7994
FRR [-]*FRR [-]	1	1	6,07989	0,2557	0,6200
N	2	2	438,93103	9,2315	0,0022*

Residual Normal Quantile Plot

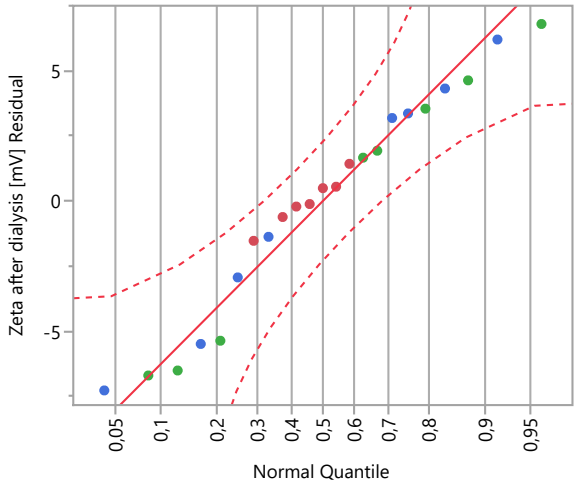

FRR [-]

Leverage Plot

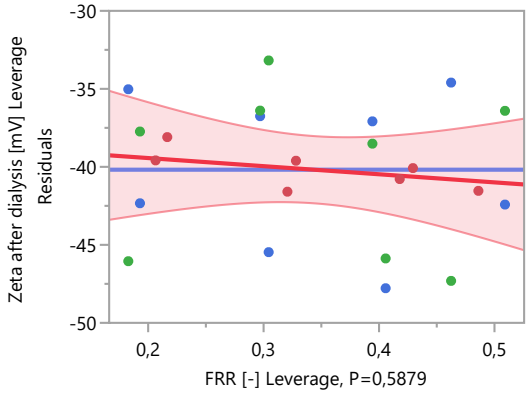

TFR [µL/min]

Leverage Plot

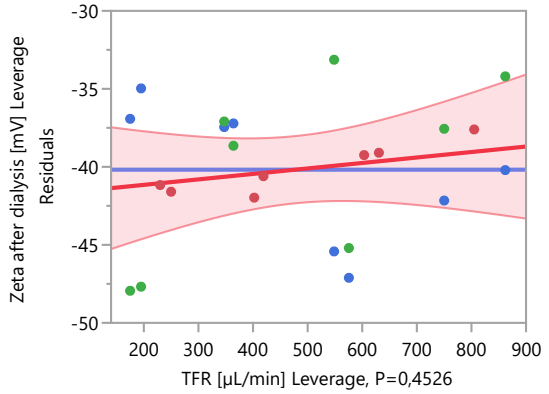

Figure C.38: Improved model of NPs zeta potential (cont.)

Response Zeta after dialysis [mV] Rapamycin=Without

FRR [-]*TFR [µL/min]

Leverage Plot

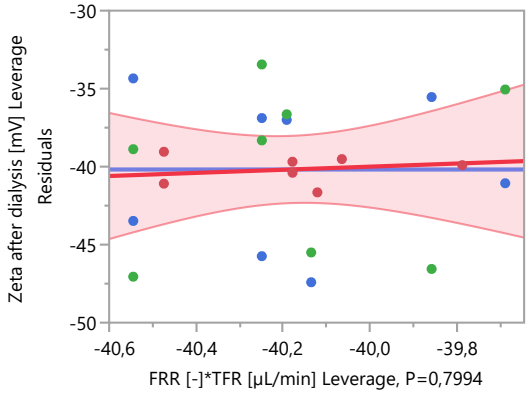

FRR [-]*FRR [-]

Leverage Plot

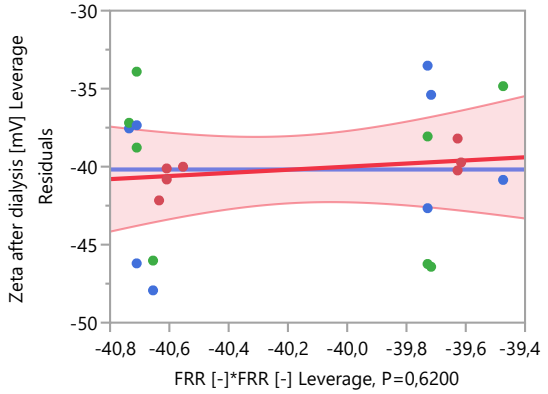

N

Leverage Plot

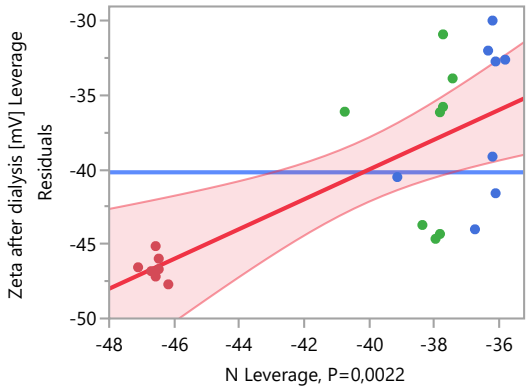

Least Squares Means Table

Level	Least Sq Mean	Std Error	Mean
1	-47,44423	2,1660589	-46,970
2	-38,68940	2,1563906	-38,023
3	-37,07065	2,1563906	-36,404

Figure C.39: Improved model of NPs zeta potential (cont.)

C.6.4 Models of NPs EE

C.6.4.1 Basic model of NPs EE

Response EE [%] Rapamycin=With

Whole Model

Actual by Predicted Plot

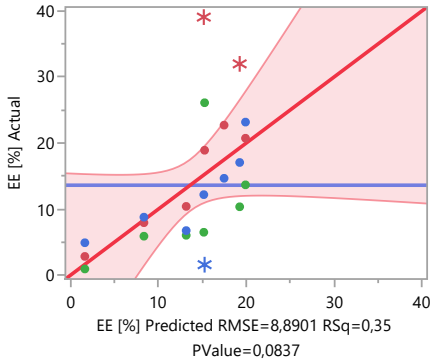

Effect Summary

Source	Logworth	PValue
FRR [-]	1,771	0,01694
FRR [-]*FRR [-]	0,706	0,19688
TFR [µL/min]	0,587	0,25904
FRR [-]*TFR [µL/min]	0,075	0,84168

Lack Of Fit

Source	DF	Sum of Squares	Mean Square	F Ratio
Lack Of Fit	3	150,8107	50,2702	0,5929
Pure Error	15	1271,8099	84,7873	Prob > F
Total Error	18	1422,6206		0,6292
				Max RSq
				0,4210

Residual by Predicted Plot

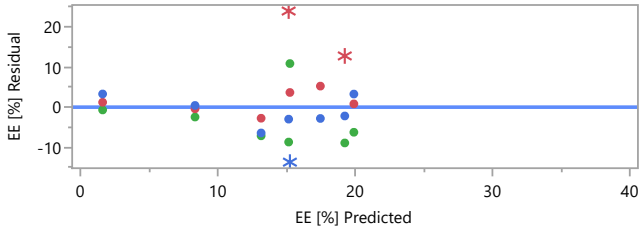

Summary of Fit

RSquare	0,352317
RSquare Adj	0,208388
Root Mean Square Error	8,890134
Mean of Response	13,60748
Observations (or Sum Wgts)	23

Analysis of Variance

Source	DF	Sum of Squares	Mean Square	F Ratio
Model	4	773,8576	193,464	2,4478
Error	18	1422,6206	79,034	Prob > F
C. Total	22	2196,4782		0,0837

Figure C.40: Basic model of NPs EE

Response EE [%] Rapamycin=With

Whole Model

Parameter Estimates

Term	Estimate	Std Error	t Ratio	Prob>|t|
Intercept	6,3339901	7,374704	0,86	0,4017
FRR [-]	43,006922	16,34333	2,63	0,0169*
TFR [µL/min]	-0,009199	0,007893	-1,17	0,2590
(FRR [-]-0,34783)*(TFR [µL/min]-485,522)	0,0111225	0,054886	0,20	0,8417
(FRR [-]-0,34783)*(FRR [-]-0,34783)	-248,7622	185,6266	-1,34	0,1969

Effect Tests

Source	Nparm	DF	Sum of Squares	F Ratio	Prob > F
FRR [-]	1	1	547,28358	6,9246	0,0169*
TFR [µL/min]	1	1	107,35591	1,3583	0,2590
FRR [-]*TFR [µL/min]	1	1	3,24561	0,0411	0,8417
FRR [-]*FRR [-]	1	1	141,94005	1,7959	0,1969

Residual Normal Quantile Plot

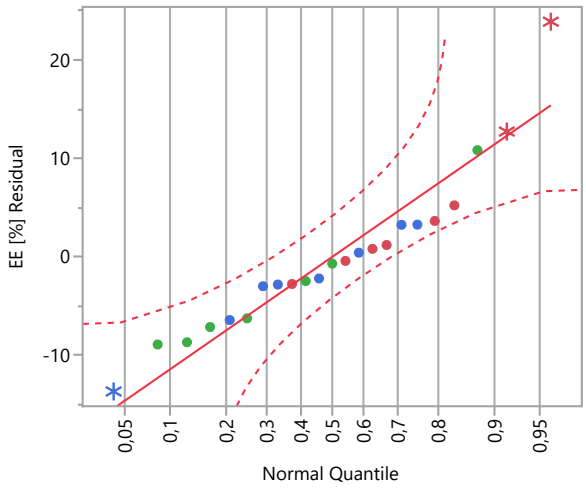

FRR [-]

Leverage Plot

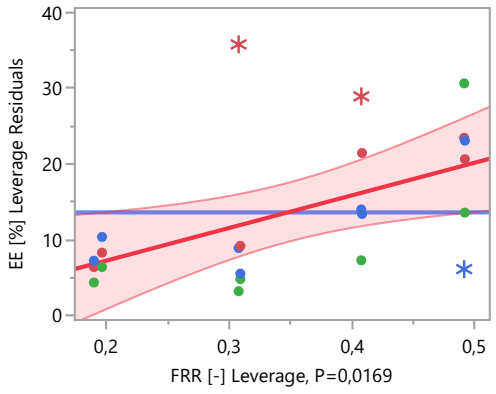

TFR [µL/min]

Leverage Plot

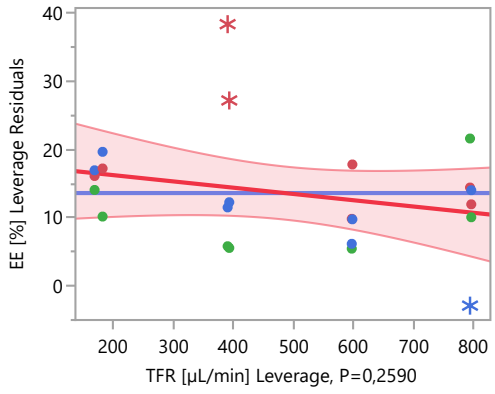

Figure C.41: Basic model of NPs EE (cont.)

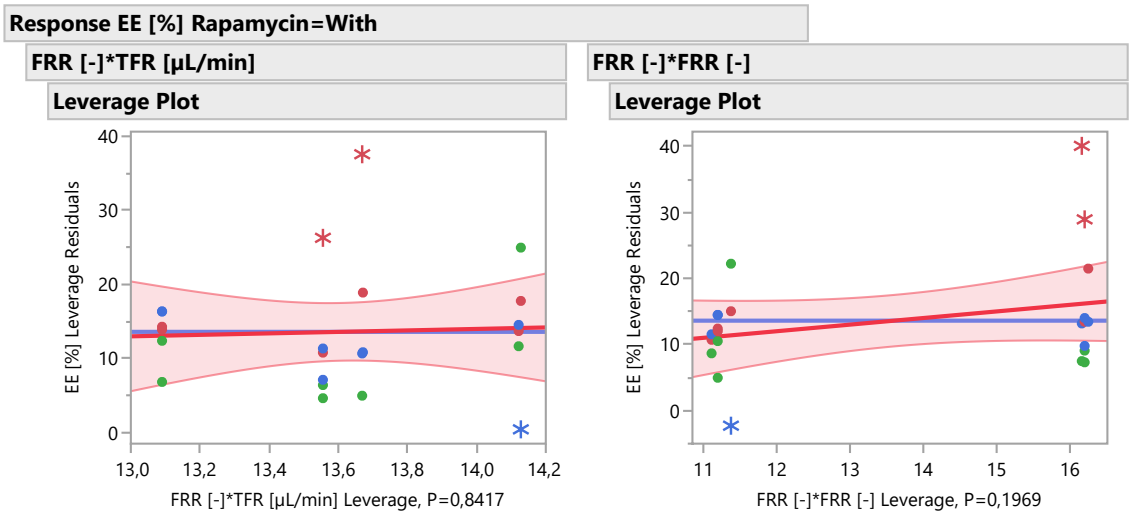

Figure C.42: Basic model of NPs EE (cont.)

C.6.4.2 Improved model of NPs EE

Response EE [%] Rapamycin=With

Whole Model

Actual by Predicted Plot

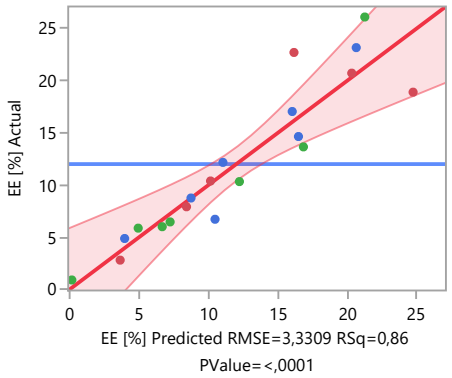

Effect Summary

Source	Logworth	PValue
FRR [-]	5,698	0,00000
FRR [-]*TFR [µL/min]	1,371	0,04260
N	0,991	0,10221
FRR [-]*FRR [-]	0,308	0,49151
TFR [µL/min]	0,092	0,80903 ^

Residual by Predicted Plot

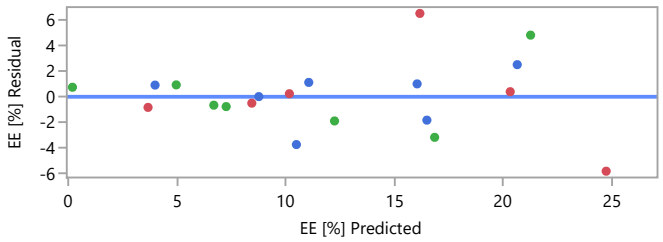

Summary of Fit

RSquare	0,858139
RSquare Adj	0,792664
Root Mean Square Error	3,330923
Mean of Response	12,01855
Observations (or Sum Wgts)	20

Analysis of Variance

Source	DF	Sum of Squares	Mean Square	F Ratio
Model	6	872,5010	145,417	13,1065
Error	13	144,2356	11,095	Prob > F
C. Total	19	1016,7366		<,0001*

Parameter Estimates

Term	Estimate	Std Error	t Ratio	Prob>|t|
Intercept	-6,282829	3,038613	-2,07	0,0592
FRR [-]	53,322753	6,599564	8,08	<,0001*
TFR [µL/min]	-0,000784	0,003178	-0,25	0,8090
(FRR [-]-0,34)*(TFR [µL/min]-479,65)	0,0493858	0,021973	2,25	0,0426*
(FRR [-]-0,34)*(FRR [-]-0,34)	54,691183	77,25983	0,71	0,4915

Figure C.43: Improved model of NPs EE

Response EE [%] Rapamycin=With

Whole Model

Parameter Estimates

Term	Estimate	Std Error	t Ratio	Prob>|t|
N[1]	1,0510947	1,114827	0,94	0,3630
N[2]	-2,424951	1,043401	-2,32	0,0370*

Effect Tests

Source	Nparm	DF	Sum of Squares	F Ratio	Prob > F
FRR [-]	1	1	724,30886	65,2822	<,0001*
TFR [µL/min]	1	1	0,67500	0,0608	0,8090
FRR [-]*TFR [µL/min]	1	1	56,04577	5,0514	0,0426*
FRR [-]*FRR [-]	1	1	5,55976	0,5011	0,4915
N	2	2	60,62638	2,7321	0,1022

Residual Normal Quantile Plot

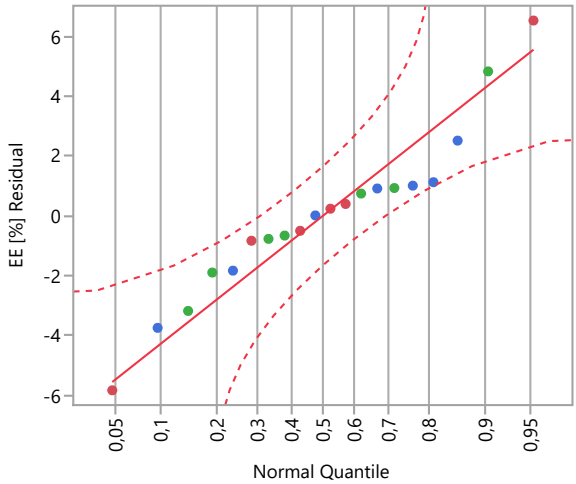

FRR [-]

Leverage Plot

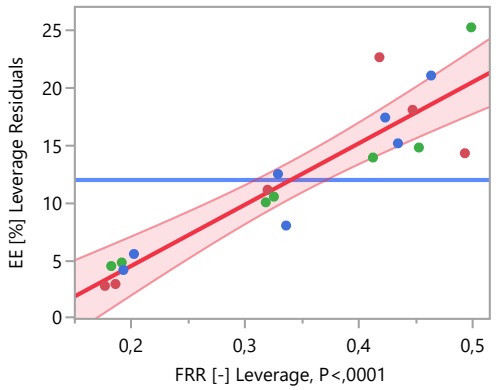

TFR [µL/min]

Leverage Plot

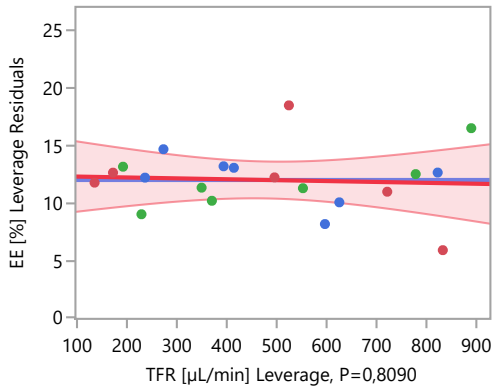

Figure C.44: Improved model of NPs EE (cont.)

Response EE [%] Rapamycin=With

FRR [-]*TFR [µL/min]

Leverage Plot

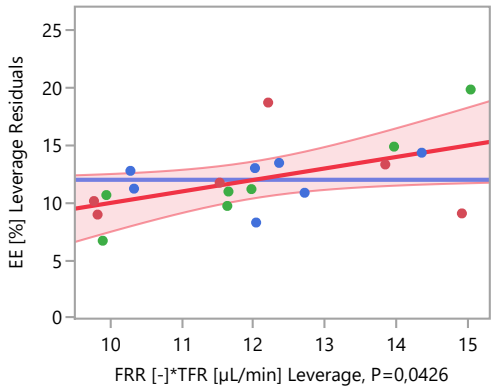

FRR [-]*FRR [-]

Leverage Plot

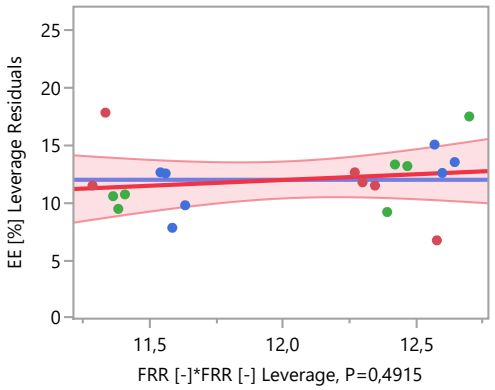

N

Leverage Plot

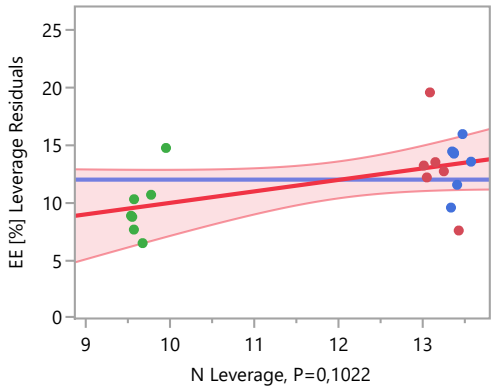

Least Squares Means Table

Level	Least Sq Mean	Std Error	Mean
1	12,521988	1,8462960	13,9137
2	9,045942	1,6501093	9,9190
3	12,844750	1,5153486	12,4937

Figure C.45: Improved model of NPs EE (cont.)

C.6.5 Prediction based on isocurve

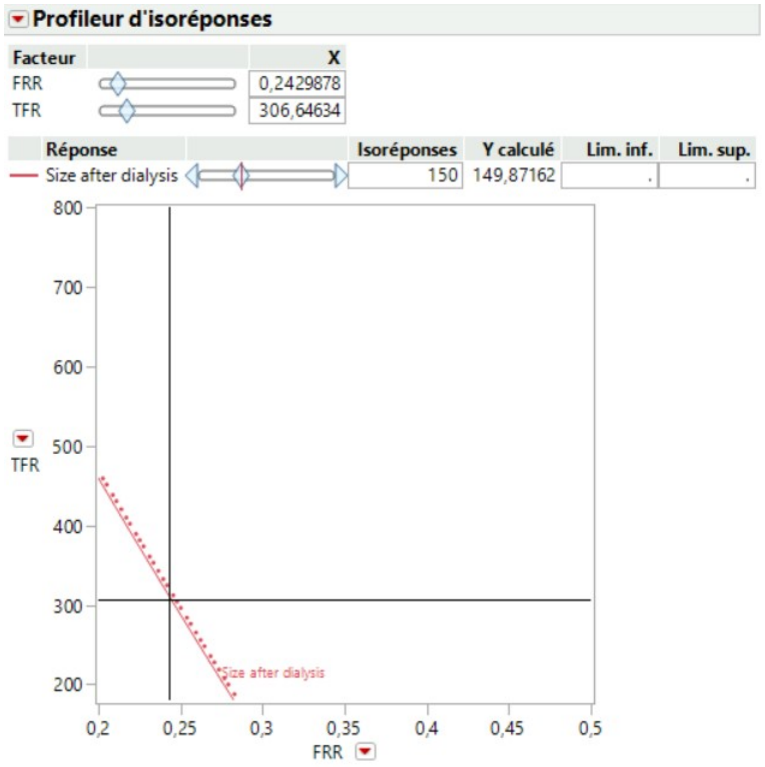

Figure C.46: Isocurve for size prediction of NPs

Bibliography

[1] Adeel M. Tuccinardi T. Cordani M. Rizzolio F. Bayda, S. The history of nanoscience and nanotechnology : From chemical–physical applications to nanomedicine. *Molecules*, 25(1):112, 2019b.

[2] Cao Y. Cao M. Wang Y. Cao Y. Gong T. Fan, D. Nanomedicine in cancer therapy. *Signal Transduction And Targeted Therapy*, 8(1), 2023.

[3] Cancer.gov. Benefits of Nanotechnology for Cancer, 2023. Accessed: 25/06/2024, https://www.cancer.gov/nano/cancer-nanotechnology/benefits.

[4] Yechezkel (Chezy) Barenholz. *Chapter 13: Doxil® – the First FDA-approved Nano-drug: from Basics via CMC, Cell Culture and Animal Studies to Clinical Use*. Martin Braddock, 2016.

[5] Y. Barenholz. Doxil® — the first fda-approved nano-drug : Lessons learned. *Journal Of Controlled Release*, 160(2):117-134, 2012.

[6] Cullis P. R. Allen, T. M. Liposomal drug delivery systems : From concept to clinical applications. *Advanced Drug Delivery Reviews*, 65(1):36-48, 2013.

[7] Shmeeda H. Barenholz Y. Gabizon, A. Pharmacokinetics of pegylated liposomal doxorubicin. *Clinical Pharmacokinetics*, 42(5):419-436, 2003.

[8] Zaks T. Langer R. Dong Y. Hou, X. Lipid nanoparticles for mrna delivery. *Nature Reviews, materials*, 6(12):1078-1094, 2021.

[9] Kester K. E. Casimiro D. Gurunathan S. DeRosa F. Jackson, N. A. C. The promise of mrna vaccines : a biotech and industrial perspective. *Npj Vaccines*, 5(1), 2020.

[10] Sahly H. M. E. Essink B. Kotloff K. Frey S. Novak R. Diemert D. Spector S. A. Rouphael N. Creech C. B. McGettigan J. Khetan S. Segall N. Solis J. Brosz A. Fierro C. Schwartz H. Neuzil K. Corey L. . . . Zaks T. Baden, L. R. Efficacy and safety of the mrna-1273 sars-cov-2 vaccine. *The new England Journal Of Medicine*, 384(5):403-416, 2021.

[11] Yves Dufrêne. LBRNA2202 - lesson : Nanobiotechnologies. *UCLouvain*, 2023.

[12] Robinson K. J. Islam J. Thurecht K. J. Corrie S. R. Bobo, D. Nanoparticle-based medicines: A review of fda-approved materials and clinical trials to date. *Pharmaceutical Research*, 33(10):2373–2387, 2016.

[13] Dobrovolskaia M. A. Ilinskaya, A. N. Nanoparticles and the blood coagulation system. part i : benefits of nanotechnology. *Nanomedicine*, 8(5):773-784, 1913.

[14] Cancer.gov. Side Effects of Cancer Treatment. Accessed: 30/07/2024, https://www.cancer.gov/about-cancer/treatment/side-effects.

[15] Bernard E. Abbosh C. André F. Auwerx J. Balmain A. Bar-Sagi D. Bernards R. Bullman S. DeGregori J. Elliott C. Erez A. Evan G. Febbraio M. A. Hidalgo A. Jamal-Hanjani M. Joyce J. A. Kaiser M. Lamia K. . . . Hanahan D. Swanton, C. Embracing cancer complexity : Hallmarks of systemic disease. *Cell*, 187(7):1589-1616, 2024.

[16] World Health Organization : WHO. Cancer, 2019. Accessed: 30/07/2024, https://www.who.int/health-topics/cancertab=tab$_1$.

[17] Sokolov A. V. Chubarev V. N. Tarasov V. V. Schiöth H. B. Namiot, E. D. Nanoparticles in clinical trials : Analysis of clinical trials, fda approvals and use for covid-19 vaccines. *International Journal Of Molecular Sciences*, 24(1):787, 2023.

[18] Jain P. K. El-Sayed I. H. El-Sayed M. A. Huang, X. Gold nanoparticles : interesting optical properties and recent applications in cancer diagnostics and therapy. *Nanomedicine*, 2(5):681-693, 2007.

[19] McNeil S. E. Mühlebach-S. Bawa R. Borchard G.-Barenholz Y. Tamarkin L. Desai N. Tinkle, S. Nanomedicines : addressing the scientific and regulatory gap. *Annals Of The New York Academy Of Sciences*, 1313(1):35-56, 2014b.

[20] Jain A. Pandurangan-G. Bastani, B. Incidence of side-effects associated with high-dose ferric gluconate in patients with severe chronic renal failure. *Nephrology*, 8(1):8-10, 2003.

[21] Rao M. Kausz-A. T. Brenner L. Pereira-B. J. G. Frigo T. B. Lewis J. M. Balakrishnan, V. S. Physicochemical properties of ferumoxytol, a new intravenous iron preparation. *European Journal Of Clinical Investigation*, 39(6):489-496, 2009.

[22] Yadav S. K. Yadav S. C. Kumari, A. Biodegradable polymeric nanoparticles based drug delivery systems. *Colloids And Surfaces B Biointerfaces*, 75(1):1-18, 2010.

[23] Pagels R. F. Wilson B. K. Ristroph K. D. Prud'homme R. K. Markwalter, C. E. Flash nanoprecipitation for the encapsulation of hydrophobic and hydrophilic compounds in polymeric nanoparticles. *Journal Of Visualized Experiments*, 143, 2019.

[24] Gupta B. Ramasamy T. Thapa R. K. Youn Y. S. Choi H. Yong C. S. Kim J. O. Poudel, B. K. Development of polymeric irinotecan nanoparticles using a novel lactone preservation strategy. *International Journal Of Pharmaceutics*, 512(1):75-86, 2016.

[25] Xie Y. El-Gendy N. Berkland C. J. Forrest M. L. Aillon, K. L. Effects of nanomaterial physicochemical properties on in vivo toxicity. *Advanced Drug Delivery Reviews*, 61(6):457-466, 2009.

[26] Dehghankhold M. Ataei S.-Davarani F. H. Javanmard R. Donikha A. Khorasani S. Mozafari M. Danaei, M. Impact of particle size and polydispersity index on the clinical applications of lipidic nanocarrier systems. *Pharmaceutics*, 10(2):57, 2018.

[27] McNeil S. E. Mühlebach-S. Bawa R. Borchard G. Barenholz Y. Tamarkin L. Desai N. Tinkle, S. Nanomedicines : addressing the scientific and regulatory gap. *Annals Of The New York Academy Of Sciences*, 1313(1):35-56, 2014.

[28] Gulati N. Nagaich U.- Pal A. Bharti, C. Mesoporous silica nanoparticles in target drug delivery system : A review. *International Journal Of Pharmaceutical Investigation*, 5(3):124, 2015b.

[29] Dewangan H. K. Yadav, D. Pegylation : an important approach for novel drug delivery system. *Journal Of Biomaterials Science Polymer Edition*, 32(2):266-280, 2020.

[30] Salman S. Ihsan-A. Elsaman T. Munir, M. U. Synthesis, characterization, functionalization and bio-applications of hydroxyapatite nanomaterials : An overview. *International Journal Of Nanomedicine*, 17:1903-1925, 2022.

[31] Cai C. Li J.-Li J. Li J. Sun T. Wang L. Wu H. Yu G. Li, J. Chitosan-based nanomaterials for drug delivery. *Molecules/Molecules Online/Molecules Annual*, 23(10):2661, 2018.

[32] Pridgen E. Molnar L. K. Farokhzad O. C. Alexis, F. Factors affecting the clearance and biodistribution of polymeric nanoparticles. *Molecular Pharmaceutics*, 5(4):505-515, 2008.

[33] Stylianopoulos T. Jain, R. K. Delivering nanomedicine to solid tumors. *Nature Reviews Clinical Oncology*, 7(11):653-664, 2010.

[34] Hunter A. C. Murray J. C. Moghimi, S. M. Nanomedicine : current status and future prospects. *The FASEB Journal*, 19(3):311-330, 2005.

[35] Shenqi Wang Richard Moore Yi Ge, Songjun Li. Nanomedicine. *Nanostructure science and technology*, 2014.

[36] Gu F. Chan J. Wang A. Langer R. Farokhzad O. Zhang, L. Nanoparticles in medicine : Therapeutic applications and developments. *Clinical Pharmacology And Therapeutics/Clinical Pharmacology Therapeutics*, 83(5):761-769, 2007.

[37] Hasani-Sadrabadi M. M. Majedi F. S. Dashtimoghadam E. Tondar M. Jacob K. I. Soleimani, S. Understanding biophysical behaviours of microfluidic-synthesized nanoparticles at nano-biointerface. *Colloids And Surfaces B Biointerfaces*, 145:802-811, 2016b.

[38] Allan S.Hoffman SCD. Frederick J.schoen M.D. Ph.D. Jack E.Lemons Ph.D. Buddy D.Ratner, Ph.D. *Biomaterials Science : An Introduction to Materials in Medicine*. Second Edition, 2004.

[39] Tagami T. Hoshikawa A. Ozeki T. Morikawa, Y. The use of an efficient microfluidic mixing system for generating stabilized polymeric nanoparticles for controlled drug release. *Biological Pharmaceutical Bulletin*, 41(6):899-907, 2018.

[40] Christensen D. Perrie Y. Roces, C. B. Translating the fabrication of protein-loaded poly(lactic-co-glycolic acid) nanoparticles from bench to scale-independent production using microfluidics. *Drug Delivery And Translational Research*, 10(3):582-593, 2020.

[41] Evonik. Biodegradable polymers for parenteral controlled release - Certificate of Analysis Resomer RG 502H, 2024, Batch Number D220500516. Accessed: 02/06/2024, https://healthcare.evonik.com/en/drugdelivery/parenteral-drug-delivery/parenteral-excipients/bioabsorbable-polymers/standard-polymers.

[42] Evonik. Biodegradable polymers for parenteral controlled release - Certificate of Analysis Resomer RG 752S, 2024, Batch number D221200539. Accessed: 02/06/2024, https://healthcare.evonik.com/en/drugdelivery/parenteral-drug-delivery/parenteral-excipients/bioabsorbable-polymers/standard-polymers.

[43] Alvarez-Fuentes J. Durán-Lobato M. Prados J. Melguizo C. Fernández-Arévalo M. Holgado M. Á. Martín-Banderas, L. Cannabinoid derivate-loaded plga nanocarriers for oral administration : formulation, characterization, and cytotoxicity studies. *International Journal Of Nanomedicine*, 5793, 2012.

[44] Pan Y.-Pham A. C.-Boyd B. J. Norton R. S. Nicolazzo J. A. Jin, L. Prolonged plasma exposure of the kv1.3-inhibitory peptide hstx1[r14a] by subcutaneous administration of a poly(lactic-co-glycolic acid) (plga) microsphere formulation. *Journal Of Pharmaceutical Sciences*, 110(3):1182-1188, 2021.

[45] Blasi P.- Deluca P. P. Schoubben, A. Effect of agitation regimen on the in vitro release of leuprolide from poly(lactic-co-glycolic) acid microparticles. *Journal Of Pharmaceutical Sciences*, 101(3):1212-1220, 2012.

[46] Bodmeier-R. Zhang, C. Direct drug milling in organic plga solution facilitates the encapsulation of nanosized drug into plga microparticles. *European Journal Of Pharmaceutics And Biopharmaceutics*, 191:1-11, 2023.

[47] M. Utzinger. *PLGA-based micro-and nanoparticle development for chemically modified messenger RNA delivery*. PhD thesis, Universität München, 2017.

[48] Kim S. G. Blenis J. Li, J. Rapamycin : One drug, many effects. *Cell Metabolism*, 19(3):373-379, 2014.

[49] National Center for Biotechnology Information. PubChem Compound Summary for CID 5284616, Sirolimus, 2024. Accessed: 06/07/2024, https://pubchem.ncbi.nlm.nih.gov/compound/Sirolimus.

[50] Gallant H. Legatt D. F. Yatscoff R. W. Trepanier, D. J. Rapamycin : distribution, pharmacokinetics and therapeutic range investigations : an update. *Clinical Biochemistry*, 31(5):345-351, 1998.

[51] Li H. Yao Q. Zhang Y. Zhu X. Xia T. Wang J. Li G. Li X. Ni S. Wang, B. Local in vitro delivery of rapamycin from electrospun peo/pdlla nanofibers for glioblastoma treatment. *Biomedicine Pharmacotherapy*, 83:1345-1352, 2016.

[52] Vladisavljević G. T. Nagy Z. K. Holdich R. G. Othman, R. Encapsulation and controlled release of rapamycin from polycaprolactone nanoparticles prepared by membrane micromixing combined with antisolvent precipitation. *Langmuir*, 32(41):10685-10693, 2016.

[53] Madni A. Li W. Correia A. Khan M. M. Rahim M. A. Santos H. A. Tahir, N. Microfluidic fabrication and characterization of sorafenib-loaded lipid-polymer hybrid nanoparticles for controlled drug delivery. *International Journal Of Pharmaceutics*, 581:119275, 2020.

[54] Kaur R. Lowry D. Moghaddam B. Wilkinson A. Perrie Y. Kastner, E. High-throughput manufacturing of size-tuned liposomes by a new microfluidics method using enhanced statistical tools for characterization. *International Journal Of Pharmaceutics*, 477(1-2):361-368, 2014.

[55] Dalvi S. V. Siril P. F. Kumar, R. Nanoparticle-based drugs and formulations : Current status and emerging applications. *ACS Applied Nano Materials*, 3(6):4944-4961, 2020.

[56] Schmidt S. Derendorf H. Gonzalez, D. Importance of relating efficacy measures to unbound drug concentrations for anti-infective agents. *Clinical Microbiology Reviews*, 26(2):274-288, 2013.

[57] E. Piacentini. *Encapsulation efficiency*. Springer, 2016.

[58] Khan F. N. Cosby L. Yang G. Winter J. O. Lee, K. H. Polymer concentration maximizes encapsulation efficiency in electrohydrodynamic mixing nanoprecipitation. *Frontiers In Nanotechnology*, 3, 2021.

[59] Siegel R.A. Rathbon M.J. Siepman, J. *Fundamentals and applications of Controlled Release Drug Delivery*. Springer New York Dordrecht Heidelberg London, 2012.

[60] Sinha A. S. K. Nigam K. D. P. Dwivedi D. Sangwai J. S. Kumar, Y. Functionalized nanoparticles : Tailoring properties through surface energetics and coordination chemistry for advanced biomedical applications. *Nanoscale*, 15(13):6075-6104, 2023.

[61] Pizzagalli L. Gerard, C. Mechanical behaviour of nanoparticles : Elasticity and plastic deformation mechanisms. *Pramana*, 84(6):1041-1048, 2015.

[62] Issadore D. Mitchell M. J. Shepherd, S. J. Microfluidic formulation of nanoparticles for biomedical applications. *Biomaterials*, 274:120826, 2021.

[63] Wathoni N. Shamsuddin S. Muchtaridi M. Herdiana, Y. Scale-up polymeric-based nanoparticles drug delivery systems : Development and challenges. *OpenNano*, 7:100048, 2022.

[64] Pillay V. Ndesendo V. M. Du Toit L. C. Kumar P. Khan R. A. Murphy C. S. Jarvis D. Choonara, Y. E. Polymeric emulsion and crosslink-mediated synthesis of super-stable nanoparticles as sustained-release anti-tuberculosis drug carriers. *Colloids And Surfaces B Biointerfaces*, 87(2):243-254, 2011.

[65] Venugopal A. Kozhikkalathil H. Valappil S. Kale M. Mann M. Ahuja P. Munjal S. Rajan, S. Synthesis of zno nanoparticles by precipitation method : Characterizations and applications in decipherment of latent fingerprints. *Materials Today : Proceedings*, 2023b.

[66] Elveflow microfluidics. La microfluidique et les puces microfluidiques - Elveflow, 2023. Accessed: 08/07/2024, https://www.elveflow.com/archives-fr/histoire-de-la-microfluidique-et-des-puces-microfluidiques/.

[67] Küçüktürkmen B. Bozkır A. Bezelya, A. Microfluidic devices for precision nanoparticle production. *Micro*, 3(4):822-866, 2023.

[68] Lizarbe-Sancha S. Campisi J. Arana S. Mujika M. Mitxelena-Iribarren, O. Different microfluidic environments for in vitro testing of lipid nanoparticles against osteosarcoma. *Bioengineering*, 8(6):77, 2021.

[69] Ozcelik A.-Grigsby C. L. Zhao Y. Guo F. Leong K. W. Huang T. J. Lu, M. Microfluidic hydrodynamic focusing for synthesis of nanomaterials. *Nano Today*, 11(6):778–792, 2016.

[70] Ren Y.-Hou L. Tao Y. Liu W. Jiang T. Jiang H. Zhang, K. Continuous microfluidic mixing and the highly controlled nanoparticle synthesis using direct current-induced thermal buoyancy convection. *Microfluidics And Nanofluidics*, 24(1), 2019.

[71] Cai L.-Liu C. Sun J. Tian, F. Microfluidic technologies for nanoparticle formation. *Lab On A Chip*, 22(3):512-529, 2022.

[72] Jeroish Z. E. Bhuvaneshwari K. S. Bayat P. Premkumar R. Samsuri F. Yusoff M. M. Narayanamurthy, V. Advances in passively driven microfluidics and lab-on-chip devices : a comprehensive literature review and patent analysis. *RSC Advances*, 10(20):11652-11680, 2020.

[73] GV. Continuous production of liposomes and lipid nanoparticles using the 5 input and micromixer chip - application note. Technical report, Dolomite, 2020, https://www.microtasconferences.org/microtas2020/images/current_support_files/dolomite/Dolomite_Application_Note-Continuous_Production_of_Liposomes_and_Lipid_NPs.pdf.

[74] GV. Continuous microfluidic synthesis of plga nanoparticles by hydrodynamic flow focusing - application note. Technical report, Dolomite, 2019, https://www.dolomite-microfluidics.com/drug-encapsulation-in-plga-particles/.

[75] Dolomite. Drug (API) microencapsulation Systems | Dolomite Microfluidics, 2024. Accessed: 28/06/2024, https://www.dolomite-microfluidics.com/microfluidic-systems/drug-api-encapsulation/.

[76] Malvern Panalytical. (s. d.). Microfluidique – présentation. Accessed: 28/06/2024, https://www.malvernpanalytical.com/fr/products/technology/microfluidics.

[77] Labarre, L., Team, E. Automated Lipid Nanoparticle Synthesis Pack - ElveFlow, 2024. Accessed: 28/06/2024, https://www.elveflow.com/microfluidics-application-packs/nanoparticles-packs/lipid-nanoparticle-synthesis/.

[78] microfluidic ChipShop GmbH. (s. d.). Microfluidics - microfluidic ChipShop. Accessed: 28/06/2024, https://www.microfluidic-chipshop.com/microfluidics/.

[79] Walczyk D. Hole P. Smith J. Lynch I. Dawson K. Montes-Burgos, I. Characterisation of nanoparticle size and state prior to nanotoxicological studies. *Journal Of Nanoparticle Research*, 12(1):47-53, 2009.

[80] Caputo F. Rösslein M. Calzolai L. Saint-Antonin F. Courant T. Wick P. Gilliland D. Mehn, D. Larger or more ? nanoparticle characterisation methods for recognition of dimers. *RSC Advances*, 7(44):27747-27754, 2017.

[81] Patrick Bogeart. LBRTI2101A - lesson : Analyse statistique de données spatiales et temporelles. *UCLouvain*, 2023.

[82] Santa T. Kato M. Itoh, N. Rapid and mild purification method for nanoparticles from a dispersed solution using a monolithic silica disk. *Journal Of Chromatography A*, 1404:141-145, 2015.

[83] Thermo Fisher Scientific. (n.d.).. Instruction Slide-A-Lyzer™ G2 Dialysis Cassette, 2013. Accessed: 06/08/2024, https://assets.fishersci.com/TFS-Assets/LSG/manuals/MAN0011668_SlideALyzer_G2_Dialy_Cassette$_UG.pdf$.

[84] Catherine Rasse, SMCS. Personal communication, 2024. Personal interview, may and june.

[85] Andy Math. Normal Distribution Empirical Rule, 2024. Accessed: 08/07/2024, https://andymath.com/normal-distribution-empirical-rule/.

[86] Wikipedia contributors. Règle 68-95-99,7, 2024. Accessed: 08/07/2024, https://fr.wikipedia.org/wiki/Poloxam

[87] Lou G. Jain N. Abraham S.-Thomas A. Halbert G. W. Perrie Y. Roces, C. B. Manufacturing considerations for the development of lipid nanoparticles using microfluidics. *Pharmaceutics*, 12(11):1095, 2020.

[88] Sieber S. Rahimi F. Shahbazi M. Rezayan-A. H. Huwyler J. Witzigmann D. Sedighi, M. Rapid optimization of liposome characteristics using a combined microfluidics and design-of-experiment approach. *Drug Delivery And Translational Research*, 9(1):404-413, 2018.

[89] Nazar A. R. S. Heshmatnezhad, F. On-chip controlled synthesis of polycaprolactone nanoparticles using continuous-flow microfluidic devices. *Journal Of Flow Chemistry*, 10(3):533-543, 2020.

[90] Saeed K. Khan I. Khan, I. Nanoparticles: Properties, applications and toxicities. arabian journal of chemistry. *International Journal Of Nanomedicine*, 12(7):908–931, 2019.

[91] Leung S. S. Quan D. H. Triccas-J. A. Britton W. J. Chan H. Parumasivam, T. Rifapentine-loaded plga microparticles for tuberculosis inhaled therapy : Preparation and in vitro aerosol characterization. *European Journal Of Pharmaceutical Sciences*, 88:1-11, 2016.

[92] B. Mukherjee. Preparation, characterization and in-vitro evaluation of sustained release protein-loaded nanoparticles based on biodegradable polymers. *International Journal Of Nanomedicine*, 487, 2008b.

[93] Solvas X. C. I. Wootton R. C. R. deMello A. J. Elvira, K. S. The past, present and potential for microfluidic reactor technology in chemical synthesis. *Nature Chemistry*, 5(11):905-915, 2013.

[94] Contributors to Wikimedia projects. Variogramme, 2021. Accessed: 06/08/2024, https://fr.wikipedia.org/wiki/Variogrammes.

[95] Dong L. Guo Z. Sun W. Mi S. Wang, A. A methacrylated hyaluronic acid network reinforced pluronic f-127 gel for treatment of bacterial keratitis. *Biomedical Materials*, 17(4):045017, 2022.

[96] Wikipedia contributors. Poloxamère, 2024. Accessed: 04/07/2024, https://fr.wikipedia.org/wiki/Poloxam

[97] Hatton T. A. Alexandridis, P. Poly(ethylene oxide) poly(propylene oxide) poly(ethylene oxide) block copolymer surfactants in aqueous solutions and at interfaces: thermodynamics, structure, dynamics, and modeling. *Colloids And Surfaces A Physicochemical And Engineering Aspects*, 96(1-2):1-46, 1995.

[98] Merck : Sigla-Aldrich. Pluronic F-127. Accessed: 13/08/2024, https://www.sigmaaldrich.com/BE/en/product/sigma/p2443?utm_source=googleutm_medium=cpcutm_campaign=8691857227utm_content=88085842275gclid=EAIaIQobChMI9MS-5c3xhwMVwaBoCR07nAsZEAAYASAAEgIfKfD_BwE.

[99] Face-centered central composite design. (s. d.). Normal Distribution Empirical Rule, 2023. Accessed: 14/06/2024, https://www.researchgate.net/figure/Face-centered-central-composite-design_fig2_369415017.

Optimisation of the microfluidic system of Dolomite for nanoparticle production

Carbon ARTHUR

In the current effort to enhance medical practices and drug delivery, optimizing the production of nanoparticles for medical applications is crucial. In the ADDB research laboratory at UCLouvain, a new microfluidic system has been purchased from the compagny Dolomite to produce nanoparticles. This system is more innovative than the conventional method and is therefore more promising.

The aim of this master thesis is to use this new device for the first time in order to understand how it works and thus obtain nanoparticles that are more suitable for medical applications and for industrialisation. In the long term, the idea would be to generate a predictive model based on this microfluidic system capable of producing nanoparticles adapted to a certain use.

Numerous experiments have been carried out with the aim of producing nanoparticles, studying the impact of changing system variables on the nanoparticles and making a first attempt to produce a predictive model. These experiments are presented in this master thesis.

UNIVERSITÉ CATHOLIQUE DE LOUVAIN
Faculté des bioingénieurs
Croix du Sud, 2 bte L7.05.01, 1348 Louvain-La-Neuve, Belgique | **www.uclouvain.be/agro**